The control design for an overactuated vehicle

Vissers, J.P.M.

Award date:
2005

The control design for an overactuated vehicle

J.P.M. Vissers

DCT 2005.114

Master's thesis

Coach: Ir. J. Ploeg (TNO)

Supervisor: Prof. dr. H. Nijmeijer

Committee: Dr. ir. A.G. de Jager
Dr. ir. K Camlibel
Dr. ir. A.J.C. Schmeitz

TNO Science & Industry, Business Unit Automotive
Department Advanced Chassis and Transport Systems

Technische Universiteit Eindhoven
Department Mechanical Engineering
Dynamics and Control Group

Eindhoven, August, 2005

Preface

This report is the result of a traineeship at TNO in Helmond in partial fulfillment of my graduation at the Technical University of Eindhoven, faculty Mechanical Engineering.
I would like to thank prof. dr. Henk Nijmeijer for this supervision and criticism, ir. Jeroen Ploeg at TNO for his support and guidance during this project and dr. ir. A.G. de Jager, dr. ir. K Camlibel and dr. ir. A.J.C. Schmeitz for participating in my graduation committee.
Further I want to thank my parents, family and friends for their support during the last couple of years.

John Vissers

Schijf, 25 August 2005

Abstract

In this report, the control design for an autonomous four wheel steered and four wheel driven robot car is considered. The main objective is to develop a structured and generic controller that can independently control the time dependent position and the orientation angle of the center of the robot car. Another objective is to let the controller function over the whole working range of the robot car (0-10 m/s^2 , 0-50 km/h). The control target over the whole velocity range differs. At high and medium velocity it is most important that the "tracking error", which is the position and orientation error, is small. At low velocities the steering angle behavior, as a reaction on position or velocity errors, is also important.

The robot car itself is an overactuated system, because the number of actuators (four steering and four driving motors) is larger than the number of degrees of freedom (three). In this report the problem is overcome by decentralizing the tracking problem. The position of the center and the orientation angle of the car are transformed to eight position-coordinates of the wheels. Also four desired orientation angles for the wheels are calculated using a kinematic approach, which guarantees that the wheels of the car are oriented so that an instantaneous center of rotation is present during the total manoeuvre. The instantaneous center of rotation represents the point around which the WMR is moving, so it is the point where the perpendiculars to the plane of each wheel (drawn from the center of the wheel) are all concurrent.

A model for a wheel that can be driven and that can be steered (unicycle) is developed using the theory on wheeled mobile robots. The controller developed for this model consists of a static-state feedback controller, which in combination with output linearizing coordinates, linearizes the (sub)system. A PD feedback controller with acceleration feedforward is designed for this linearized system. Finally, a tyre slip compensation is also designed to improve the tracking behavior.
The total robot controller that consists of four separate controllers is tested by evaluating typical vehicle manoeuvres through simulations and experiments in the VEHIL test facility. The simulation and experimental results show that the controller is capable of controlling the car over the whole specified range.

Samenvatting

Het regelontwerp voor een vier wiel gestuurd en vier wiel aangedreven voertuig wordt besproken in dit rapport. Het belangrijkste doel is om een gestructureerde en generieke regelaar te ontwerpen welke de tijdsafhankelijke positie en de oriëntatie hoek van het centrum van het voertuig kan regelen. Een andere doel is om de regelaar te laten functioneren over het hele werkgebied van het voertuig (0-10 m/s^2 , 0-50 km/h). Het regeldoel is verschillend over dit werkgebied, want bij hoge en gemiddelde snelheden is het belangrijk om een zo klein mogelijke fout in de positie en de oriëntatie hoek te hebben. Bij lage snelheden is het echter ook belangrijk dat het stuurgedrag, als reactie op positie- of snelheidsfouten, rustig is ook al gaat dit bijvoorbeeld ten koste van een grotere positiefout.

Het voertuig zelf is een overgeactueerd systeem, wat wil zeggend dat het aantal actuatoren (vier stuur- en vier aandrijfmotoren) groter is dan het aantal vrijheidsgraden (drie). Dit probleem is aangepakt door het regelprobleem te decentralizeren. De positie van het centrum en de orientatiehoek van de wagen worden vertaald naar acht positie-coördinaten van de wielen. Tevens worden er vier oriëntatie hoeken voor de stuurwielen bepaald, welke worden berekend volgens een kinematische aanpak. Dit garandeert dat de wielen zo worden georiënteerd dat er tijdens de beweging een uniek "instantaneous center of rotation" is. Het ICR is het punt rond welk het voertuig draait tijdens de manoeuvre, dus het is het punt waar de loodlijnen op de vlakken van de wielen tezamen komen.

Een model voor een wiel dat kan worden aangedreven en kan worden gestuurd (unicycle) is ontwikkeld gebruik makend van de theorie over mobiele robots. De regelaar die voor dit systeem is ontworpen bestaat uit een toestandsterugkoppeling, welke in combinatie met de juiste uitgangs (linearisatie) variabelen, een (sub)systeem lineariseert. Een simpele PD regelaar met "feedforward" is ontworpen voor dit gelineariseerde systeem. Er is ook nog een bepaalde bandenslip compensatie ontwikkeld voor de regelaar welke ervoor moet zorgen dat het volggedrag van het voertuig verbeterd.
De uiteindelijke regelaar, welke bestaat uit een regelaar voor elke hoek, is getest door simulaties en experimenten in de VEHIL test faciliteit met typische manoeuvres voor het voertuig. Het blijkt dat de regelaar in staat is om het voertuig over het hele gespecificeerde gebied te regelen met de aparte regeldoelen die daarbij horen.

List of Symbols

Symbol	Unit	Description
D	N	Cornering stiffness
F_z	N	Vertical load
G	N	Slip stiffness
I	kgm^2	Inertia
K_p	$-$	Proportional gain of the PD controller
K_v	$-$	Differential gain of the PD controller
L	m	Distance from vehicle center of gravity to wheel axle
N_{cs}	$-$	Number of conventional steerable wheels
N_f	$-$	Number of fixed wheels
N_w	$-$	Total number of wheels
O	$-$	Order
SA	rad	Slip angle
V	m/s	Velocity
W	m	Distance from the center of the wheel axle to the end
W	Nm/s	Power of interaction forces
a	m/s^2	Acceleration
e	m	Error
e_c	m	Distance from the center of the wheel/tyreto the "control point"
g	m/s^2	Gravitational constant
h_{car}	m	Height of the center of gravity
m	kg	Mass
m	$-$	Number of independent constraints
n	$-$	Number of configuration variables
n	$-$	Total number of data-points
r	m	Radius of the wheel/tyre
t	s	Time
x	m	x position in the global coordinate frame
$\dot{x}$	m/s	First derivative of x
$\ddot{x}$	m/s^2	Second derivative of x
y	m	y position in the global coordinate frame
$\dot{y}$	m/s	First derivative of y
$\ddot{y}$	m/s^2	Second derivative of y
α	rad	The angle that defines how the wheel is orientated at the car
β	rad	The steering angle

Symbol	Unit	Description
δ_m	$-$	Degree of mobility
δ_s	$-$	Degree of steerability
ε	$-$	Normalization parameter
φ	rad	Rotation angle of the wheel/tyre
$\dot{\varphi}$	rad/s	Rotation angle velocity of the wheel/tyre
$\ddot{\varphi}$	rad/s^2	Rotation angle acceleration of the wheel/tyre
θ	rad	Vehicle orientation angle
$\dot{\theta}$	rad/s	Vehicle orientation angle velocity
$\ddot{\theta}$	rad/s^2	Vehicle orientation angle acceleration
A	$-$	Matrix with the roll and slip constraints
A_1	$-$	Submatrix of the A matrix related to the posture coordinates (q_1)
B	$-$	Matrix that relates the input torques to the configuration variables
C	$-$	Matrix constructed by coriolis, centrifugal, gravity and resistant torques
C_1	$-$	Matrix constructed of slip constraints
F	$-$	Total generalized force vector
H	$-$	Matrix that relates the total input-vector η with z_2
H_ε	$-$	Matrix constructed by the slow manifolds
J	$-$	Matrix constructed by the matrices M, S and A
J_1	$-$	Matrix with the part of the roll constraints related to ξ
J_2	$-$	Matrix with the part of the roll constraints related to φ
K	$-$	Matrix constructed by e.g. tyre parameters
K_{pT}	$-$	Positive definite matrix of the "K_p" value(s) of the PD controller(s)
K_{vT}	$-$	Positive definite matrix of the "K_v" value(s) of the PD controller(s)
L	$-$	Matrix transforming the slip velocities to the longitudinal and lateral components
M	$-$	Inertia matrix
Q	$-$	Matrix that relates z_2 to $\dot{z}_3$
$R(\theta)$	$-$	Rotation matrix
S	$-$	Matrix that links the total input-vector η with the configuration variables
S_1	$-$	Matrix that links the total input-vector η with the posture coordinates
f_0	$-$	A vector of the system in singular perturbation form
f_1	$-$	A vector of the system in singular perturbation form
f_2	$-$	A vector of the system in singular perturbation form
g_0	$-$	A vector of the system in singular perturbation form
g_1	$-$	A vector of the system in singular perturbation form
g_2	$-$	A vector of the system in singular perturbation form
h	$-$	Vector with linearizing output functions (equal to z_1)
q	$-$	Vector with configuration variables
q_1	$-$	Vector of posture coordinates (ξ and β)
w	$-$	Vector with an arbitrary reference input
z_1	$-$	Vector with linearizing output functions (equal to h)
z_2	$-$	First derivative of z_1
z_3	$-$	Non-linearizing output functions
β	$-$	Vector of steering angles
ζ	$-$	Input-vector with steering angle velocities
η_a	$-$	Input-vector with generalized velocities

Symbol	Unit	Description
η	–	The total input-vector with generalized velocities
λ	–	Lagrange multipliers vector
μ	–	Vector that describes the importance of the violation of the constraints
ν	–	Vector with an arbitrary reference input
τ	–	Vector of input torques
ξ	–	Vector of the coordinates x, y, θ
Σ	–	Matrix where the columns form a basis of the null-space of C_1

Indices	Description
$_f$	Front
$_r$	Rear
$_l$	Left
$_l$	Local coordinate system
$_r$	Right
$_1$	Front wheel
$_2$	Rear wheel
$_i$	wheel index (bicycle)
$_{ij}$	wheel index (4ws4wd car)
$_{ref}$	Reference variable
$_{lat}$	Lateral component
$_{long}$	Longitudinal component

Table of Contents

Chapter 1

Introduction

1.1 Motivation

Wheeled mobile robots (WMR's) are widely used nowadays in the industry. The goal is often to let the center of the robot follow a certain time dependent reference path. TNO owns such a wheeled mobile robot, which is used in the VEHIL test facility. VEHIL is a hardware in the loop test facility that is used to efficiently develop and test intelligent vehicles. The idea is to bring the real world to a hall, where, instead of real velocities, the relative velocities between vehicles are used. The wheeled mobile robot is used to simulate this relative motion of the other car(s) in the surrounding traffic of the testing vehicle. The wheeled mobile robot used in the VEHIL test facility is different from most common wheeled mobile robots, because it is a high dynamic wheeled mobile robot. The wheeled mobile robot is capable of extreme manoeuvres at high velocities and exceeds the handling performance of modern road vehicles. The control goal, for the wheeled mobile robot used in VEHIL, is not only to let the center follow a certain (time-dependent) reference path, but also to control the orientation angle of the wheeled mobile robot during the manoeuvre.
Because of this, the wheeled mobile robot used is a four wheel steered and four wheel driven car (4ws4wd car) that is equipped with four driving motors and four steering motors. The research in this report focusses on the control design for this type of wheeled mobile robot.

The 4ws4wd robot is equipped with eight actuators but there are only three degrees of freedom in the horizontal plane, so the system is an over-actuated system.
The control methods developed before all focus on the forces and moments that act on the system. Most of the control methods do not take into account the tyre behavior (e.g. slip), which can have a great influence on the system if extreme manoeuvres are executed. The methods are also often ad-hoc. Therefore two important reasons can be stated why to develop a new control method for the 4ws4wd robot.

1. A more structured and generic control method is desired.

2. The control method has to take into account the tyre behavior.

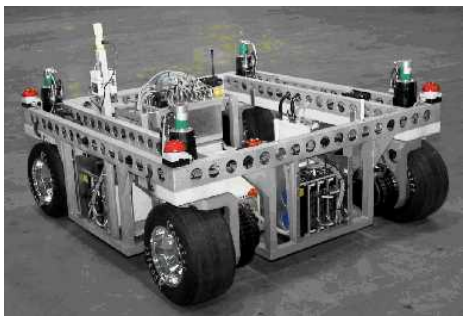

Figure 1.1: 4ws4wd WMR robot of TNO automotive

The field of robotics provides structured and generic methods for the control problem of a wheeled mobile robot. The starting idea of the method is that the tyre behaviour is ideal, which here means that no tyre slip is present. A model for the WMR is constructed using the approach from the field of robotics for WMR's with ideal tyres. Finally a controller is developed for this model. However, if these controllers are tested on real systems then it often concluded that tyre slip is an effect which cannot be neglected. This is the reason that a procedure to include the tyre behavior in the controller is developed in the field of robotics.

1.2 Problem statement

In this project, the control of a 4ws4wd vehicle is considered. The objectives of this project are:

- Develop a tracking controller for the x and y position of the center and the orientation angle (θ) of the 4ws4wd car.
- Develop a controller that takes into account the tyre behavior.
- Evaluate and tune the controller by means of simulations and experiments with the 4ws4wd robot used in the VEHIL test facility.

1.3 Outline of the report

The outline of the report is as follows. In chapter 2 the 4ws4wd robot that has to be controlled will be described. Also some requirement will be stated here. In chapter 3 an overview of the main literature in the field of robotics will be presented. Chapter 4 will construct the core of this report. Here the general procedure to derive a model and a controller for a wheeled mobile robot with and without tyre slip will be presented. A case study with a simple example will be conducted to demonstrate the procedures. In chapter 5 a controller for a bicycle model is developed using the procedures described in chapter 4. The bicycle model has the same manoeuvrability as a full (4ws4wd) car, however the equations are much more simple. This is the reason that the bicycle model is

often used in the development process of a (4ws4wd) car. As a start a controller is developed using the theory for a wheeled mobile robot without tyre slip. The following step is to introduce a "new" controller for the bicycle to overcome the problems with the controller from the standard theory. The "new" controller aims to decentralize the control problem to come to a more generic solution for the control problem. Each wheel of the wheeled mobile robot will have its own controller. Each wheel has a so called "unicycle" controller, which is a controller for a wheel that can be driven and that can be steered. So in total there are multiple unicycle controllers, because multiple wheels are attached on the 4ws4wd robot. For this reason the term "multicycle" controller (**multi**ple uni**cycle** controller) is introduced. Also a controller for a bicycle with tyre slip will be derived using the procedure described in chapter 4. The (multiple) unicycle controller is extended with a tyre slip compensation. At the end of this section, simulations are performed to investigate the advantage of the tyre slip compensation. In chapter 6 the multicycle controller will be changed so that the controller can be used for the 4ws4wd robot. At the end of this chapter, simulations using a full dynamic model of the 4ws4wd robot used in the VEHIL testing facility will be performed. The main text concludes with a chapter about the experiments performed in the VEHIL testing facility. Finally conclusions about the obtained results and also recommendations will be given.

Chapter 2

System description

A general description of the WMR, where the controller will be designed for, is desired before a start can be made with the control design. First of all the specifications of the WMR are described. Secondly, a list of requirements for the controller that follow out of the specifications will be given. These requirements will later on in the report be used to choose a certain type of controller during the control design process.

2.1 Specifications

The wheeled mobile robot used in VEHIL is a vehicle that responds to position commands issued. The WMR requires the independent control of its x and y position of the center, as well as its orientation (yaw) angle θ in order to carry out the desired manoeuvres (e.g. figure 2.1). Such a manoeuvring flexibility is accomplished through a four wheel steered and four wheel driven vehicle platform equipped with eight actuators. The maximum "longitudinal" acceleration and de-acceleration of the WMR is about 10 m/s^2. Also the maximum "lateral" acceleration, during e.g. driving a corner, is 10 m/s^2. There is a not to be underestimated amount of weight transfer with an acceleration level of 10 m/s^2, because of the height of the center of gravity of the WMR. The more vertical force on a tyre, the more lateral and longitudinal force the tyre can deliver (up to a certain limit) (appendix B). Therefore it is important to separately control the torques for all the four wheels to assure that the maximum performance of the WMR can be obtained.
The maximum velocity of the WMR in VEHIL is 50 km/h, however it is important for the controller to work well over the whole working range from 0-50 km/h. Position tracking is most important, but the steering angle behaviour, as a reaction on errors, is also important at low velocities. It is for example not desired for the steering angles to change 45^o or more as a response on an *error* in the lateral direction if the car itself is driving slowly in the longitudinal direction.
Motors capable of steering the wheels in a range of -350^o till 350^o are implemented for all four wheels. These large steering angles are needed, because of the trajectories driven by the WMR in VEHIL. One example is a straight line, where during this manoeuvre the orientation angle varies from -200^o till 200^o.

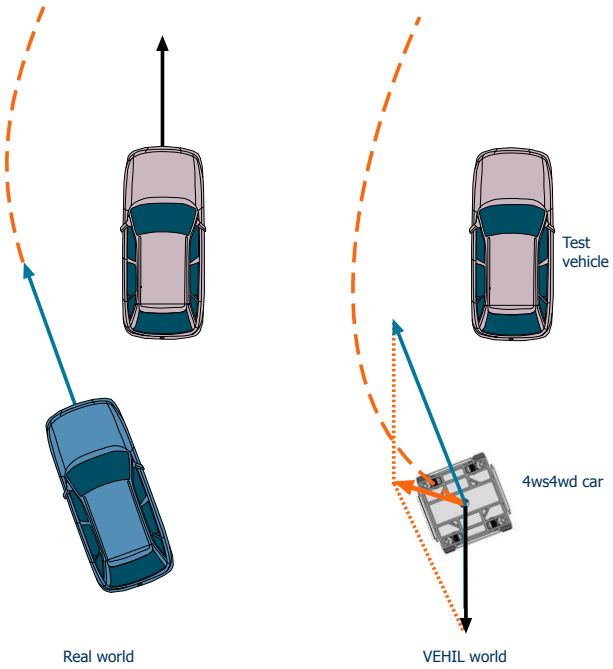

Figure 2.1: The reason for the independent control of x, y and θ.

Because of this, a controller is needed that is able to control the steering angle of the wheels over the whole range of 700^o.
Finally, it is important for the controller to work real-time with a sample rate of 500 Hz, so a numerically complicated controller is not desired.
The most important specifications of the WMR used in VEHIL are summarized in table 2.1.

Table 2.1: Specifications

Vehicle mass:	620 kg
Wheel base:	1.4 m
Track width:	1.4 m
Maximum speed:	50 km/h
Maximum acceleration:	10 m/s^2
Installed power:	52 kW
Steering angle range:	-350^o - 350^o

2.2 Requirements

The (extra) requirements following from the specifications are:

1. The controller has to distribute the forces according to the weight shift.

2. The controller has to work over the whole velocity range of 0-50 km/h. Position tracking is most important, but the steering angle behaviour is also important at low velocities.

3. The controller must be able to control the steering angle of the wheels over the whole range of 700^o.

4. The controller has to work real time with a sample rate of 500 Hz.

2.3 Summary

The (extra) requirements for the controller and some specifications of the four wheel driven four wheel steered car used in VEHIL are defined. The result is that a "simple" (velocity scaled) controller that takes into account weight shift has to be designed.

Chapter 3

Literature survey

This chapter provides an overview of the literature that constitutes the basis of this report. The studied literature focusses on **W**heeled **M**obile **R**obots (WMR's). A WMR is effectively a body with wheels mounted on the body so that the body can move in the horizontal plane. Different wheel types are known, such as fixed wheels, conventional steering wheels, swedish wheels and castor wheels. The most common wheels are conventional steering wheels (e.g. front wheel(s) of a passenger car) and fixed wheels (e.g. rear wheel(s) of a passenger car).
The first point of attention of the literature study is the theory on wheeled mobile robots and the resulting controllers. The second point of attention is the possibility to implement a tyre slip compensation in the controller that is based on the theory on wheeled mobile robots.
In section 3.1 the term "constraints" will be explained and the possibilities to describe models using the constraints is explained. Section 3.2 gives a short overview of the possible models for WMR's. Section 3.3 gives an overview of the possibilities of the robot theory to model the tyre slip. Finally a summary will be given that also describes how this literature constitutes the basis of this research.

3.1 Constraints

The first thing explained in every book or paper about WMR's is the term "constraints". Constraints are mathematical formulas describing the limitations of the position/movability of the system. There are two important type of constraints; position and velocity constraints. Velocity constraints are often described as not integrable kinematic constraints [3]. Kinematic constraints are not integrable if the constraints have no restrictions on the collection of possible positions of the robot, but have restrictions on the movability of the robot.
A common example to explain constraints is a normal front wheel steered car. This car can reach every position in the horizontal plane, but the car cannot move sideways. The front wheel steered car in figure 3.1 cannot move from A to B using path number 1. This is because of the restriction in the sideways direction of the wheel, which is a restriction of the velocity in this direction, which limits the (total) movability of the car. Instead of path number 1, path

number 2 has to be followed to get from A to B.

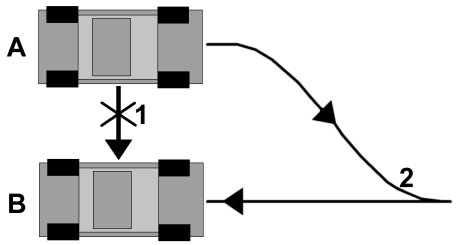

Figure 3.1: Parking problem for a normal front wheel steered car.

Campion, Bastin and D'Andréa-Novel state that all WMR's are characterized by velocity constraints [3]. The two important velocity constraints for WMR's are the slip and roll constraint (see figure 3.2). The slip constraint states that no movement is possible in the lateral (sideways) direction of a wheel and the roll constraint states that the longitudinal (forward) velocity of a wheel is equal to the rotation velocity of the wheel multiplied by the radius of the wheel.

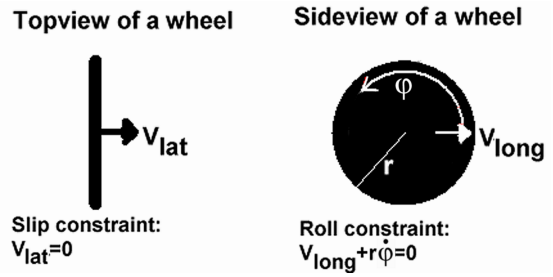

Figure 3.2: The slip and roll constraint of a wheel.

3.2 Classification

WMR's are subjected to constraints, as is known from the previous section. Campion et al. [3] have developed an approach to use these constraints to describe models for WMR's [3] [8].
The constraints contain information about the restrictions of the system with respect to velocities, so these constraints can be used to formulate a kinematic model of the system that describes the movement of the system. The idea is that the movement of the system is hidden in the null-space of the set of constraint equations [3] [8].
Using this approach, Campion et al. [3] suggest that four different kinds of (state space) models can be described to understand the behavior of a WMR.

- The posture kinematic model

- The configuration kinematic model
- The configuration dynamic model
- The posture dynamic model

The posture kinematic model describes the motion of the robot in the horizontal plane, but not all the evolutions of the configuration variables (e.g. wheel rotation) are described. These are described in the configuration kinematic model. The configuration dynamic model also models the dynamics of the robot. The posture dynamic model describes the system dynamics between the control input and the posture coordinates, which are the positions of the center of the car, the orientation angle of the car and the steering angles of the conventional steering wheels attached to the car.
As said before, the kinematic part of the models can be described using the velocity constraints. Extra dynamical equations are needed to be able to describe the dynamic models. These dynamic equations contain information about the mass of the car, the rotation inertia of the wheel, the positioning of the motors etc.
The velocity constraints of a WMR describe the so-called "mobility" of a WMR according to Campion et al. [3]. Not every WMR has the same "mobility properties", therefore it is possible to describe *five* general type of WMR's. These five types will often be characterized as type (δ_m,δ_s)-WMR's, where (δ_m) is the *degree of mobility* and (δ_s) is the *degree of steerability*.

If a WMR is equipped only with fixed wheels and conventional steering wheels, then the degree of mobility and the degree of steerability can be described as:
The degree of mobility is the number of degrees of freedom manipulatable directly without re-orienting the conventional steering wheels and the degree of steerability is the number of independent conventional steering wheels.

The sum of the degree of mobility and the degree of steerability is always three or less, because the number of degrees of freedom, of a WMR that moves in the horizontal plane, is three. Two different WMR types are described in figure 3.3. On the left side a bicycle with two conventional steering wheels is illustrated and on the right side a unicycle with two fixed wheels is illustrated. The bicycle is a (1,2)-WMR, because it has two conventional steering wheels and it can move in one direction (tangential of the circle) without reorientation of its conventional steering wheels. The unicycle is a (2,0)-WMR, because it is equipped with zero conventional steering wheels and it can manipulate "two" directions. First of all it can move forward by driving both wheels in the same directions. Secondly the unicycle can rotate around its vertical axis by driving both wheels in opposite direction.
The term independent in the description of the steerability is important, because this is the reason why the maximum number for the degree of steerability is two. This is also the reason for the maximum of two independent steering wheels on a WMR. Two wheels is the maximum number of wheels needed to describe the ICR (figure 3.3), which is the instantaneous center of rotation. If more wheels are attached to the WMR, the wheels have to be directed so that the movement around the ICR is not restricted. This is the reason that a four

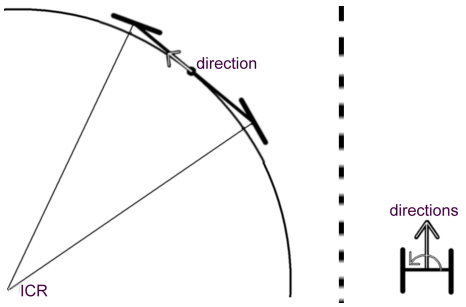

Figure 3.3: Driving possibilities of a "bicycle" and a "unicycle" without the reorientation of a conventional steering wheel. (Topview)

wheel steering (4ws) car is often modelled as a 2ws WMR with two steering wheels that both are a combination of two of the four steering wheels of the 4ws car. Therefore there have to be steering wheels on the 4ws car that are linked together in a mathematical way [2], so that an unique ICR is present.

The goal of the report is to find a controller for a WMR to track not only the reference x and y position of the center of the robot, but also the reference orientation angle and the reference steering angles (if defined) of the robot. A number of different controllers for different WMR's are described in the literature. Some are based on state feedback [4], while others are based on e.g sliding mode control [6] [7].
The basis of the controller suggested by D'Andréa-Novel [4] is a static state feedback controller. This controller linearizes the (sub)system if the right output linearizing coordinates are used. A PD feedback controller with acceleration feedforward is designed for this linearized system.

3.3 Slip modelling

The strong point of the discussed approach, which is the development of the controller for the model that is developed using the null-space of the total set of constraints, is at the same time the drawback of the approach. Constraints of the wheels are in reality often violated due to tyre slip, which is a result of the fact that tyres only can deliver forces if there is a difference in direction/velocity of movement between the tyre and the ground [1]. By Motte and Campion [5] it is suggested to model this slip as a linear system. The slipping effects introduce an extra (fast) dynamic effect to the known equations from the standard WMR theory. These equations together are formulated in a standard form for a system with "fast" and "slow" dynamics (i.e. a stiff system), the so called singular perturbation form. Fast relates to the fact that the new "slip" variable of the tyre-forces is multiplied by a small factor so that the variable can change fast without having a lot of influence on the other slow variables of the system.
A controller based on the so-called "slow manifold approach" is suggested by Motte and Campion [5]. The slow manifold approach allows to design feedback control laws taking into account the tyre slip. The system is output linearized

on the slow manifold, so tracking of the desired variables can be achieved by choosing the right output linearizing coordinates.

3.4 Summary

The standard approach in the theory on wheeled mobile robots is to model a 4ws4wd car as a 2ws2wd car with the front wheels modelled as one wheel and the rear wheels modelled as one wheel. This approach however has the disadvantage that for example the weight distribution between the four wheels cannot be modelled properly anymore. So a controller based on this model has the same disadvantages. Therefore another approach to control a 4ws4wd car will be discussed in this report next to the straight forward controller from the field of robotics for a 4ws4wd car.
Reviewing the literature of WMR's, the conclusion is that a lot of literature is available about WMR's, especially for the most simple WMR; the unicycle (type(2,0)) [3]. A unicycle is described in different ways in the literature; one wheel that can be rotated and oriented, or two wheels that can rotate and that are mounted on a fixed axle. The kinematic model of a unicycle is the most simple model of the collection of WMR's, still containing relevant WMR characteristics. For this reason it is the most interesting one for modelling and simulating. Because of the amount of literature about unicycles and because of the complexity of the system the choice is made to study if it is possible to use them in a certain way to develop a controller for the 4ws4wd car. The idea presented is inspired on an idea described in a paper of Borenstein [10]. In this paper two two-wheeled unicycles are linked together using a compliant linkage.

The literature about tyre slip is substantial, but the literature linking the tyre slip and the theory on wheeled mobile robots is limited. However, slip is a not to be underestimated factor, due to the large working range (e.g. large speed and acceleration) of the 4ws4wd car where the controller will be developed for. The slip modelling suggested by Motte and Campion is only suited to model linear tyre behavior, but in reality the tyre has a non-linear tyre behavior (see appendix B). However the linear approach is a good step in the right direction. Therefore the slip modelling suggested by Motte and Campion will be discussed in this report.

Chapter 4

Wheeled mobile robot control design

This chapter describes the general procedure for the development of a model for a wheeled mobile robot and the control design. A result of the literature survey is that the theory on wheeled mobile robots provides structured solutions to describe a model and develop a controller for a WMR. The theory on WMR's can be split up in a theory for wheeled mobile robots with wheels that have no "slip" and wheeled mobile robots with wheels that do have "slip". Slip is a non-avoidable effect since real tyres only can deliver forces if there is a difference in direction/velocity of movement between the tyre and the ground. In section 4.1 the procedure to develop the model and a controller for a WMR without tyre slip will be described. In section 4.2 this procedure is used to develop a controller for a 1DOF car without slip. In section 4.3 the procedure to develop the model and a controller for a WMR with slip will be described. Finally, the procedure of section 4.3 is used to develop a controller for a 1DOF car with tyre slip.

4.1 Theory on wheeled mobile robots

The focus in this report is on the modelling of WMR's with conventional steering wheels and fixed wheels (e.g. front and rear wheels of a car). The theory on wheeled mobile robot discussed is rewritten for these type of WMR's.
The first step is to define the coordinate-system(s). In figure 4.1 the local and the global coordinate systems are illustrated.
An orthogonal rotation matrix called $R(\theta)$ is introduced to switch between the velocity (and acceleration) vectors of the global and local axis systems.

$$R(\theta) = \begin{pmatrix} \cos(\theta) & \sin(\theta) & 0 \\ -\sin(\theta) & \cos(\theta) & 0 \\ 0 & 0 & 1 \end{pmatrix} \tag{4.1}$$

where θ is the orientation angle of the car.

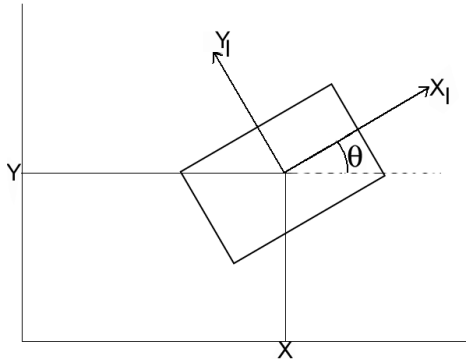

Figure 4.1: Coordinate definition

The matrix $R(\theta)$ is defined so that:

$$\begin{pmatrix} \dot{x}_l \\ \dot{y}_l \\ \dot{\theta} \end{pmatrix} = R(\theta)\dot{\xi} \quad where \quad \xi = \begin{pmatrix} x \\ y \\ \theta \end{pmatrix} \tag{4.2}$$

As stated before, a wheel has two important constraints; The slip constraint, which limits the movability in the horizontal plane and the roll constraint, which relates the rotation of the wheels to the forward speed of the wheels. Both constraints are defined relative to the local coordinate system and translated to the global coordinate system using the matrix $R(\theta)$.
The slip constraint restricts the movement in the lateral direction of a tyre. This can be defined as [3]:

$$\begin{pmatrix} \sin(\alpha+\beta) & -\cos(\alpha+\beta) & -L\cos(\beta) \end{pmatrix} R(\theta)\dot{\xi} = 0 \tag{4.3}$$

where β is the steering angle, L is the distance from the local coordinate origin of the car to the wheel, α is an angle that defines how the wheel is oriented at the car, φ is the rotation of the wheel and r is the radius of the tyre. These variables are illustrated in figure 4.2.
The roll constraint defines that the forward velocity plus the rotation-velocity of the tyre multiplied with the radius of the tyre is zero. This can be defined as [3]:

$$\begin{pmatrix} \cos(\alpha+\beta) & \sin(\alpha+\beta) & L\sin(\beta) \end{pmatrix} R(\theta)\dot{\xi} + r\dot{\varphi} = 0 \tag{4.4}$$

4.1.1 Model development using the theory on wheeled mobile robots

The WMR's discussed in this report are equipped with N_{cs} conventional steering wheels and N_f fixed wheels, so the total number of wheels is $N_w = N_{cs} + N_f$. The WMR satisfies a set of m independent constraints [5]. The set of slip constraints is:

$$C_1 R(\theta)\dot{\xi} = 0 \tag{4.5}$$

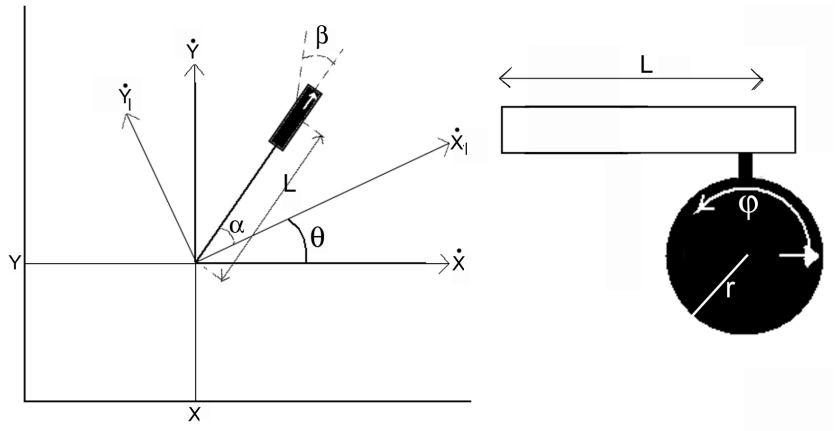

Figure 4.2: Coordinate definition for the constraints

where C_1 is a (N_wx3)-matrix. The set of roll constraints is:

$$J_1 R(\theta)\dot{\xi} + J_2\dot{\varphi} = 0 \tag{4.6}$$

where J_1 is a (N_wx3)-matrix and J_2 is a (N_wxN_w)-matrix.

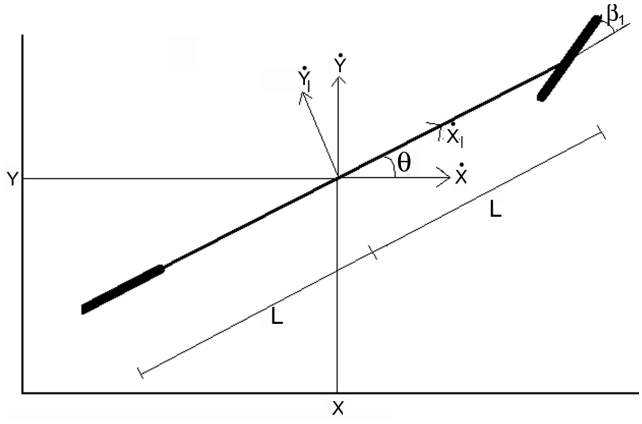

Figure 4.3: Bicycle with one conventional steering wheel and one fixed wheel.

As an example, the constraints of a bicycle with one conventional steering wheel and one fixed wheel (figure 4.3) will be determined and written in the standard form.
The front conventional steering wheel and the rear fixed wheel both have two constraints. To obtain these constraints from the general form (4.3) - (4.4), α, L and β have to be defined. For the front wheel α=0, L=L and β=β_1. For the rear wheel α=π, L=L and β=0. The set of slip constraints now is (4.5):

$$C_1 R(\theta)\dot{\xi} = \begin{pmatrix} \sin(\beta_1) & -\cos(\beta_1) & -L\cos(\beta_1) \\ 0 & 1 & -L \end{pmatrix} R(\theta)\dot{\xi} = 0 \tag{4.7}$$

The total set of roll constraints now is (4.6):

$$J_1 R(\theta)\dot{\xi} + J_2\dot{\varphi} = \begin{pmatrix} \cos(\beta_1) & \sin(\beta_1) & L\sin(\beta_1) \\ -1 & 0 & 0 \end{pmatrix} R(\theta)\dot{\xi} + \begin{pmatrix} r & 0 \\ 0 & r \end{pmatrix}\dot{\varphi} = 0 \tag{4.8}$$

The following step is to introduce the variable q, which is the set of n-configuration variables, which are the position coordinates ξ, the steering angle coordinates of the conventional steering wheels β and the rotation angles coordinates of the wheels φ, so:

$$q = \begin{pmatrix} \xi \\ \beta \\ \varphi \end{pmatrix} \tag{4.9}$$

Therefore, the system of constraints (4.5) - (4.6) can be written in a more general form:

$$A^T(q)\dot{q} = 0 \tag{4.10}$$

where $A^T(q)$ is a mxn matrix:

$$A^T(q) = \begin{pmatrix} C_1 R(\theta) & 0 & 0 \\ J_1 R(\theta) & 0 & J_2 \end{pmatrix} \tag{4.11}$$

Before the kinematic and dynamic models can be defined, it is important to state how the degree of steerability (δ_s), which is the number of degrees of freedom that can manipulated without re-orienting the conventional steering wheels, and the degree of mobility (δ_m), which is the number of independent conventional steering wheels, are defined.
The degree of mobility is [8]:

$$\delta_m = dim(N[C_1]) = 3 - rank[C_1] \tag{4.12}$$

where $dim(N[C_1])$ is the dimension of the null-space of C_1. So the dimension of the null-space of C_1 is equal to the degree of mobility. This can be explained by looking at what C_1 effectively is. The matrix C_1 defines the mobility limitations of the system in the horizontal plane, so the possible movements of the system are hidden in the null-space of C_1. These possible movements are the mobility of the system. For the bicycle with one conventional steering wheel and one fixed wheel, the C_1 matrix is defined in (4.7). The rank of this matrix is equal to two, so the degree of mobility is one.
The degree of steerability is [8]:

$$\delta_s = rank[C_1(\beta)] \tag{4.13}$$

where $C_1(\beta)$ is the part of the C_1 matrix constructed from the constraints for the conventional steering wheels. The $C_1(\beta)$ matrix for the bicycle with one conventional steering wheel and one fixed wheel is defined as:

$$C_1(\beta) = \begin{pmatrix} \sin(\beta_1) & -\cos(\beta_1) & -L\cos(\beta_1) \end{pmatrix} \tag{4.14}$$

Therefore, the degree of steerability is one. Concluding, the bicycle with one fixed and one conventional steering wheel is a so called (1,1)-WMR.

The most simple model for a WMR is the posture kinematic model, so therefore this is the first model to derive. The posture kinematic model is a model that describes the motion of the robot in the horizontal plane, without describing all evolutions of the configuration variables. The most important matrix for this model is the C_1 matrix, because C_1 describes the limitation on the coordinates velocities in the horizontal plane $(\dot{x}, \dot{y}, \dot{\theta})$. The matrices J_1 and J_2 are not relevant for the posture kinematic model, because J_1 in combination with the J_2 matrix (4.6) describes the relation between the posture coordinates and the wheel rotation coordinates, which aren't posture coordinates.
The following step is to define a matrix $\Sigma(\beta)$, which is a $(3\text{x}\delta_m)$ matrix where the columns form a basis of the null-space of C_1, so $C_1\Sigma(\beta) = 0$.
Using this definition it is possible to rewrite (4.5) as:

$$R(\theta)\dot{\xi} = \Sigma(\beta)\eta_a \tag{4.15}$$

so

$$\dot{\xi} = R^T(\theta)\Sigma(\beta)\eta_a \tag{4.16}$$

where η_a is an input-vector of dimension δ_m with generalized velocities. Now the posture kinematic model is almost known. It is however desired that the posture kinematic model is a linear system with respect to the inputs. The steering angles are also an input, so the system is not a linear system with respect to the inputs, because of the possible nonlinearities in β in $\Sigma(\beta)$. For this reason the extra differential equation $\dot{\beta} = \zeta$ that defines the movement of the steering angles is added. So the *posture kinematic model* is:

$$\begin{pmatrix} \dot{\xi} \\ \dot{\beta} \end{pmatrix} = \begin{pmatrix} R^T(\theta)\Sigma(\beta) & 0 \\ 0 & I \end{pmatrix} \begin{pmatrix} \eta_a \\ \zeta \end{pmatrix} \tag{4.17}$$

The following step is to find the configuration kinematic model, which is the posture kinematic model expanded with the description of the wheel rotation variables. The description is determined using (4.6) and (4.15).

$$\dot{\varphi} = -J_2^{-1}J_1R(\theta)\dot{\xi} = -J_2^{-1}J_1\Sigma(\beta)\eta_a \tag{4.18}$$

The *configuration kinematic model* is:

$$\dot{q} = \begin{pmatrix} \dot{\xi} \\ \dot{\beta} \\ \dot{\varphi} \end{pmatrix} = \begin{pmatrix} R^T(\theta)\Sigma(\beta) & 0 \\ 0 & I \\ -J_2^{-1}J_1\Sigma(\beta) & 0 \end{pmatrix} \begin{pmatrix} \eta_a \\ \zeta \end{pmatrix} = S(q)\eta \tag{4.19}$$

where q are the configuration coordinates and η is the total generalized velocities input of dimension $\delta_m + \delta_s$.
Looking at (4.10) and (4.19) the conclusion is that

$$A^T(q)S(q) = 0 \tag{4.20}$$

if $\eta \neq 0$. The statement $A^T(q)S(q) = 0$ is important for the theory on wheeled mobile robots as will be explained later on.

A WMR with fixed wheels and/or conventional steering wheels is equipped with motors that can orient and rotate the wheels, so in total there are two "types" of torques; steering torques (τ_s) and driving torques (τ_d).
The coupling between all configuration coordinates, generalized velocities and torques of the motors is made in the configuration dynamic model. An extra dynamic equation that links the torque inputs to the movement of the configuration coordinates is needed. This extra dynamic equation is the differential equation describing a mechanical system, which has the following standard form:

$$M(q)\ddot{q} = C(q,\dot{q}) + F + B(q)\tau \tag{4.21}$$

where $C(q,\dot{q})$ is the matrix constructed by coriolis, centrifugal, gravity and resistant torques, $M(q)$ is the inertia matrix, τ is the vector of input torques, $B(q)$ is a matrix that relates the input torques to the generalized coordinates and F is the total generalized force vector.
The force F in this case consists of constraint forces, which are the forces that ensure that the constraints are satisfied. The power for these forces is equal to zero for any motion satisfying the constraints [4], so:

$$A^T(q)\dot{q} = 0 \;\rightarrow\; F^T\dot{q} = 0 \tag{4.22}$$

This implies that a m-vector (A is a (nxm) matrix) exists, called the 'Lagrange multipliers vector' λ so

$$F = A(q)\lambda \tag{4.23}$$

The system is now completely described by the configuration kinematic model ($\dot{q} = S(q)\eta$) and the differential equation. Because of (4.20) it is possible to eliminate the Lagrange forces in the differential equation by left-multiplying the equation with $S^T(q)$:

$$S^T(q)M(q)\ddot{q} = S^T(q)\{C(q,\dot{q}) + B(q)\tau\} \tag{4.24}$$

Using the configuration kinematic model and the derivative of the configuration kinematic model, which is $\ddot{q} = \dot{S}(q)\eta + S(q)\dot{\eta}$, the *configuration dynamic model* can be written as:

$$\begin{pmatrix} \dot{q} \\ \dot{\eta} \end{pmatrix} = \begin{pmatrix} S(q)\eta \\ \{S^TM(q)S(q)\}^{-1}S^T(q)\{-M(q)\dot{S}(q,\dot{q})\eta + C(q,\dot{q}) + B(q)\tau\} \end{pmatrix} \tag{4.25}$$

where q are the configuration variables and η is the total generalized velocities vector. A complete model, describing the relation between the configuration variables and the real inputs (the torques of the steering and driving motors), is available now.

The configuration dynamic model is feedback equivalent (by a static state feedback) to the following system:

$$\begin{aligned} \dot{q} &= S(q)\eta \\ \dot{\eta} &= \nu \end{aligned} \tag{4.26}$$

with

$$\tau = \{S^T(q)B(q)\}^+\{S^T(q)\{M(q)S(q)\nu + M(q)\dot{S}(q,\dot{q})\eta - C(q,\dot{q})\}\} \quad (4.27)$$

where the superscript + stands for the pseudo inverse and ν is an arbitrary (reference) input. The pseudo inverse of $S^T(q)B(q)$ is calculated instead of the "normal" inverse, because $S^T(q)B(q)$ can be a non-square matrix. This is for example the case if the WMR is "overactuated". An example of this is a bicycle with two conventional steering wheels, both having a steering and driving motor. Effectively only one driving motor is needed to move the WMR, because the mobility of the WMR is one. The matrix $S^T(q)B(q)$ will be non-square if two driving motors are attached to the bicycle. Using the pseudo-inverse, the total driving force will be distributed between the two driving motors.

The feedback equivalent model of the configuration dynamic model (4.26) can be rewritten by choosing only the posture coordinates ($q_1 = [\xi, \beta]$, dimension $3 + \delta_s$). This model is then called the *posture dynamic model.*

$$\begin{aligned} \dot{q_1} &= S_1(q)\eta \\ \dot{\eta} &= \nu \end{aligned} \quad (4.28)$$

where $S_1(q_1)$ is the sub-matrix of $S(q)$ that is related to the q_1 variables.

4.1.2 Controller development for a wheeled mobile robot

The main goal of the controller is to let the center of the WMR track a certain reference trajectory ($[x_{ref},\ y_{ref},\ \theta_{ref}]$). Also, it is desired that the reference steering angles β_{ref} are tracked if they are given. It is investigated if a nonlinear control method that output linearizes the (sub)system can be used. The advantage of this is that the normal linear control techniques can be used for the linearized system.
All type of WMR's discussed in this report are not full state linearizable by a smooth static time-invariant state feedback. The largest (sub)system of the posture dynamic model linearizable by a smooth static state feedback is of dimension $2(\delta_m+\delta_s)$. The nonlinear subsystem that remains next to the linear subsystem is of dimension $3 - \delta_m$. A feedback controller will be developed for the linearized (sub)system [4], [8].

This first step in the procedure to derive a output linearized system is to select $(\delta_m + \delta_s)$ linearizing output functions $z_1(q_1)$.

$$z_1 = h(x, y, \theta, \beta) = h(q_1) \quad (4.29)$$

Next, this function is differentiated with respect to time:

$$z_2 = \dot{z}_1 = \frac{\partial h}{\partial q_1}\dot{q}_1 = \frac{\partial h}{\partial q_1}S_1(q_1)\eta = H(q_1)\eta \quad (4.30)$$

where $H(q_1)$ is a $(\delta_m+\delta_s)$x$(\delta_m+\delta_s)$ matrix. This function is again differentiated with respect to time:

$$\dot{z}_2 = \ddot{z}_1 = H(q_1)\dot{\eta} + \dot{H}\eta = H(q_1)\nu + b(q_1, \eta) \quad (4.31)$$

where ν is defined according to (4.26).
Summarizing, the following change of coordinates is used:

$$\begin{aligned} z_1 &= h(q_1) \\ z_2 &= H(q_1)\eta \\ z_3 &= k(q_1) \end{aligned} \tag{4.32}$$

where $k(q_1)$ is defined so that the mapping

$$q_1 = \begin{pmatrix} x \\ y \\ \theta \\ \beta \end{pmatrix} \rightarrow \begin{pmatrix} h(q_1) \\ k(q_1) \end{pmatrix} = \begin{pmatrix} z_1 \\ z_3 \end{pmatrix} \tag{4.33}$$

is a diffeomorphism on R^{δ_s+3} ($\delta_s + 3 = dimension(q_1)$), which means that the map between both the coordinate systems is differentiable and has a differentiable inverse [9]. Finally $\dot{z}_3$ can be defined:

$$\dot{z}_3 = \frac{\partial k}{\partial q_1}\dot{q}_1 = \frac{\partial k}{\partial q_1}S_1(q_1)\eta = \frac{\partial k}{\partial q_1}S_1(q_1)H(q_1)^{-1}z_2 = Q(q_1)z_2 \tag{4.34}$$

The inverse of the matrix $H(q_1)$ influences the nonlinear subsystem of dimension $3 - \delta_m$ as can be concluded from (4.34). Therefore, the output coordinates (z_1) have to be chosen so that the inverse of $H(q_1)$ always exists, or that the singularity is never reached in the working range of the WMR.
All the variables from the model (4.38) are defined, so the last step is to define ν so that a linear system, $\dot{z_2} = w$, remains.

$$\nu = H(q_1)^{-1}(w - b(q_1, \eta)) \tag{4.35}$$

where w is the new input. The goal of the whole procedure is to track the coordinates $[\xi_{ref}, \beta_{ref}]$. It is not possible to track these variables directly because the dimension of $[\xi_{ref}, \beta_{ref}]$ is larger than the dimension of z_1. Therefore, the reference variables have to be rewritten in a reference variable z_{1ref} using (4.29). A solution for the input w, which ensures that the error in z_1 and z_2 exponentially converge to zero, is:

$$w = \ddot{z}_{1ref} - K_{pT}(z_1 - z_{1ref}) - K_{vT}(\dot{z}_1 - \dot{z}_{1ref}) \tag{4.36}$$

where K_{pT} and K_{vT} are two positive definite matrices. The total torque input is a combination of (4.36) and (4.27).

$$\tau = \{S^T(q)B(q)\}^+\{S^T(q)\{M(q)S(q)H^{-1}(w - b(q_1, \eta)) + M(q)\dot{S}(q, \dot{q})\eta - C(q, \dot{q})\}\} \tag{4.37}$$

The end result of the procedure is the following system:

$$\begin{aligned} \dot{z_1} &= z_2 \\ \dot{z_2} &= b + H(z)\nu = w \\ \dot{z_3} &= Q(q_1)z_2 \end{aligned} \tag{4.38}$$

A schematic overview of the system is plotted in figure 4.4.

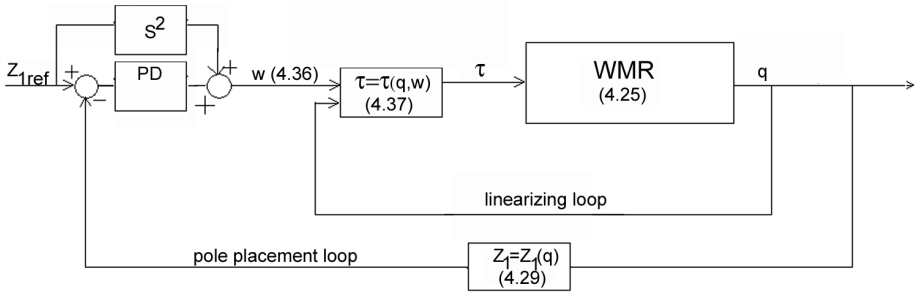

Figure 4.4: Schematic overview

4.2 Case study - one degree of freedom example - part 1

In this paragraph, a simple example of a car that is capable of driving in one direction (forwards-backwards) will be studied to clarify the procedure. The model and the controller for a front wheel driven 1DOF car without tyre slip will be developed using the theory on wheeled mobile robots.

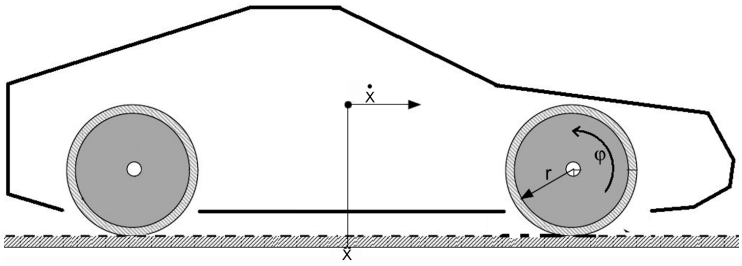

Figure 4.5: Car with front-wheel drive

The 1DOF-Car is a car that can accelerate and brake along a straight line (figure 4.5). The two configuration variables (n=2) are the position x and the rotation of the wheel φ. The local and global coordinates are equal, so the $R(\theta)$ matrix is 1.

Wheeled mobile robot theory - 1DOF model

The configuration coordinates q are:

$$q = \begin{pmatrix} x \\ \varphi \end{pmatrix} \tag{4.39}$$

The car is a 1DOF car, so only one constraint (m=1), which is the roll constraint, consists. Using (4.4), this constraint is:

$$\dot{x} + \dot{\varphi} r = 0 \tag{4.40}$$

which is in the standard form $A^T\dot{q} = 0$:

$$\begin{pmatrix} 1 & r \end{pmatrix} \begin{pmatrix} \dot{x} \\ \dot{\varphi} \end{pmatrix} = 0 \tag{4.41}$$

The procedure to determine S for the 1DOF car is a bit different from the method for a normal 3DOF WMR. Therefore, a trivial procedure instead of the formal procedure will be used to determine the S of the 1DOF car.
It is known that $A^T S = 0$ [5] and it is clear that the mobility of the 1DOF car is one, because the only movement possible is in the x-direction. The result is that a possible solution for S is:

$$S = \begin{pmatrix} 1 \\ -\frac{1}{r} \end{pmatrix} \tag{4.42}$$

So the *configuration kinematic model* is:

$$\dot{q} = S\eta = \begin{pmatrix} 1 \\ -\frac{1}{r} \end{pmatrix} \eta \tag{4.43}$$

which is a model that looks pretty straightforward. The first line describes that the forward velocity $\dot{x}$ is equal to the velocity input η. The second line describes that the rotation velocity of the wheel is equal to the negative velocity input divided by the radius. So the rotation velocity of the wheel is also equal to the negative forward velocity $\dot{x}$ divided by the radius, which is exactly the roll constraint from which the model is derived (4.40).
The desired model is the configuration dynamic model. An extra dynamic equation (4.21) has to be introduced to get from the configuration kinematic model to the configuration dynamic model. It is assumed that the car has no external disturbances, such as rolling friction and air resistance. A driving motor is attached to the front wheel. This motor accelerates the wheel in negative φ direction if the torque is positive. The total generalized force vector consists of constraint forces (4.23).
The extra equation can now be defined as:

$$\begin{gathered} M\ddot{q} = F + C + B\tau = \\ \begin{pmatrix} m & o \\ o & I_\varphi \end{pmatrix} \begin{pmatrix} \ddot{x} \\ \ddot{\varphi} \end{pmatrix} = \begin{pmatrix} 1 \\ r \end{pmatrix} \lambda + \begin{pmatrix} 0 \\ 0 \end{pmatrix} + \begin{pmatrix} 0 \\ -1 \end{pmatrix} \tau \end{gathered} \tag{4.44}$$

where m is the mass of the car, λ is the "Lagrange multiplier" and I_φ is the rotation inertia of the wheel. The conclusion is that the Lagrange multiplier is equal to the force in x-direction F_x.
The matrices that are needed to introduce the configuration dynamic model (4.25) are M, $\dot{S}$, C and B. S is a time-independent vector here, so $\dot{S} = 0$. Hence, the resulting *configuration dynamic model* is:

$$\begin{aligned} \dot{q} &= \begin{pmatrix} 1 \\ \frac{1}{-r} \end{pmatrix} \eta \\ \dot{\eta} &= \frac{r}{mr^2 + I_\varphi} \tau \end{aligned} \tag{4.45}$$

In this case, the posture is equal to the position of the center of the car (x), so the feedback equivalent of the *posture dynamic model* is:

$$\begin{aligned} \dot{q}_1 &= \eta \\ \dot{\eta} &= \nu \end{aligned} \tag{4.46}$$

where the used torque input is:

$$\tau = (m + \frac{I_\varphi}{r^2})\nu r \tag{4.47}$$

1DOF car controller

For this case it is easy to develop a controller, but the formal approach of section 4.1.2 will be followed to explain the procedure. It is desired that the center of the car follows a specified reference trajectory (x_{ref}), so the output function z_1 is equal to x. The variable z_2 is equal to $\dot{x}$, which is equal to η, so H is 1 for this 1DOF system. The variable $\dot{z_2}$ is equal to $\dot{\eta}$, so $b = 0$. The variable z_3 is equal to 0, because z_1 is equal to the full posture.
Therefore, the total linearized system, using that

$$\nu = H^{-1}(w - b) = w \tag{4.48}$$

is:

$$\begin{aligned} \dot{z_1} &= z_2 \\ \dot{z_2} &= w \end{aligned} \tag{4.49}$$

So the torque input of the system is:

$$\tau = (m + \frac{I_\varphi}{r^2})wr \tag{4.50}$$

where w is chosen as:

$$w = \ddot{z}_{1ref} - K_p(z_1 - z_{1ref}) - K_v(\dot{z}_1 - \dot{z}_{1ref}) \tag{4.51}$$

where K_p and K_v are two gains. The variable z_{1ref} is equal to x_{ref}, because z_1 is x. If the system is ideal system, $w = \ddot{z}_{1ref}$ is enough to assure a perfect tracking if no starting errors are present. However, in reality there can be disturbances, starting errors or parameter uncertainties. Therefore, a PD feedback loop is added to the input w.

4.3 Wheeled mobile robot extended with tyre slip

The main difference between wheeled mobile robots with and without tyre slip are the generalized forces, which are no longer constraint forces, but real contact forces. The constraints are violated because of the tyre slip. This is the reason why a reformulation of the theory on wheeled mobile robot that is described is needed.

4.3.1 Model extended with tyre slip

An ideal wheeled mobile robot has no tyre slip, but reality is different (see appendix B), because a real tyre can only deliver forces if there is a certain amount of slip. The velocity constraints are violated as a result of the slip,

so $A^T(q)\dot{q} \neq 0$. The slip results in interaction forces, which have a dissipative nature [4]. The assumption is made that the power of interaction forces (W) is a negative definite function of the generalized slip velocities [4]. A negative definite function has the standard form of $x^T U x \leq 0$. The generalized slip velocities here are $A^T(q)\dot{q}$. This results in the following equation for the power of interaction forces:

$$W = -\frac{1}{\varepsilon}[\dot{q}^T A(q)]K(q,\dot{q})[A^T(q)\dot{q}] \leq 0 \tag{4.52}$$

where ε is a small normalization parameter ($\varepsilon \geq 0$) and $K(q,\dot{q})$ is a positive definite m x m matrix to ensure that (4.52) is a negative definite function. $K(q,\dot{q})$ is for instance constructed by tyre parameters, such as cornering stiffness.
Power can be described as a force multiplied by a velocity, so it is possible to write (4.52) as:

$$W = \dot{q}^T F \; so \; F = -\frac{1}{\varepsilon}A(q)K(q,\dot{q})A^T(q)\dot{q} \tag{4.53}$$

where F is the generalized force.
The following procedure is set-up to determine the unknown matrix K. A normal tyre can generate forces in both the lateral and longitudinal direction of the tyre (see appendix B). Both effects are decoupled in the linear approximation, so the forces for every tyre i of the WMR can be expressed as [4]:

$$\begin{pmatrix} F_{lat\ i} \\ F_{long\ i} \end{pmatrix} = \frac{1}{V_i}\begin{pmatrix} D & 0 \\ 0 & G \end{pmatrix}\begin{pmatrix} V_{lat\ i} \\ V_{long\ i} - r\dot{\varphi}_i \end{pmatrix} \tag{4.54}$$

where V_i is the *absolute* velocity of the center of the tyre, $V_{lat\ i}$ and $V_{long\ i}$ are the velocities in respectively lateral and longitudinal direction of the tyre. $D = \frac{D_0}{\varepsilon}$ is the cornering stiffness and $G = \frac{G_0}{\varepsilon}$ is the slip stiffness.
The lateral velocity ($V_{lat\ i}$) of the tyre is zero if the slip constraint is not violated ("ideal" case). The expression $V_{long\ i} - r\dot{\varphi}_i$ is zero if the roll constraint is not violated. However, in the current situation the constraints have to be violated to develop a tyre force. Both the lateral and longitudinal velocity can be expressed as a combination of the generalized slip velocities.

$$\begin{pmatrix} V_{lat\ i} \\ V_{long\ i} - r\dot{\varphi}_i \end{pmatrix} = L_i(q)A^T(q)\dot{q} \tag{4.55}$$

where $L_i(q)$ is a matrix that transforms the slip velocities to the longitudinal and the lateral velocity components.
The generalized force is also a combination of the longitudinal and lateral force of the tyre. The lateral force is pointed in the direction of the lateral slip and the longitudinal force is pointed in the direction of the longitudinal slip. It is now possible to define the generalized force, using the same principle as in (4.55).

$$F_i = -A(q)L_i^T(q)\begin{pmatrix} F_{lat\ i} \\ F_{long\ i} \end{pmatrix} \tag{4.56}$$

If (4.54), (4.55) and (4.56) are combined, the generalized force can be expressed as:

$$F_i = -\frac{1}{\varepsilon}A(q)L_i^T(q)\frac{1}{V_i}\begin{pmatrix} D_0 & 0 \\ 0 & G_0 \end{pmatrix}L_i(q)A^T(q)\dot{q} \tag{4.57}$$

Using (4.53), the expression for K_i is.

$$K_i = L_i^T(q)\frac{1}{V_i}\begin{pmatrix} D_0 & 0 \\ 0 & G_0 \end{pmatrix} L_i(q) \tag{4.58}$$

The total generalized force (4.53) is the summation of all the generalized forces of the tyres (4.57). The only difference between the forces (F_i) of each tyre is the K_i matrix, so the only difference between the total and the separate generalized forces is the K matrix. Therefore, K is the summation of the K_i's of all the tyres.

Considering the above, the configuration kinematic model expression (4.19) is not valid anymore, because the constraints, on which the model is based, are violated. Instead, a possible expression for the configuration coordinate velocity vector is:

$$\dot{q} = S(q)\eta + A(q)\varepsilon\mu \tag{4.59}$$

where μ is an m-vector describing the importance of the violation of the constraints, because if (4.59) is pre-multiplied by $A^T(q)$ and if (4.20) is used,(4.59) becomes:

$$A^T(q)\dot{q} = A^T(q)A(q)\varepsilon\mu \tag{4.60}$$

Equation (4.20) can still be used, because the matrices A and S are not changed. Equation (4.59) is equal to a standard no-slip WMR system if ε is zero, which is expected, because the slip is zero if ε is zero.
Using (4.60) and (4.53), the total generalized force can be written as:

$$F = -A(q)K(q,\dot{q})A^T(q)A(q)\mu \tag{4.61}$$

All dynamic models describing a mechanical model, so also the dynamical model for a wheeled mobile robot can be written in a standard form (4.21). The generalized force vector F is no longer equal to $F = A(q)\lambda$, but is equal to (4.61). Furthermore the rest of the matrices are equal to the matrices of the wheeled mobile robot without tyre slip.
The vectors $\dot{q}$ and $\ddot{q}$ in (4.21) can be replaced by (4.59) and the time derivative of (4.59) respectively.

$$\begin{aligned} &M(q)(S(q)\dot{\eta} + \dot{S}(q)\eta + A(q)\varepsilon\dot{\mu} + \dot{A}(q)\varepsilon\mu) = \\ &C(q, S(q)\eta + A(q)\varepsilon\mu) - A(q)K(q, S(q)\eta + A(q)\varepsilon\mu)A^T(q)A(q)\mu + B(q)\tau \end{aligned} \tag{4.62}$$

If the above system is pre-multiplied by the matrix $[S(q)A(q)]^T$, the following equation is obtained:

$$\begin{aligned} J(q)\begin{pmatrix} \dot{\eta} \\ \varepsilon\dot{\mu} \end{pmatrix} = \begin{pmatrix} S^T(q) \\ A^T(q) \end{pmatrix}[C(q, S\eta + A\varepsilon\mu) + B(q)\tau - M(q)(\dot{S}\eta + \dot{A}\varepsilon\mu)] + \\ \begin{pmatrix} 0 \\ -A^T(q)A(q)K(q, S(q)\eta + A(q)\varepsilon\mu)A^T(q)A(q)\mu \end{pmatrix} \end{aligned} \tag{4.63}$$

where $J = \begin{pmatrix} S^T(q)M(q)S(q) & S^T(q)M(q)A(q) \\ A^T(q)M(q)S(q) & A^T(q)M(q)A(q) \end{pmatrix}$

Using (4.59) and (4.63), front multiplied by J^{-1}, the resulting system can be written in the so called singular perturbation form, which is:

$$\begin{aligned} \dot{q} &= S(q)\eta + A(q)\varepsilon\mu \\ \dot{\eta} &= f_o(q,\eta) + \varepsilon f_1(q,\eta,\mu) + \varepsilon^2 f_2(q,\eta,\mu) + B_1(q)\tau - R_{12}A^T AKA^T A\mu \\ \varepsilon\dot{\mu} &= g_o(q,\eta) + \varepsilon g_1(q,\eta,\mu) + \varepsilon^2 g_2(q,\eta,\mu) + B_2(q)\tau - R_{22}A^T AKA^T A\mu \end{aligned} \tag{4.64}$$

If these equations are compared to the equations for a wheeled mobile robot without tyre slip (4.25), the conclusion is that a third equation is added to the system. This is an equation describing the dynamics of the variable μ, which is the so called fast variable. Notice that μ is a fast variable because ε is a small variable. The variables μ and $\dot{\mu}$ are multiplied by ε or K ($K = K(\varepsilon, ..)$, using that $G_0 = \varepsilon G$ and $D_0 = \varepsilon D$) in all the three equations, so the variable can change fast in time without having a lot of influence on the other so called slow variables of the system.

4.3.2 Controller with tyre slip compensation

The slow manifold approach [5] is used for the development of the controller. The idea behind the approach is to define an invariant and attractive "slow manifold" on which the system is output linearizable. This assures that the results are comparable with the results of the controller without tyre slip compensation.
The first step is to transform the model in singular perturbation form to the slow manifold. A continuous feedback law is introduced: $\tau_\varepsilon(q(t), \eta(t), t)$. If $\varepsilon = 0$, then

$$\mu = H_0(q, \eta, \tau_\varepsilon) \tag{4.65}$$

is the unique solution of:

$$0 = g_o(q,\eta) + B_2(q)\tau_\varepsilon - R_{22}A^T AKA^T A\mu \tag{4.66}$$

which is the last equation of (4.64) for $\varepsilon = 0$. Solution (4.65) is a so called "integral manifold" for system (4.64) with $\varepsilon = 0$. A manifold can be described as a kind of space that locally looks like an "ordinary" Euclidean/Cartesian space, which is often denoted as $\mathbb{R}^n$. A simple example is a sphere, which in total is not a plane, but small patches of the sphere are "homeomorph" to patches of the Euclidean plane.
Equation (4.65) is called an integral manifold of system (4.64) with $\varepsilon = 0$, because a trajectory that starts in the manifold will remain in the manifold for all future time. Consequently the motion on the manifold is described by:

$$\begin{aligned} \dot{q} &= S(q)\eta \\ \dot{\eta} &= f_o(q,\eta) + B_1(q)\tau_\varepsilon - R_{12}A^T AKA^T AH_o \end{aligned} \tag{4.67}$$

Start intermezzo

It is important to give a short introduction of Tikhonov's theorem [5] first. A system in singular perturbation form has the following standard form:

$$\begin{aligned} \dot{x} &= f(t, x, z, \varepsilon) \\ \varepsilon \dot{z} &= g(t, x, z, \varepsilon) \end{aligned} \tag{4.68}$$

where the first equation describes the slow dynamics and the second equation describes the fast dynamics. The main idea is to approximate x using the solution of the reduced problem, which is:

$$\dot{\bar{x}} = f(t, \bar{x}, h(t, \bar{x}), 0) \quad \bar{x}(0) = x_0 \tag{4.69}$$

where $\bar{z} = h(t, \bar{x})$ is the solution of $0 = g(t, x, z, 0)$. For small values of ε it can be expected that $\bar{x}$ is a good approximation of x. However it cannot be expected directly that $\bar{z}$ is a good approximation of z. The difference between z and $\bar{z}$ is expressed as: $\hat{z} = z - \bar{z}$. Now Tikhonov introduces the following so called "boundary system" for a fixed (t_0, x_0).

$$\frac{d\hat{z}}{d\tau} = g(t_0, x_0, \hat{z} + h(t_0, x_0), 0), \quad \hat{z}(0) = z_0 - h(0, x_0) \quad \tau = t/\varepsilon \tag{4.70}$$

The boundary layer describes the fast dynamics, disregarding variation in the slow variables (t, x), since of $\tau = t/\varepsilon$. Tikhonov's theorem uses that $\hat{z} = 0$ is an exponentially stable equilibrium of the boundary layer problem. This condition implies that $lim_{\tau \to +\infty} \hat{z}(\tau) = 0$. If this is used,

$$\begin{aligned} x(t, \varepsilon) &= \bar{x}(t) + O(\varepsilon) \\ z(t, \varepsilon) &= h(t, \bar{x}(t)) + \hat{z}(\tau) + O(\varepsilon) \end{aligned} \tag{4.71}$$

where $O(\varepsilon)$ stands for the order of ε, i.e. when $\varepsilon \to 0$ then $O(\varepsilon) \to 0$.

End intermezzo

The following step is to use Tikhonov's theorem for (4.64). If $\varepsilon > 0$ and the same feedback control law is used for the complete system instead of the reduced system, then using Tikhonov's theorem it is possible to conclude that trajectories of (4.64) starting in an $O(\varepsilon)$ neighborhood of (4.65) will remain in an $O(\varepsilon)$ neighborhood of (4.65) [5]. This means that the total error at the end will be bounded and quite small if ε is small.

It also follows that for any control law $\tau_\varepsilon(t) = \tau_\varepsilon(q, \eta, t)$, $\varepsilon_1 > 0$ exists and a function $H_\varepsilon(q, \eta, \tau_\varepsilon)$, that defines a slow manifold ($\mu = H_\varepsilon(q, \eta, \tau_\varepsilon)$), for all $\varepsilon \in [0, \varepsilon_1]$ exists [5].
The dynamics on this manifold are described by:

$$\begin{aligned} \dot{q} &= S(q)\eta + A(q)\varepsilon H_\varepsilon \\ \dot{\eta} &= f_o(q, \eta) + \varepsilon f_1(q, \eta, H_\varepsilon) + \varepsilon^2 f_2(q, \eta, H_\varepsilon) + B_1(q)\tau_\varepsilon - R_{12}A^T AKA^T AH_\varepsilon \end{aligned} \tag{4.72}$$

The dynamics are only depending on the slow variables q, η and t. This is the reason why the integral manifold $\mu = H_\varepsilon(q, \eta, \tau_\varepsilon)$ is called a slow manifold for (4.64).

The slow manifold is, independently of the choice of the feedback control law (τ_ε), attractive for sufficiently small values of ε, provided that η remains bounded [5]. So if the system is not to far from the ideal case (the constraints are satisfied) and if the start is not to far from the slow manifold, the system will converge:

$$\lim_{t\to\infty}(\mu - H_\varepsilon) = 0 \tag{4.73}$$

The main goal of the controller for the wheeled mobile robot with tyre slip is to let the center of the WMR track a certain reference trajectory ([x_{ref}, y_{ref}, θ_{ref}]). It is also desired that the reference steering angles β_{ref} are tracked if they are given. The goal is to first output linearize the system on the corresponding slow manifold using the right output coordinates. A feedback controller will consequently be developed for this linearized system [5].
All type of WMR's discussed in this report are not full state output linearizable on the corresponding slow manifold. The largest (sub)system of the posture dynamic model output linearizable is of dimension $2(\delta_m+\delta_s)$. The nonlinear subsystem that remains next to the linear subsystem is of dimension $3-\delta_m$. The following ($\delta_m+\delta_s$) output functions (z_1) can be defined.

$$z_1 = h(x, y, \theta, \beta) = h(q_1) \tag{4.74}$$

The first derivative of this function is equal to:

$$z_2 = \dot{z}_1 = S_s\eta + A_s\varepsilon\mu \tag{4.75}$$

where S_s and A_s are determined in the similar way as H (4.30). The nonlinear subsystem z_3 is defined in the similar way as for the wheeled mobile robot without tyre slip ($z_3 = k(q_1)$). The desired linear subsystem and the nonlinear subsystem on the manifold are (see also (4.38)).

$$\begin{aligned}\dot{z_1} &= z_2\\ \dot{z_2} &= \dot{S}_s\eta + \dot{A}_s\varepsilon H_\varepsilon + S_s\dot{\eta} + A_s\varepsilon\dot{H}_\varepsilon = w\\ \dot{z_3} &= Q_1 z_2 + Q_2\end{aligned} \tag{4.76}$$

where $\dot{z}_3$ is:

$$\begin{aligned}\dot{z}_3 = \tfrac{\partial k}{\partial q_1}\dot{q}_1 = \tfrac{\partial k}{\partial q_1}(S_1\eta + A_1\varepsilon H_\varepsilon) =\\ \tfrac{\partial k}{\partial q_1}(S_1(S_s^{-1}z_2 - S_s^{-1}A_s\varepsilon H_\varepsilon) + A_1\varepsilon H_\varepsilon)\end{aligned} \tag{4.77}$$

where S_1 and A_1 are sub-matrices of S and A, so that ($q_1 = S_1\eta + A_1\varepsilon H_\varepsilon$) and Q_1 and Q_2 are

$$Q_1 = [\frac{\partial k}{\partial q_1}S_1]S_s^{-1} \tag{4.78}$$

$$Q_2 = \frac{\partial k}{\partial q_1}(-S_1(S_s^{-1}A_s\varepsilon H_\varepsilon) + A_1\varepsilon H_\varepsilon) \tag{4.79}$$

where Q_1 is equal to Q from the wheeled mobile robot without tyre slip. Q_2 is determined by the variable $\varepsilon H_\varepsilon$, so Q_2 is zero if ε is zero, so the variable $\dot{z}_3$ will convert to the variable $\dot{z}_3$ for the wheeled mobile robot without slip if ε is zero. Q_2 will also be zero if H_ε is zero, which is the case when the tyre has no absolute velocity. The new input w, similar to (4.36), is:

$$w = \ddot{z}_{1ref} - K_{pT}(z_1 - z_{1ref}) - K_{vT}(S_s(q)\eta + A_s(q)\varepsilon H_\varepsilon - \dot{z}_{1ref}) \tag{4.80}$$

where K_{pT} and K_{vT} are two positive definite matrices and $S_s(q)\eta + A_s(q)\varepsilon H_\varepsilon$ is equal to $\dot{z}_1$ on the slow manifold. The reference z_{1ref} is determined by rewriting the reference posture variables using the output linearizing coordinate(s) z_1.
In the slow manifold approach, it is determined that a τ_ε and a H_ε exist, but they are still unknown. To construct these variables a Taylor series expansion is made:

$$\begin{aligned} \tau_\varepsilon &= \tau_0 + \varepsilon\tau_1 + \varepsilon^2\tau_2 + ... \\ H_\varepsilon &= H_0 + \varepsilon H_1 + \varepsilon^2 H_2 + ... \end{aligned} \tag{4.81}$$

where

$$\begin{aligned} \tau_u &= \tfrac{1}{u!}\left(\tfrac{\partial \tau_\varepsilon}{\partial \varepsilon^u}\right)_{\varepsilon=0} \\ H_u &= \tfrac{1}{u!}\left(\tfrac{\partial H_\varepsilon}{\partial \varepsilon^u}\right)_{\varepsilon=0} \end{aligned} \tag{4.82}$$

These expressions of τ_ε and H_ε can be inserted into the linearization condition, which is the second equation of (4.76), and in the manifold condition, which is the third equation of (4.64).

$$\begin{aligned} &\dot{z}_2 = \ddot{z}_1 = \dot{S}_s(q,\eta,H_\varepsilon)\eta + \dot{A}_s(q,\eta,H_\varepsilon)\varepsilon\mu + S_s(q)\dot{\eta} + A_s(q)\varepsilon\dot{H}_\varepsilon = w \\ &\varepsilon\dot{H}_\varepsilon = g_o(q,\eta) + \varepsilon g_1(q,\eta,H_\varepsilon) + \varepsilon^2 g_2(q,\eta,H_\varepsilon) + B_2(q)\tau_\varepsilon - R_{22}A^T AKA^T AH_\varepsilon \end{aligned} \tag{4.83}$$

As a result of this for each power ε^u of ε there is a system of two equations linearly depending on τ_u and H_u, which can now be obtained solving the equations (4.83).

- *Determine H_0 and τ_0*
  To determine H_0 and τ_0, ε in (4.83) has to be set to zero. This results in the following two equations:

  $$\begin{aligned} &\dot{S}_s(q,\eta)\eta + S_s(q)f_o(q,\eta) + S_s(q)B_1(q)\tau_0 - S_s(q)R_{12}A^T AKA^T AH_0 = \\ &\ddot{y}_r - K_{pT}(y_1 - y_r) - K_{vT}(S_s(q)\eta - \dot{y}_r) \\ &0 = g_o(q,\eta) + B_2(q)\tau_0 - R_{22}A^T AKA^T AH_0 \end{aligned} \tag{4.84}$$

  These are two algebraic equations with two unknowns, so it should be possible to determine them. However, problems can arise if a combination of matrices is singular, e.g. to determine τ_0 the inverse of S_sB_1 is needed.

- *Determine H_u and τ_u ($u \geq 1$)*
  To determine H_u and τ_u first the equations (4.83) have to be differentiated with respect to ε^u. After this ε has to be set to zero and the total has to be divided by $u!$. This results in the following two equations:

  $$\begin{aligned} &\dot{S}_s(q,\eta,H_{u-1})\eta + \dot{A}_s(q,\eta,H_{u-1})H_{u-1} + S_s(q)f_u(q,\eta,H_{u-1}) + \\ &S_s(q)B_1(q)\tau_u - S_s(q)R_{12}A^T AKA^T AH_u + A_s(q)\dot{H}_{u-1} = -K_{vT}A_s(q)H_{u-1} \\ &\dot{H}_{u-1} = g_u(q,\eta,H_{u-1}) + B_2(q)\tau_u - R_{22}A^T AKA^T AH_u \end{aligned} \tag{4.85}$$

  These are two equations with two unknowns if $\dot{H}_{u-1}$ is known. This is true if it is stated that $\dot{H}_{u-1}$ is the time derivative of the known variable H_{u-1}. Again problems can arise with a combination of matrices that is singular.

4.4 Case study - one degree of freedom example - part 2

In this paragraph, the model and the controller for the 1DOF car (figure 4.5) with tyre slip will de derived. The procedure up to the equation for the configuration kinematic model (4.43) is the same. From there on this method follows the general procedure for a WRM with tyre slip.

WMR model extended with tyre slip - 1DOF

The configuration kinematic model is known, so the first step is to introduce an extra differential equation, which is equal to (4.44). The only difference is the general force F, which is no longer equal to $A\lambda$, but is determined by the contact forces.

$$\begin{pmatrix} m & o \\ o & I_\varphi \end{pmatrix} \begin{pmatrix} \ddot{x} \\ \ddot{\varphi} \end{pmatrix} = F + \begin{pmatrix} 0 \\ -1 \end{pmatrix} \tau \tag{4.86}$$

where m is the mass of the car and I_φ is the rotation inertia of the wheel. The general procedure gives a formulation for the contact forces, which is $F = -AKA^T A\mu$. The model for a WMR with tyre slip can be written in the standard form described by (4.64). To be able to write the model in this form a few steps have to be taken. Given that the longitudinal tyre force is

$$F_{long} = \frac{G_0}{\varepsilon} \frac{V_{long} - r\dot{\varphi}}{V} \tag{4.87}$$

and using (4.55), the conclusion is that $L = -1$. Using this and (4.58), it is possible to define K for the 1DOF example:

$$K = \frac{G_0}{V} \tag{4.88}$$

After pre-multiplying (4.86) with $\begin{pmatrix} S^T \\ A^T \end{pmatrix}$ and substituting $\ddot{q}$ by $\begin{pmatrix} S & A \end{pmatrix} \begin{pmatrix} \dot{\eta} \\ \varepsilon\dot{\mu} \end{pmatrix}$ the dynamic model reduces to:

$$\begin{pmatrix} m + \frac{I_\varphi}{r^2} & m - I_\varphi \\ m - I_\varphi & m + I_\varphi r^2 \end{pmatrix} \begin{pmatrix} \dot{\eta} \\ \varepsilon\dot{\mu} \end{pmatrix} = \begin{pmatrix} \frac{1}{r} \\ -r \end{pmatrix} \tau + \begin{pmatrix} 0 \\ \frac{-(1+r^2)^2 G_0}{V} \end{pmatrix} \mu \tag{4.89}$$

This is, rewritten in the standard form (4.64):

$$\begin{aligned} \dot{q} &= \begin{pmatrix} 1 \\ \frac{1}{-r} \end{pmatrix} \eta + \begin{pmatrix} 1 \\ r \end{pmatrix} \varepsilon\mu \\ \dot{\eta} &= \frac{r\tau}{I_\varphi(1+r^2)} - \frac{G_0(-m+I_\varphi)r^2\mu}{VI_\varphi m} \\ \varepsilon\dot{\mu} &= \frac{-r\tau}{I_\varphi(1+r^2)} - \frac{G_0(mr^2+I_\varphi)\mu}{VI_\varphi m} \end{aligned} \tag{4.90}$$

Comparing this with the configuration dynamic model of the 1DOF car without tyre slip (4.45), the conclusion is that tyre characteristics are added to the equation (G_0) and an extra dynamic equation of the fast variable μ is added.

The system itself looks strange, because of the problems with the dimensions (e.g. $m+I_\varphi$). However the idea is here to see it as a "dimensionless" system. If $\varepsilon = 0$ is implemented in (4.90) and if equation three of (4.90) is implemented in equation two of (4.90), a system equivalent to the system of the 1DOF car without tyre slip remains (4.45).

Controller with tyre slip compensation - 1DOF

The following step is to develop a controller for the system in singular perturbation form using the theory from section 4.3.2. It is desired that the center of the car follows a specified reference trajectory (x_{ref}), so the output function z_1, is equal to x. The derivative of z_1 is $\dot{z}_1 = S_s\eta + A_s\varepsilon\mu$, is

$$\dot{z}_1 = \eta + \varepsilon\mu \tag{4.91}$$

so $S_s = 1$ and $A_s = 1$ and their time derivatives are zero. The variable z_2 is equal to $\dot{z}_1$ and $z_3 = 0$, because z_1 is equal to the full posture.
The (desired) linear subsystem on the slow manifold (H_ε) is:

$$\begin{aligned} \dot{z_1} &= z_2 \\ \dot{z_2} &= \dot{S}_s\eta + \dot{A}_s\varepsilon H_\varepsilon + S_s\dot{\eta} + A_s\varepsilon\dot{H}_\varepsilon = \dot{\eta} + \varepsilon\dot{H}_\varepsilon = w \end{aligned} \tag{4.92}$$

The linearizing condition and manifold condition (4.83) are:

$$\begin{aligned} \ddot{z_1} &= \dot{\eta} + \varepsilon\dot{H}_\varepsilon = w \; so \; \tfrac{r\tau_\varepsilon}{I_\varphi(1+r^2)} - \tfrac{G_0(-m+I_\varphi)r^2H_\varepsilon}{VI_\varphi m} + \varepsilon\dot{H}_\varepsilon = w \\ \varepsilon\dot{H}_\varepsilon &= \tfrac{-r\tau_\varepsilon}{I_\varphi(1+r^2)} - \tfrac{G_0(mr^2+I_\varphi)H_\varepsilon}{VI_\varphi m} \end{aligned} \tag{4.93}$$

where $w = \ddot{z}_{1ref} - K_p(z_1 - z_{1ref}) - K_v(\eta + \varepsilon H_\varepsilon - \dot{z}_{1ref})$.
The resulting system in state-space form is:

$$\begin{aligned} \dot{z}_1 &= z_2 \\ \dot{z}_2 &= w \end{aligned} \tag{4.94}$$

Now the variables τ_ε and H_ε have to be determined. The first step is to derive τ_0 and H_0 using the procedure described in section 4.3.2. If $\varepsilon = 0$, the linearizing condition and manifold condition are:

$$\begin{aligned} \tfrac{r\tau_0}{I_\varphi(1+r^2)} - \tfrac{G_0(-m+I_\varphi)r^2H_0}{VI_\varphi m} &= w_{p1} \\ 0 = \tfrac{-r\tau_0}{I_\varphi(1+r^2)} - \tfrac{G_0(mr^2+I_\varphi)H_0}{VI_\varphi m} & \end{aligned} \tag{4.95}$$

where $w_{p1} = \ddot{z}_{1ref} - K_p(z_1 - z_{1ref}) - K_v(\eta - \dot{z}_{1ref})$. Equation (4.95) is a pair of algebraic equations that has a solution for τ_0 and H_0, which is:

$$\begin{aligned} \tau_0 &= (m + \tfrac{I_\varphi}{r^2})w_{p1}r \\ H_0 &= \tfrac{-w_{p1}Vm}{(1+r^2)G_0} \end{aligned} \tag{4.96}$$

The variable τ_0 shows already similarities with (4.50), which is obvious, because τ_0 is the part of the Taylor series expansion that remains if ε (zero slip).
The following step is to derive τ_1 and H_1. First the linearizing condition and the

manifold condition have to be differentiated with respect to ε. By implementing $\varepsilon = 0$, the two equations become:

$$\begin{array}{l} \frac{r\tau_1}{I_\varphi(1+r^2)} - \frac{G_0(-m+I_\varphi)r^2H_1}{VI_\varphi m} + \dot{H}_0 = -K_vH_0 \\ \dot{H}_0 = \frac{-r\tau_1}{I_\varphi(1+r^2)} - \frac{G_0(mr^2+I_\varphi)H_1}{VI_\varphi m} \end{array} \tag{4.97}$$

where $\dot{H}_0$ is:

$$\dot{H}_0 = \frac{(-\dot{w}_{p1}V - w_{p1}\dot{V})m}{(1+r^2)G_0} \tag{4.98}$$

where

$$\begin{array}{l} \dot{w}_{p1} = (\dddot{z}_{1ref} - K_p(\ddot{z}_1 \mid_{\varepsilon=0} - \ddot{z}_{1ref})) - K_v(\dot{\eta} \mid_{\varepsilon=0} - \ddot{z}_{1ref}) = \\ \quad (\dddot{z}_{1ref} - K_p(\eta - \dot{z}_{1ref})) - K_v(-K_p(z_1 - z_{1ref}) - K_v(\eta - \dot{z}_{1ref}))) \end{array} \tag{4.99}$$

The solutions for τ_1 and H_1 are:

$$\begin{array}{l} \tau_1 = \\ \frac{K_v w_{p1} V m(mr^2+I_\varphi)}{G_0(1+r^2)r} + \frac{(w_{p1}\dot{V}+\dot{w}_{p1}V)I_\varphi m}{G_0 r} = -K_vH_0r(m + \frac{I_\varphi}{r^2}) + \frac{(w_{p1}\dot{V}+\dot{w}_{p1}V)I_\varphi m}{G_0 r} \\ H_1 = \frac{-K_v w_{p1} V^2 m^2}{(1+r^2)^2 G_0^2} \end{array} \tag{4.100}$$

The following step is to derive τ_2 and H_2. First the linearizing condition and the manifold condition have to be differentiated with respect to ε^2. By implementing $\varepsilon = 0$, the two equations become:

$$\begin{array}{l} \frac{r\tau_2}{I_\varphi(1+r^2)} - \frac{G_0(-m+I_\varphi)r^2H_2}{VI_\varphi m} + \dot{H}_1 = -K_vH_1 \\ \dot{H}_1 = \frac{-r\tau_2}{I_\varphi(1+r^2)} - \frac{G_0(mr^2+I_\varphi)H_2}{VI_\varphi m} \end{array} \tag{4.101}$$

where $\dot{H}_1$ is:

$$\dot{H}_1 = \frac{K_v(-\dot{w}_{p1}V - 2w_{p1}\dot{V})Vm^2}{(1+r^2)^2G_0^2} \tag{4.102}$$

The solutions for τ_2 and H_2 are:

$$\begin{array}{l} \tau_2 = \frac{K_v^2 w_{p1} V^2 m^2(mr^2+I_\varphi)}{G_0^2(1+r^2)^2 r} + \frac{(2w_{p1}\dot{V}+\dot{w}_{p1}V)K_vI_\varphi Vm^2}{G_0^2(1+r^2)r} = \\ \quad -K_vH_1r(m + \frac{I_\varphi}{r^2}) - K_vV\dot{H}_0\frac{I_\varphi m}{G_0 r} - K_v\dot{V}H_0\frac{I_\varphi m}{G_0 r} \\ H_2 = \frac{-K_v^2 w_{p1} V^3 m^3}{(1+r^2)^3 G_0^3} \end{array} \tag{4.103}$$

This process can be continued an infinite number of times with as a final result:

$$\begin{array}{l} \tau_\varepsilon = \tau_0 + \varepsilon\tau_1 + \varepsilon^2\tau_2 + ... \\ \quad = (m + \frac{I_\varphi}{r^2})(w_{p1} - \varepsilon K_vH_0 - \varepsilon^2K_vH_1 - ..)r + \\ \quad \varepsilon\frac{((w_{p1}-\varepsilon K_vH_0-..)\dot{V}+(\dot{w}_{p1}-\varepsilon K_v\dot{H}_0-..)V)I_\varphi m}{G_0 r} \end{array} \tag{4.104}$$

Using that

$$\begin{array}{l} w = \ddot{z}_{1ref} - K_p(z_1 - z_{1ref}) - K_v(\eta + \varepsilon H_\varepsilon - \dot{z}_{1ref}) \\ w_{p1} = \ddot{z}_{1ref} - K_p(z_1 - z_{1ref}) - K_v(\eta - \dot{z}_{1ref}) \end{array} \tag{4.105}$$

it is possible to state that:

$$\begin{aligned} w &= w_{p1} - \varepsilon K_v(H_0 + \varepsilon H_1 + ..) = w_{p1} - \varepsilon K_v H_\varepsilon \\ \dot{w} &= \dot{w}_{p1} - \varepsilon K_v(\dot{H}_0 + \varepsilon \dot{H}_1 + ..) = \dot{w}_{p1} - \varepsilon K_v \dot{H}_\varepsilon \end{aligned} \tag{4.106}$$

so τ_ε is:

$$\tau_\varepsilon = (m + \frac{I_\varphi}{r^2})wr + \varepsilon \frac{(w\dot{V} + \dot{w}V)I_\varphi m}{G_0 r} \tag{4.107}$$

The conclusion is that the input τ_ε is equal to the input τ of the 1DOF system without slip (4.50) if $\varepsilon = 0$. The extra "slip compensation" term has the dimension of a torque, but furthermore it is difficult to give an interpretation of the slip compensation term. This is mainly due to the fact that slip itself is velocity-based and that torque is acceleration-based.

4.5 Summary

In this chapter, all necessary steps to develop the model and controller for a wheeled mobile robot with and without tyre slip are described. A case study is presented to show how to use the general procedures. In the case study a simple system is described, so that it is still possible to understand what the procedure consists of without losing the overview.
In the following chapters the concepts presented in this chapter will be used to develop models and controllers for different kind of wheeled mobile robots.

Chapter 5

Bicycle control design

The model of a (4ws4wd) car is quite complex. That is the reason why a simplified model for a car, which is called the bicycle model, can be used as a starting point in the modelling process. The longitudinal dynamics of the car are modelled in the bicycle model, but the lateral dynamics are simplified. For example, the two tyres at the front are combined to one tyre and the two tyres at the rear are also combined to one tyre.
The car that will be studied consists of two wheels that both can be driven and steered. The manoeuvrability properties are equal to final controllable 4ws4wd car. The wheels of the car are subjected to velocity constraints, which are restrictions on the movability.
As a start, a controller from the theory on wheeled mobile robots for a bicycle (model) with two conventional steering wheels will be discussed. In section 5.2 another type of controller, with improved properties, will be developed. In section 5.3 a first step will be made in the tuning process of the controller. From here on it is assumed that the velocity constraints are violated during normal driving, which will be described as slip. A model and a controller with slip compensation will be developed for a bicycle model with tyre slip. Finally a study will be made in section 5.7 to compare the controllers with and without slip compensation.

5.1 Bicycle model and controller from the theory on wheeled mobile robots

A model is made (appendix C) for the two wheel steered and two wheel driven car using the theory on wheeled mobile robots.
It is desired that the center of the car will follow a specified reference trajectory $(x_{ref}, y_{ref}, \theta_{ref})$. One of the possible control techniques to achieve this is output linearization via static state feedback [8]. Such a controller for the bicycle model is described in detail in appendix C. The controller has some drawbacks looking at the requirements summed up in section 2.2.
The largest drawbacks of the controller are the singular steering angles. The result is that not the whole specified steering range of 700^o can be controlled. Another drawback is the incapability of the controller to distribute the torques according to the vertical force on the wheels. This is desired, because of the

huge amount of weight transfer during the trajectories in combination with the knowledge that the controller later on will be used by a wheeled mobile robot with normal tyres. Normal tyres cannot deliver an infinite amount of force, but can deliver a larger force, up to a certain limit, if the vertical load is increased. Another drawback of the controller, using static state feedback, for a bicycle is that the error in lateral direction is regulated using the front wheel. The rear wheel is not used to compensate for the lateral error. However, this is a direct result of the choice of the output coordinates.
The static state feedback controller for the bicycle model does not satisfy the requirements summed up in section 2.2. Therefore, it is studied whether a dynamic state feedback controller [8] is an option. The idea is to delay some "combination of inputs" simultaneously affecting several outputs, via the addition of integrators, in order to enable other inputs to act in the meanwhile and therefore hopefully to obtain an extended decoupled system. The conclusion is that the drawbacks of the singular steering angles and the incapability to distribute the torque according to the weight transfer remain.
It follows therefore that a non standard control method has to be constructed because of the specific requirements of the controlled wheeled mobile robot.

5.2 Basic idea of the double unicycle controller

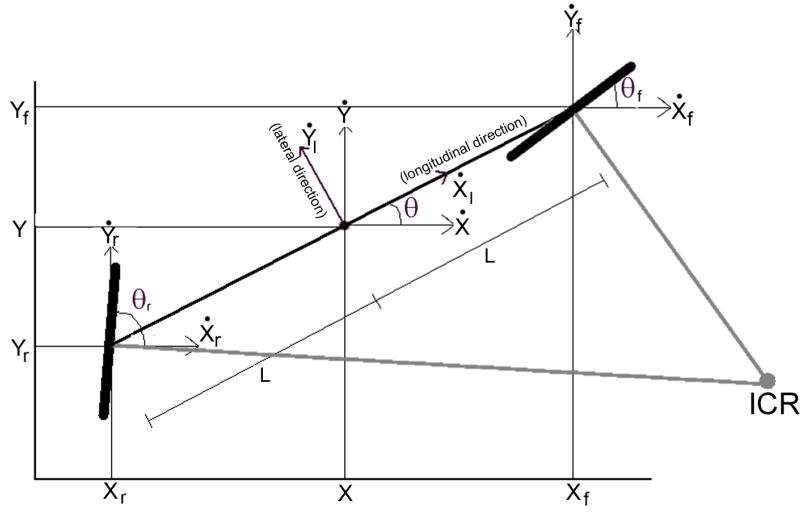

Figure 5.1: Bicycle model - Rewritten for double unicycle controller

The control method is inspired on the concept presented in the paper of Borenstein [10]. The basic idea of the double unicycle controller is to decentralize the tracking problem, which is to let the center of the car (x, y, θ) follow the reference trajectory $(x_{ref}, y_{ref}, \theta_{ref})$. The concept is to convert the (reference) position and (reference) orientation angle of the center to (reference) positions x_i, y_i $(i = f(ront), r(ear))$ (figure 5.1). The same procedure is followed to calculate the first and second derivative of the (reference) positions of the

corners.
The (reference) orientation angles of the wheels (θ_i) are calculated using the kinematic approach, which means that the orientation angles are calculated using the reference velocity signals of the front and the rear. This approach guarantees that the wheels are oriented so that instantaneous center of rotation (ICR figure 6.1) is present during the total manoeuvre. The ICR represents the point around which the WMR is moving, so it is the point where the perpendiculars to the plane of each wheel (drawn from the center of the wheel) are all concurrent. The (reference) positions, velocities and accelerations front and rear are:

$$\begin{aligned}
x_f &= x + L\cos(\theta) \\
x_r &= x - L\cos(\theta) \\
y_f &= y + L\sin(\theta) \\
y_r &= y - L\sin(\theta) \\
\dot{x}_f &= \dot{x} - L\dot{\theta}\sin(\theta) \\
\dot{x}_r &= \dot{x} + L\dot{\theta}\sin(\theta) \\
\dot{y}_f &= \dot{y} + L\dot{\theta}\cos(\theta) \\
\dot{y}_r &= \dot{y} - L\dot{\theta}\cos(\theta) \\
\ddot{x}_f &= \ddot{x} - L\ddot{\theta}\sin(\theta) - L\dot{\theta}^2\cos(\theta) \\
\ddot{x}_r &= \ddot{x} + L\ddot{\theta}\sin(\theta) + L\dot{\theta}^2\cos(\theta) \\
\ddot{y}_f &= \ddot{y} + L\ddot{\theta}\cos(\theta) - L\dot{\theta}^2\sin(\theta) \\
\ddot{y}_r &= \ddot{y} - L\ddot{\theta}\cos(\theta) + L\dot{\theta}^2\sin(\theta)
\end{aligned} \tag{5.1}$$

and,

$$\theta_i = \arctan(\frac{\dot{y}_i}{\dot{x}_i}) \tag{5.2}$$

and $\dot{\theta}_i$ and $\ddot{\theta}_i$ are the first and second time derivative of (5.2).
The system with some of the new coordinates is illustrated in figure 5.1. Looking at the front and the rear of the car, the conclusion is that the car consists effectively of two systems, which both consists of a wheel that can be oriented and driven. Both systems have their own reference signal ($x_{iref}, y_{iref}, \theta_{iref}$) and their own mass ($m_i$), so effectively two control problems remain. A single wheel that can be oriented and that can be driven independently is called a unicycle [3] in the theory on wheeled mobile robots. A schematic overview that illustrates the idea of the control method is plotted in figure 5.2. At the top of the schema the reference and measured position and orientation angle (plus the derivatives) enter. These are translated to reference and measured positions (plus the derivatives) of the front and the rear of the car using geometric model information. The reference orientation angles of the wheels (plus the derivatives) are calculated and are used as an input for the unicycle controller in combination with the reference and measured position of the corner (plus the derivatives) and the reference and measured orientation angle of the center (plus the derivatives). Also other measured data, such as the velocity of the wheels, steering angles etc, enter the unicycle controllers. The output of the controllers are four torques that are sent to the motors of the car.

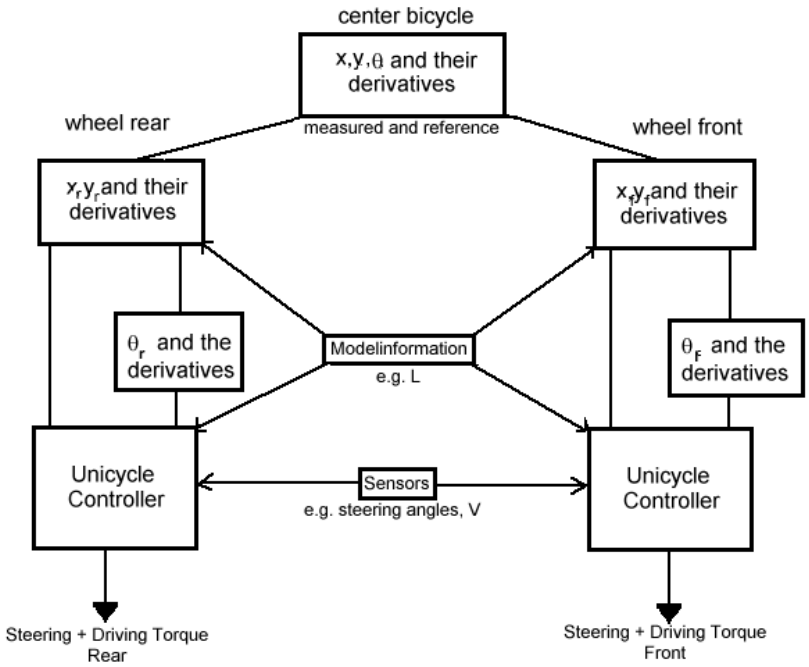

Figure 5.2: Schematic overview double unicycle controller

5.2.1 Unicycle model

The first step, in developing the double unicycle controller, is to develop a model for a single unicycle using the wheeled mobile theory presented in section 4.1.1. The unicycle with the relevant coordinates is illustrated in figure 5.3. The unicycle is a so called (2,0)-type WMR, so the degree of mobility is two and the degree of steerability is zero. The degree of mobility is two, because the unicycle can manipulate two "directions" directly. The unicycle can drive forward and backward, which is the first possible movement. The unicycle can also move around its vertical axis, which is the second possible movement. The degree of steerability is zero, because no conventional steerable wheels are mounted on the unicycle.

A unicycle has four configuration variables (n=4), which are the position of the center (x_i and y_i), the orientation angle θ_i and the rotation of the wheel φ_i.

$$q_i = \begin{pmatrix} x_i \\ y_i \\ \theta_i \\ \varphi_i \end{pmatrix} \tag{5.3}$$

The unicycle described here consists of one wheel that is subject to two constraints (m=2), which are the roll and the slip constraint. The slip constraint limits the movability of the system in the horizontal plane ($\dot{y}_{li} = 0$). The roll constraint relates the rotation of the wheel to the forward speed of the wheel ($\dot{x}_{li} + r\dot{\varphi} = 0$).

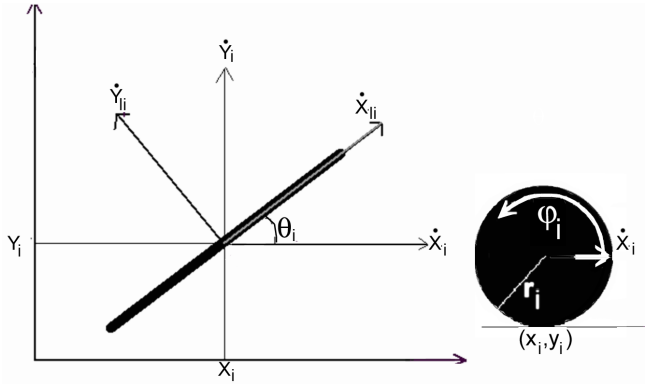

Figure 5.3: Unicycle model

The total procedure to develop the complete model for a unicycle is described in appendix D. Here only the the resulting model(s) will be stated. The *configuration dynamic model* of a unicycle is:

$$\begin{pmatrix} \dot{x}_i \\ \dot{y}_i \\ \dot{\theta}_i \\ \dot{\varphi}_i \\ \dot{\eta}_{1i} \\ \dot{\eta}_{2i} \end{pmatrix} = \begin{pmatrix} \cos(\theta_i)\eta_{1i} \\ \sin(\theta_i)\eta_{1i} \\ \eta_{2i} \\ \frac{-\eta_{1i}}{r_i} \\ \frac{r_i \tau_{di}}{m_i r_i^2 + I_{\varphi_i}} \\ \frac{\tau_{si}}{I_{\theta_i}} \end{pmatrix} \tag{5.4}$$

where m_i is the mass of the unicycle, I_{θ_i} is the inertia of the unicycle around the vertical axis, I_{φ_i} is the rotation inertia of the wheel, η_{1i} is the forward velocity of the unicycle, η_{2i} is the orientation velocity of the unicycle, τ_{di} is the driving torque and τ_{si} is the steering torque.
The driving motor is implemented so that a positive τ_{di} results in an acceleration in negative φ_i direction. The steering motor is implemented so that a positive τ_{si} results in an acceleration in positive θ_i direction.
The analogy with the configuration dynamic model of the 1DOF car is visible. The term for $\dot{\eta}_{1i}$ is equal to the term for $\dot{\eta}$ of the 1DOF car (4.45).
The system that is feedback equivalent (by static state feedback) to the configuration dynamic model can be described using the following torque input τ_i:

$$\begin{pmatrix} \tau_{di} \\ \tau_{si} \end{pmatrix} = \begin{pmatrix} \frac{\nu_{1i}(m_i r_i^2 + I_{\varphi_i})}{r_i} \\ \nu_{2i} I_{\theta_i} \end{pmatrix} \tag{5.5}$$

where $\nu_i = [\nu_{1i}\ \nu_{2i}]$ is a new system input. The posture dynamic model, which is the part of the configuration dynamic model related to the posture variables

($q_{1i} = [x_i \ y_i \ \theta_i]$) now becomes:

$$\begin{pmatrix} \dot{x}_i \\ \dot{y}_i \\ \dot{\theta}_i \\ \dot{\eta}_{1i} \\ \dot{\eta}_{2i} \end{pmatrix} = \begin{pmatrix} \cos(\theta_i)\eta_{1i} \\ \sin(\theta_i)\eta_{1i} \\ \eta_{2i} \\ \nu_{1i} \\ \nu_{2i} \end{pmatrix} \tag{5.6}$$

5.2.2 Unicycle controller

Looking at (5.6), the conclusion is that it is possible to directly have control of the forward velocity of the unicycle and the orientation angle of the unicycle. However, it is not easy to have a direct control of the position of the unicycle, because there is not something as the forward position of the unicycle to control. Therefore, a "master" controller should be introduced that transforms the position errors in adapted (velocity) reference signals, which are used by the "slave" controller that controls the velocity. The drawback of this is that the total controller consists of more parameters, which is more difficult to tune. Therefore, the choice is made to design a controller that directly controls the position and orientation angle of the unicycle. It is important to control the orientation angle next to the position of the unicycle, since then the orientation angle will always be as close as possible to the ideal orientation angle (5.2). This is desired, because it is necessary that an ICR is present during the manoeuvre and because the controller will be used for a car with real tyres that have slip. Because of the tyre characteristic diagram of real tyres (appendix B), it is desired to keep the orientation angle as close as possible to the ideal (kinematic) steering angle, so that the so called slip angle is minimized.
The goal of the controller is to control the three variables (x_i, y_i and θ_i), but only two inputs are available (steering and driving motor). Because of this the control method, using output linearization, described in section 4.1.2, will be used. The goal of the control design method is to get a controllable linear subsystem with dimension 4 ($\dot{z}_{1i}, \dot{z}_{2i}$) and a nonlinear subsystem of dimension 1 ($\dot{z}_{3i}$), which will result in a 5-dimensional system, which is also the dimension of the posture dynamic model (5.6).
First, the linearizing output vector z_{1i} is selected, which is of dimension 2 because of the degree of mobility. The vector z_{1i} is constructed from the posture variables ($q_i = [x_i, y_i, \theta_i]$) so that a controllable system will remain. The variable z_{1i} is of dimension 2, so effectively a point tracking problem remains. If the point x_i, y_i would be chosen, then it is not possible to assure that the orientation angle will be equal or convert to the reference orientation angle. However, if a point in front of the wheels is chosen, it is assured that the variables x_i, y_i, θ_i will convert to the reference variables if there is a forward velocity. A simple example that can illustrate this concept is a truck with a trailer. The reference is that the orientation angle between the truck and the trailer is zero. If the trailer is oriented with a certain angle relative to the truck while the truck stands still, this orientation angle will remain. However, if the truck starts driving forward in a straight line, the orientation angle of the trailer (relative to the truck) will convert to zero which is the reference signal. The chosen "virtual control point" in front of the wheel, illustrated in figure 5.4 [8], is:

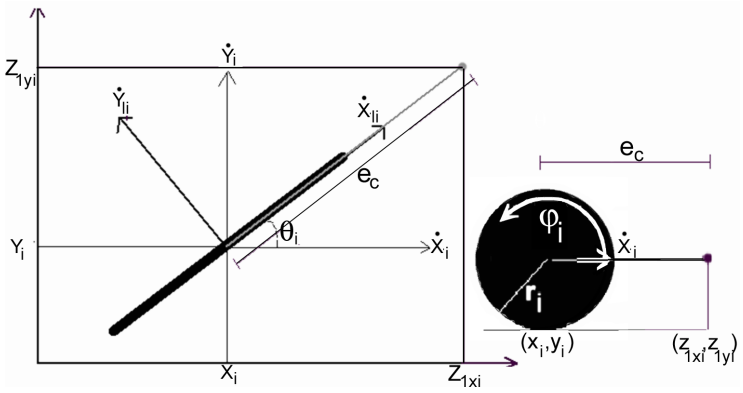

Figure 5.4: Output linearizing coordinates z_{1i}.

$$z_{1i} = \begin{pmatrix} z_{1xi} \\ z_{1yi} \end{pmatrix} = \begin{pmatrix} x_i + e_c \cos(\theta_i) \\ y_i + e_c \sin(\theta_i) \end{pmatrix} \tag{5.7}$$

where e_c is the distance between the center of the unicycle and the "virtual control point" (z_{1i}).
The variable $z_{2i} = \dot{z}_{1i}$, using (5.6) and (5.7), is:

$$z_{2i} = \dot{z}_{1i} = H_i \eta_i = \begin{pmatrix} \cos(\theta_i) & -e_c \sin(\theta_i) \\ \sin(\theta_i) & e_c \cos(\theta_i) \end{pmatrix} \begin{pmatrix} \eta_{1i} \\ \eta_{2i} \end{pmatrix} \tag{5.8}$$

The determinant of H_i is equal to e_c. If e_c is zero, this would mean that $z_{1i} = [x_i \; y_i]$, so $\dot{z}_{1xi} = \cos(\theta_i)\eta_{1i}$ and $\dot{z}_{1yi} = \sin(\theta_i)\eta_{1i}$. As a result of this $\dot{z}_{1i}$ will not see the input η_{2i} anymore.
Now z_{1i} and z_{2i} are known, but the nonlinear subsystem, which is z_{3i}, is still unknown. A possible choice for z_{3i} is θ_i [8], because then the mapping between q_{1i} and $[z_{1i}, z_{3i}]$ is a diffeomorphism on $\mathbb{R}^3$. The following step is to determine $\dot{z}_{2i}$ and $\dot{z}_{3i}$. Using that $\dot{\eta}_i = \nu_i$, it is possible to define $\dot{z}_{2i}$ as:

$$\dot{z}_{2i} = \ddot{z}_{1i} = H_i \dot{\eta}_i + \dot{H}_i \eta_i = H_i \nu_i + b_i \tag{5.9}$$

where H_i is defined in (5.8) and b_i is:

$$b_i = \begin{pmatrix} -\eta_{1i}\eta_{2i} \sin(\theta_i) - e_c \eta_{2i}^2 \cos(\theta_i) \\ \eta_{1i}\eta_{2i} \cos(\theta_i) - e_c \eta_{2i}^2 \sin(\theta_i) \end{pmatrix} \tag{5.10}$$

$\dot{z}_{3i}$ is equal to:

$$\dot{z}_{3i} = \frac{\partial \theta_i}{\partial q_1} \dot{q}_1 = Q_i(q_{1i}) z_{2i} = \begin{pmatrix} \frac{-\sin(\theta_i)}{e_c} & \frac{\cos(\theta_i)}{e_c} \end{pmatrix} \begin{pmatrix} z_{2xi} \\ z_{2yi} \end{pmatrix} \tag{5.11}$$

where $\dot{q}_1$ is defined in (5.6). The variable e_c will influence the behavior of the nonlinear subsystem as can be concluded from (5.11).
Finally it is possible to state that $\ddot{z}_{1i} = w_i$ using that:

$$\nu_i = H_i^{-1}(w_i - b_i) \tag{5.12}$$

where w_i is a new to be defined input. It follows again that e_c has to be a non-zero number, because the determinant of H_i is equal to e_c. The system that remains is :

$$\begin{aligned} \dot{z_{1i}} &= z_{2i} \\ \dot{z_{2i}} &= w_i \\ \dot{z_{3i}} &= Q_i(q_{1i})z_{2i} \end{aligned} \tag{5.13}$$

where Q_i is defined in (5.11). The new input w_i is:

$$w_i = \begin{pmatrix} w_{1i} \\ w_{2i} \end{pmatrix} \tag{5.14}$$

where a possible choice for w_i is a PD controller with a feedforward acceleration signal.

$$\begin{aligned} w_{1i} &= \ddot{z}_{1xiref} - K_v(\dot{z}_{1xi} - \dot{z}_{1xiref}) - K_p(z_{1xi} - z_{1xiref}) \\ w_{2i} &= \ddot{z}_{1yiref} - K_v(\dot{z}_{1yi} - \dot{z}_{1yiref}) - K_p(z_{1yi} - z_{1yiref}) \end{aligned} \tag{5.15}$$

where K_p and K_p are gains and $z_{1iref} = [z_{1xiref} \; z_{1yiref}] = z_{1i}(x_{iref}, y_{iref}, \theta_{iref})$. The choice is made to apply the same control gains, K_p and K_v, for both w_{1i} and w_{2i} in order to make the system behaviour independent of the direction. If for example the control gains in w_{1i} and w_{2i} would not be equal, the response on a position error in the longitudinal direction of the wheel would be different for orientation angles of respectively 0^o and 90^o. The total torque input is now a combination of (5.12) and (5.5).

$$\begin{pmatrix} \tau_{di} \\ \tau_{si} \end{pmatrix} = \begin{pmatrix} \frac{(m_i r_i^2 + I_{\varphi_i})}{r_i}(\cos(\theta_i)w_{1i} + \sin(\theta_i)w_{2i} + e_c\eta_{2i}^2 \\ I_{\theta_i}(\frac{-\sin(\theta_i)}{e_c}w_{1i} + \frac{\cos(\theta_i)}{e_c}w_{2i} - \frac{\eta_{1i}\eta_{2i}}{e_c}) \end{pmatrix} \tag{5.16}$$

The internal dynamics of this system are described by the last equation of (5.13). It is interesting to determine the behaviour of these dynamics. While driving, the the variable z_3 is bounded as long as $e_c \neq 0$, because the error in z_2 exponentially converges to zero (see 4.1.2). A useful procedure to check if the internal dynamics are stable if the unicycle stands still is to verify if the zero-dynamics [14], which are the dynamics that remain if the outputs are zero, are stable.
The two relative degrees, which are loosely speaking the number of integrators between the inputs (w_i) and the defined outputs (z_{1i}), of the system are two [14], so the first step in the procedure to determine the zero-dynamics is to implement that z_{1i}=z_{2i}=0. The input w_i has to be zero to keep the variable z_{2i} zero. The zero-dynamics of the system are thus equal to $\dot{z}_{3i} = 0$. Therefore, a possible solution for $z_{3i}(t)$ is θ_{it}, which is a stable solution. The result is that $z_{1xi} = x_{it} + e_c\cos\theta_{it} = 0$, $z_{1yi} = y_{it} + e_c\sin\theta_{it} = 0$ are solutions for the situation that the unicycle stands still at the (0,0)-position of the virtual control point z_{1i}.

5.2.3 Double unicycle controller

The idea behind the double unicycle controller is to model the front and the rear of the car as a unicycle. The unicycle controller is developed, but a small change

has to be made to the controller. The motor that steers the wheels on the bicycle only has to steer the wheels relative to the body of the bicycle. This angle is the so called "steering angle" (β_i). The steering angle is equal to the orientation angle of the wheel minus the orientation angle of the car ($\beta_i = \theta_i - \theta$). The total steering torque (5.16) from the unicycle controller is equal to $I_{\theta_i}\ddot{\theta}_i$. The steering torque that has to be sent to the car is equal to $I_{\theta_i}\ddot{\beta}_i$. So a compensation term of $-I_{\theta_i}\ddot{\theta}$ has to be added to the calculated steering torque (5.16) to get the real steering torque for the motors on the car.
The total torque, for each of the 2 wheels on the car, is:

$$\begin{pmatrix} \tau_{di} \\ \tau_{si} \end{pmatrix} = \begin{pmatrix} \frac{(m_i r_i^2 + I_{\varphi_i})}{r_i}(\cos(\theta_i)w_{1i} + \sin(\theta_i)w_{2i} + e_c\eta_{2i}^2 \\ I_{\theta_i}(\frac{-\sin(\theta_i)}{e_c}w_{1i} + \frac{\cos(\theta_i)}{e_c}w_{2i} - \frac{\eta_{1i}\eta_{2i}}{e_c}) - I_{\theta_i}\ddot{\theta} \end{pmatrix} \tag{5.17}$$

where θ_i ($i = f, r$) etc are illustrated in figure 5.1 and w_i is defined in (5.15). Especially for a real car with tyres, it is important to implement a certain weight transfer. This is important, because the more vertical force on a normal tyre, the more lateral and longitudinal force a tyre can deliver (up to a certain limit). For example, the rear driving torque has to be larger than the front driving torque to obtain the maximum performance if a car is accelerating in longitudinal direction.
This effect can be implemented in the double unicycle controller by implementing a (varying) mass for the unicycles according to:

$$\begin{aligned} m_f &= \tfrac{1}{2}m - \tfrac{h_{car}m}{4Lg}a_{long} \\ m_r &= \tfrac{1}{2}m + \tfrac{h_{car}m}{4Lg}a_{long} \end{aligned} \tag{5.18}$$

where h_{car} is the height of the center of gravity, g is the gravity constant, m is the total mass of the car and a_{long} is the longitudinal acceleration (figure 5.1). The orientation and the rotation inertia of the unicycle are equal to the orientation and rotation inertia of the wheel(s) of the bicycle model.

5.3 Tuning the double unicycle controller

The control method of controlling a virtual point at a distance of e_c in front of the wheel introduces an extra controller parameter (e_c) next to the controller gains K_p and K_v. The PD controller with feedforward controls the position of the virtual point (z_{1i}, $i = f, r$). However, in reality it is more important that the center of the bicycle has a good tracking behaviour. This is studied by simulations with the configuration dynamic model of a bicycle (appendix C). Different trajectories are driven using the double unicycle controller. The result is that the tracking of the center is perfect when no starting errors and no slip is present. The system is output feedback linearized, which in combination with the correct feedforward signal of the reference trajectory, is the reason that the tracking is perfect. Therefore, it is more interesting to see how the response of the system is on position/starting errors.
It is desired that the response on a position error in lateral direction and the response on a position error in longitudinal direction is equal in the time domain because of the equal performance of the controllable 4ws4wd car in lateral and longitudinal direction (see chapter 2). However, steering angle behavior, as a

reaction on a lateral error, is also important at low velocities ($< 2\ km/h$).
The relation between e_c, the orientation angle, the forward velocity η_{1i} and the lateral error will be studied. This analysis is done using the idea that the car is driving in positive x direction with an orientation angle of zero. If feedback is used, then the PD controller will cause the car to react on an error in lateral direction. The input w_{2i} will have the most influence on the dynamics, especially at orientation angles close to the reference orientation angles of zero (see e.g. (5.17)). To get an insight in the orientation angle dynamics the (open loop) transfer function between the input w_{2i} and θ_i, (linearized) around $\theta_i = 0$ will be given. Using (5.4), (5.16) and $\eta_{2i} = \dot{\theta}_i$, the transfer function can be described as:

$$H_{steer} = \frac{\theta_i}{w_{2i}} = \frac{1}{e_c s^2 + \eta_{1i} s} \tag{5.19}$$

The conclusion is that the forward velocity of the unicycle (η_{1i}) is effectively a damper that influences the steering system. So the faster the unicycle is driving, the more damping in the steering system. The parameter e_c is effectively a mass for the steering system.
At low velocities, the gain between the input w_{2i} and the output $\theta_i = 0$ is relatively high compared to the gain at higher velocities, so the output will be larger at lower velocities for an equal input. If the variable e_c is increased, the gain is lowered, so the output will be lower for an equal input. It has to be considered that the variable e_c only has an influence if there is an *error* in the position or velocity of the point z_{1i}. The "normal" steering angle behaviour, which is the steering angle behaviour while driving a trajectory with no position and velocity error, is determined by the defined trajectory (e.g. ICR position) and is not changed by the variable e_c.

5.3.1 Simulations with starting errors

To get a more detailed view on the influence of e_c on the reaction of the system at position errors, simulations with a starting error in the position are performed. They are performed using the configuration dynamic model of the bicycle (appendix C) in combination with the double unicycle controller as described in section 5.2.3. Two different simulations with starting errors are performed (figure 5.5). The starting errors are 0.5 m, which is the maximum allowed position error for the real 4ws4wd car in VEHIL.

1. A simulation with a longitudinal starting error of 0.5 meter ($e_{x0} = -0.5$).
2. A simulation with a lateral starting error of 0.5 meter ($e_{y0} = -0.5$).

The orientation angle of the bicycle is chosen to be zero, so the lateral error corresponds to the y error ($e_y = y - y_{ref}$) and the longitudinal error corresponds to the x error ($e_x = x - x_{ref}$). The reference trajectory for the simulations is a straight line with a constant velocity:

$$x_{ref} = Vt,\ \dot{x}_{ref} = V,\ \ddot{x}_{ref} = y_{ref} = \dot{y}_{ref} = \ddot{y}_{ref} = \theta_{ref} = \dot{\theta}_{ref} = \ddot{\theta}_{ref} = 0 \tag{5.20}$$

Simulation 1 is performed with four different values for the velocity V. The value of e_c is not changed, because this factor has no influence on the dynamics

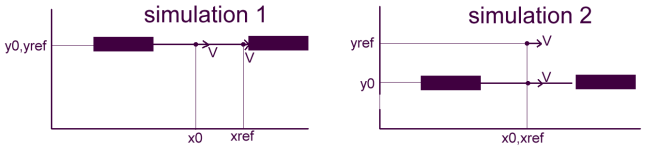

Figure 5.5: Simulation 1 and 2

if there is only a longitudinal error, because $\ddot{z}_{1xi}$ reduces to $\ddot{x}_i = \ddot{x}_{iref} - K_v(\dot{x}_i - \dot{x}_{iref}) - K_p(x_i - x_{iref})$ if $\theta_i, \dot{\theta}_i, \ddot{\theta}_i = 0$. Simulation 2 is performed with four different values for the velocity V and three different values for e_c.
The gains of the PD controller (K_p and K_v) are respectively chosen as 41 and 9, which results in a natural damped system. For a more detailed discussion about the tuning of the gains, see appendix A. All the simulations are performed using Matlab/Simulink, using the ode5 solver with a fixed step size of 0.002 s. The results of the simulations are shown in figure 5.6, figure 5.7 and figure 5.8.

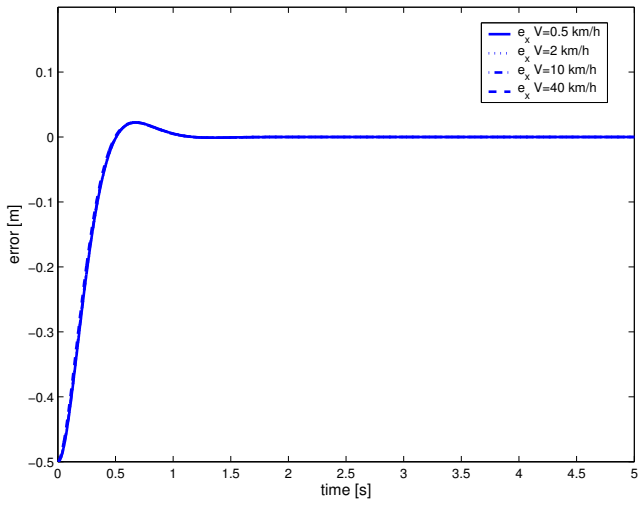

Figure 5.6: Position error for simulation 1 - e_x is the error in x and V is the forward velocity of the bicycle

Figure 5.6 shows the error in x direction for simulation 1 for four different velocities V. From figure 5.6 it follows that the response on the error in x-direction is equal for different velocities. This can be explained by looking at the equation for $\ddot{z}_{1xi}$, which reduces to $\ddot{x}_i = \ddot{x}_{iref} - K_v(\dot{x}_i - \dot{x}_{iref}) - K_p(x_i - x_{iref})$ if $\theta_i, \dot{\theta}_i, \ddot{\theta}_i = 0$. So the resulting behaviour is the behaviour of the PD controller, because $\ddot{x}_{iref} = 0$.
Figure 5.7 and figure 5.8 show respectively the errors in x and y direction and the steering angles for simulation 2 for three different values of e_c and four different values of the velocity V. From figure 5.7 it follows that a smaller e_c value results in a faster decrease of the error in the y-direction. It can also be concluded that the response on the starting error in the y-direction causes a

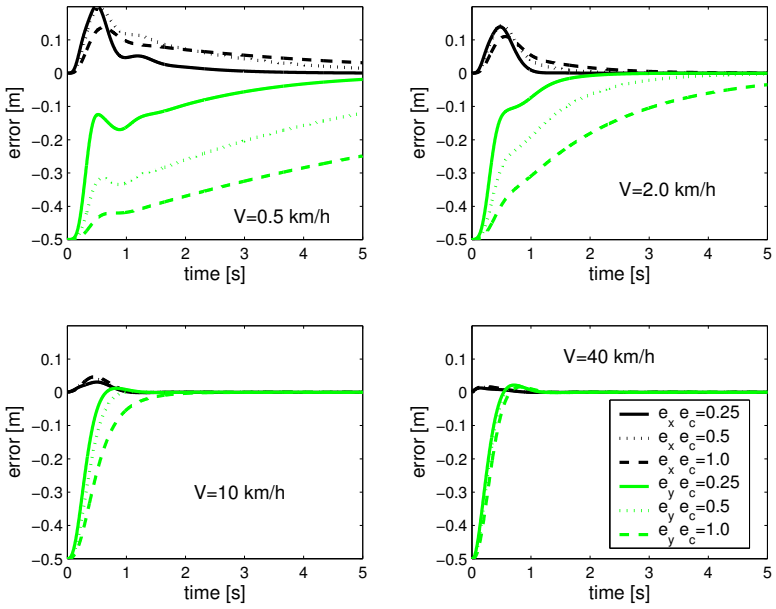

Figure 5.7: Position error for simulation 2 for three different values of e_c and for four different forward velocities V - e_x is the error in x (dark lines) and e_y is the error in y (light lines)

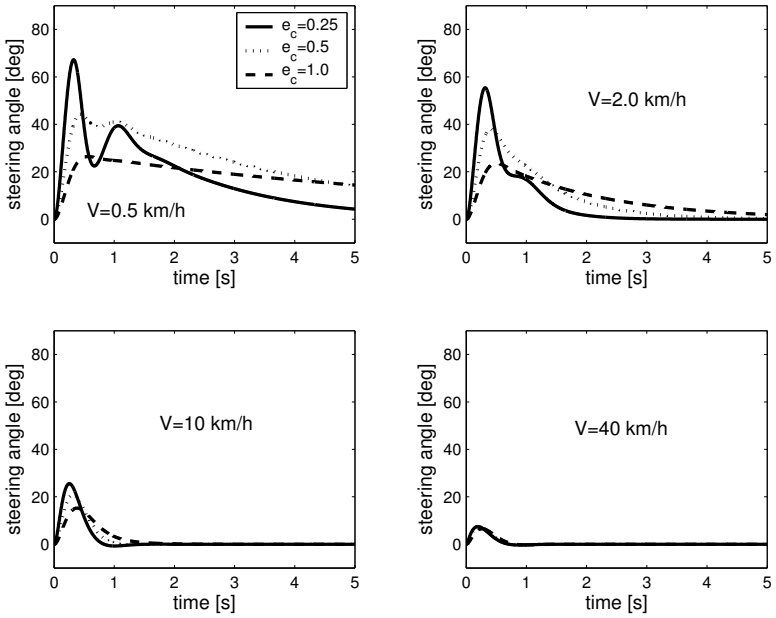

Figure 5.8: Steering angles for simulation 2 for three different values of e_c and for four different forward velocities V

small error in the x-direction at low velocities. This is both the result of the effect that the steering angles increase if the e_c variable decreases (figure 5.8). If the velocity increases, then the error in the x-direction, due to the response on the on the starting error in y-direction, reduces. This is because the steering angles decrease if the velocity is increased (figure 5.8), which is expected from (5.19). It can also be concluded that the responses for the different values of e_c get more comparable if the velocity increases. This is because the influence of the velocity on the gain of (5.19) is relatively larger than the influence of e_c if the velocity is high.
As can be expected from (5.19), small values of e_c and low velocities result in large steering angles (figure 5.8).

A few additional requirements (see chapter 2) are needed to be able to draw final conclusions for the desired value of e_c. These extra requirements follow from the desired behaviour of the 4ws4wd car that has to be controlled.

- For low velocities, the steering behaviour is more important than the (lateral) error.
- For medium and high velocities, the tracking error is more important than the steering behaviour.
- For medium and high velocities, the response on errors in lateral and longitudinal direction is desired to be equal.

Using these extra requirements, the conclusion is that e_c has to be different for different trajectories. From figure 5.6, figure 5.7 and figure 5.8 it follows that a value for e_c between 0.25 m (or lower) and 0.5 m is desired for trajectories with mostly medium ($>$10 km/h) and high velocities, because then the response on an error in lateral direction is comparable to the response on an error in longitudinal direction. A value of e_c of 0.5 m or higher is desired for trajectories with mostly low velocities ($<$2 km/h), because then the orientation angles, as a reaction on lateral position errors (max 0.5 m), are less then 45^o off the reference orientation angles (see chapter 2).
It is recommended for further research to implement a velocity dependent variable e_c for trajectories that have a more even distributed velocity range. Using a velocity dependent e_c it is possible to have the most desirable value of e_c for high and low velocity periods of the trajectory.

5.4 Bicycle with tyre slip control design

In reality, wheeled mobile robot cars always have tyres that only can deliver forces if there is slip. A tyre can deliver forces in the longitudinal and the lateral direction, so there is slip in these directions: First, when the forward velocity of the car is not equal to the rotation of the tyres multiplied by the radius of the tyres (longitudinal). Secondly when the direction in which the tyre is pointing is different than the direction in which the tyre is moving (lateral) (see appendix B).
The tyre slip can result in an (extra) error, so it is useful to include a certain tyre slip compensation in the controller. The controller that is developed consists of two separate controllers for the wheels, the so called unicycle controllers.

Not a lot of literature, related to wheeled mobile robots, about tyre slip and the compensation of the tyre slip is available. One of the few slip compensations for wheeled mobile robots with tyre slip is developed by Motte and Campion [5]. They suggest to model this slip as a linear system, so as a starting point a linear tyre model will be implemented into the unicycle model and a controller will be developed for this system.

5.5 Unicycle model and controller with slip compensation

The controller, developed for the bicycle model without tyre slip, is the so called "double unicycle controller", which is based on the idea to decentralize the tracking problem. The unicycle is the most important part of this controller. This section just briefly discuss the model and controller of the unicycle with slip, which has the same system properties as the unicycle discussed in section 5.2.1. For a more detailed discussion of the procedure, see appendix E.

5.5.1 Unicycle model extended with tyre slip

A wheeled robot with tyre slip can be described with a model written in the standard singular perturbation form (4.64), which is a standard form for systems that consist of fast and slow variables. The procedure, described in section 4.3.1, is used to get to this model description for the unicycle (appendix E).
The unicycle (see figure 5.3) with tyre slip in singular perturbation form is:

$$
\begin{aligned}
\dot{q}_i &= \begin{pmatrix} \cos(\theta_i) & 0 \\ \sin(\theta_i) & 0 \\ 0 & 1 \\ \frac{-1}{r_i} & 0 \end{pmatrix} \eta_i + \begin{pmatrix} \sin(\theta_i) & \cos(\theta_i) \\ -\cos(\theta_i) & \sin(\theta_i) \\ 0 & 0 \\ 0 & r_i \end{pmatrix} \varepsilon\mu_i \\
\dot{\eta}_i &= \varepsilon \begin{pmatrix} \frac{-\mu_{1i}\eta_{2i}r_i^2}{r_i^2+1} \\ 0 \end{pmatrix} + \begin{pmatrix} \frac{r_i}{(r_i^2+1)I_{\varphi_i}} & 0 \\ 0 & \frac{1}{I_{\theta_i}} \end{pmatrix} \tau_{\varepsilon i} - \begin{pmatrix} 0 & \frac{-(m_i - I_{\varphi_i})r_i^2 G_0}{V_i m_i I_{\varphi_i}} \\ 0 & 0 \end{pmatrix} \mu_i \\
\varepsilon\dot{\mu}_i &= \begin{pmatrix} \eta_{1i}\eta_{2i} \\ 0 \end{pmatrix} + \varepsilon \begin{pmatrix} \eta_{2i}\mu_{2i} \\ \frac{-\mu_{1i}\eta_{2i}}{r_i^2+1} \end{pmatrix} + \begin{pmatrix} 0 & 0 \\ \frac{-r_i}{(r_i^2+1)I_{\varphi_i}} & 0 \end{pmatrix} \tau_{\varepsilon i} - \\
&\quad \begin{pmatrix} \frac{D_0}{V_i m_i} & 0 \\ 0 & \frac{(m_i r_i^2 + I_{\varphi_i})G_0}{V_i m_i I_{\varphi_i}} \end{pmatrix} \mu_i
\end{aligned}
\tag{5.21}
$$

where η_{1i} is the forward velocity of tyre i, η_{2i} is the orientation velocity of tyre i, V_i is the absolute velocity of tyre i, m_i is the mass of unicycles, τ_i is the torque vector ($[\tau_{di}\ \tau_{si}]$), r_i is the radius of tyre i, G_0 and D_0 are tyre parameters, I_{φ_i} is the rotation inertia of tyre i, I_{θ_i} is the orient inertia of tyre i and μ_i is the so called "fast" variable that gives an indication for the amount of tyre slip.

5.5.2 Unicycle controller with tyre slip compensation

The goal of the control method is to assure that the unicycle center tracks the reference variables $x_{iref}, y_{iref}, \theta_{iref}$ and their derivatives. The control method

that is used is a combination of the slow manifold theory and output linearization. The idea behind the slow manifold approach is to define an invariant and attractive slow manifold on which the system is output linearizable.
Output linearization is needed, because the unicycle is a non-linear system with two inputs, which are the steering and driving motor. By choosing appropriate output variables, a linear subsystem of dimension 4 $[z_{1i}, z_{2i}]$ and a nonlinear subsystem of dimension 1 $[z_{3i}]$ remain.
The whole procedure is described in detail in appendix E. Here only the output variables will be stated and the final controller with the slip compensation term will be stated.
The appropriate output linearization variables to perform the procedure described in section 4.3.2 have to be defined.
The same output linearizing variables as for the unicycle without tyre slip are chosen to be able to make a valid comparison:

$$z_{1i} = \begin{pmatrix} x_i + e_c \cos(\theta_i) \\ y_i + e_c \sin(\theta_i) \end{pmatrix} \tag{5.22}$$

where e_c is the distance from the center of the unicycle to the "virtual control point" (z_{1i}) (see figure 5.4).
The first derivative of this equation is:

$$\dot{z}_{1i} = z_{2i} = S_{si}\eta + A_{si}\varepsilon\mu_i = \begin{pmatrix} \dot{x}_i - e_c\dot{\theta}_i \sin(\theta_i) \\ \dot{y}_i + e_c\dot{\theta}_i \cos(\theta_i) \end{pmatrix} \tag{5.23}$$

The variable z_{3i} is equal to the z_{3i} variable of the unicycle without tyre slip, being θ_i. The desired linearization condition is $\ddot{z}_{1i} = w_i$ (4.92), where w_i is a new input. The *linearization condition* for a unicycle is:

$$\ddot{z}_{1i} = S_{si}\dot{\eta}_i + A_{si}\varepsilon\dot{H}_{\varepsilon_i} + \dot{S}_{si}\eta_i + \dot{A}_{si}\varepsilon H_{\varepsilon_i} = w_i \tag{5.24}$$

where $\mu_i = H_{\varepsilon_i}$ is the so called "slow manifold" solution. The system that remains is almost equal to the system that remains for the unicycle without slip. The linearized system for the unicycle with slip is equal to:

$$\begin{aligned} \dot{z}_{1i} &= z_{2i} \\ \dot{z}_{2i} &= w_i \\ \dot{z}_{3i} &= Q_{1i}(q_{1i})z_{2i} + Q_{2i}(H_{\varepsilon i}, q_{1i}) \end{aligned} \tag{5.25}$$

where Q_{1i} is equal to Q_i that is defined in (5.11), so:

$$Q_{1i} = \begin{pmatrix} \frac{-\sin(\theta_i)}{e_c} & \frac{\cos(\theta_i)}{e_c} \end{pmatrix} \tag{5.26}$$

The variable Q_{2i} is:

$$Q_{2i} = \begin{pmatrix} \frac{1}{e_c} & 0 \end{pmatrix} \varepsilon H_{\varepsilon_i} \tag{5.27}$$

The variable Q_{2i} is dependent of $H_{\varepsilon_{i1}}$, which is (partly) described in appendix E. Confirming expectations, $H_{\varepsilon_{i1}}$ is related to the variable D_0, because D_0 is the cornering stiffness which is related to the slip angle of the tyre. Besides, $H_{\varepsilon i1}$ is zero if the velocity is zero, which is expected on beforehand, because there is no slip if the tyre is not moving.

A possible choice for the new input w_i, to assures that the error in the velocity and position of z_{1i} exponentially converges to zero, is:

$$w_i = \begin{array}{l} w_{1i} = \ddot{z}_{1xiref} - K_v(\dot{z}_{1xi} - \dot{z}_{1xiref}) - K_p(z_{1xi} - z_{1xiref}) \\ w_{2i} = \ddot{z}_{1yiref} - K_v(\dot{z}_{1yi} - \dot{z}_{1yiref}) - K_p(z_{1yi} - z_{1yiref}) \end{array} \tag{5.28}$$

where $z_{1iref} = [z_{1ixref}\ z_{1iyref}] = z_1(x_{iref}, y_{iref}, \theta_{iref})$ and K_p and K_v are two positive gains.

The linearization condition (5.24) in combination with the manifold condition (equation 3 of (5.21) with $\mu_i = H_{\varepsilon_i}$) is a set of two equations with two unknowns (τ_{ε_i} and H_{ε_i}). These two variables are constructed using a Taylor series expansion. The variables of this Taylor series expansion, which are τ_{0i} and H_{0i} and τ_{1i} etc, are determined in the similar way as for the 1DOF example. This procedure is described in detail in appendix E.
The result of the procedure for the torque input is:

$$\tau_{\varepsilon_i} = \begin{pmatrix} \frac{m_i r_i^2 + I_{\varphi_i}}{r_i} \\ \frac{I_{\theta_i}}{e_c} \end{pmatrix} \left(\begin{pmatrix} c(\theta_i) & s(\theta_i) \\ -s(\theta_i) & c(\theta_i) \end{pmatrix} \begin{pmatrix} w_{1i} \\ w_{2i} \end{pmatrix} + \begin{pmatrix} e_c\eta_{2i}^2 \\ -\eta_{1i}\eta_{2i} \end{pmatrix} \right) + \varepsilon TCRT_{ti} \tag{5.29}$$

where $TCRT_{ti}$ is the tyre characteristic related slip compensation term, which is:

$$TCRT_{ti} = \begin{pmatrix} TCRT_{1ti} \\ TCRT_{2ti} \end{pmatrix} \tag{5.30}$$

where $TCRT_{1ti}$ and $TCRT_{2ti}$ are:

$$\begin{array}{l} TCRT_{1ti} = \\ \frac{m_i I_{\varphi_i}}{r_i G_0}(V_i(\cos(\theta_i)\dot{w}_{1i} + \sin(\theta_i)\dot{w}_{2i} + 2\eta_{2i}(-\sin(\theta_i)w_{1i} + \cos(\theta_i)w_{2i} - \eta_{1i}\eta_{2i})) + \\ \dot{V}_i(\cos(\theta_i)w_{1i} + \sin(\theta_i)w_{2i} + e_c\eta_{2i}^2) + \eta_{2i}V_i(-\sin(\theta_i)w_{1i} + V_i\cos(\theta_i)w_{2i})) - \\ \frac{I_{\varphi_i}V_i m_i}{r_i D_o}\eta_{1i}\eta_{2i}^2 \end{array} \tag{5.31}$$

$$TCRT_{2ti} = \begin{array}{l} \frac{m_i I_{\theta_i}}{e_c^2 D_0}(e_c\eta_{2i}(V_i\cos(\theta_i)w_{1i} + V_i\sin(\theta_i)w_{2i} + V_i e_c\eta_{2i}^2 + \eta_{1i}\dot{V}_i) + \\ \eta_{1i}V_i(-\sin(\theta_i)w_{1i} + \cos(\theta_i)w_{2i} - \eta_{1i}\eta_{2i})) + \\ \frac{V_i m_i I_{\theta_i}}{e_c G_0(1+r_i^2)}\eta_{2i}(\cos(\theta_i)w_{1i} + \sin(\theta_i)w_{2i} + e_c\eta_{2i}^2) \end{array} \tag{5.32}$$

The similarity between the controller for a model without tyre slip and the controller with slip compensation with $\varepsilon = 0$ is visible in the 1DOF example (chapter 4). The same similarity can be found for the unicycle, because (5.29) with $\varepsilon = 0$ is equal to (5.16).
Also similarities between the controller with slip compensation for the 1 DOF model and the unicycle model can be found. The driving part of the unicycle controller (first row of (5.29)) is equal to the torque input with tyre slip compensation of the 1 DOF model (4.107), if $\theta_i = 0$ and $\dot{\theta}_i = \eta_{2i} = 0$ are implemented in (5.29).

To give an interpretation of the slip compensation term is again difficult. However, it is clear that both tyre characteristics are implemented in the compensation term.
The internal dynamics of this system are described by the last equation of (5.25). Just like for the unicycle without slip it is interesting to determine the zero-dynamics for the unicycle with slip and check if they are stable. The first step in the procedure to determine the zero-dynamics is to implement that z_{1i}=z_{2i}=0, because the two relative degrees of the system are two. The input w_i will have to be zero to keep the variable z_{2i} zero. The variable Q_{2i} is zero, because the slip is zero if the velocity is zero, so $H_{\varepsilon i1} = 0$. The zero-dynamics of the system are equal to $\dot{z}_{3i} = 0$. The result of this is that a possible solution for $z_{3i}(t)$ is θ_{it}, which is a stable solution. The result is that $z_{1xi} = x_{it} + e_c \cos\theta_{it} = 0$, $z_{1yi} = y_{it} + e_c \sin\theta_{it} = 0$ are solutions for the situation that the unicycle stands still at the (0,0)-position of the virtual control point z_{1i}.

5.5.3 Double unicycle controller with tyre slip compensation

The double unicycle controller with tyre slip compensations can be derived just like the double unicycle controller without slip compensation (5.17). The steering torque is changed, because the tyres only have to be oriented relative to the body of the bicycle. Because of this, a compensation term of $-I_{\theta_i}\ddot{\theta}$ is added. The result for the input torque for each of the two wheels on the car is:

$$\tau_{\varepsilon i} = \begin{pmatrix} \frac{m_i r_i^2 + I_{\varphi_i}}{r_i} \\ \frac{I_{\theta_i}}{e_c} \end{pmatrix} \left(\begin{pmatrix} c(\theta_i) & s(\theta_i) \\ -s(\theta_i) & c(\theta_i) \end{pmatrix} \begin{pmatrix} w_{1i} \\ w_{2i} \end{pmatrix} + \begin{pmatrix} e_c \eta_{2i}^2 \\ -\eta_{1i}\eta_{2i} \end{pmatrix} \right) + \varepsilon TCRT_{ti} - \begin{pmatrix} 0 \\ I_{\theta_i}\ddot{\theta} \end{pmatrix} \tag{5.33}$$

where θ_i $(i = f, r)$ etc are illustrated in figure 5.1, $TCRT_{ti}$ is the tyre characteristic related term for tyre i, w_{1i} and w_{2i} are defined in (5.28) and m_i is the (varying) mass of the unicycle.

5.6 Analysis of the effect of the tyre slip compensation

In this section, it will be analytical studied whether the controller with slip compensation can assure perfect tracking of trajectories for the center of the two wheel steered two wheel driven car.
The most important goal of the unicycle controller (with feedback) is to assure that $z_{1i} = z_{1iref}$. The variable z_{1iref} consists of the reference position variables x_{iref} and y_{iref} and the reference orientation angle θ_{iref}. The reference orientation angle is determined using the idea that the wheels should be directed so that an ICR is present during the manoeuvre. The reference orientation angle is the kinematic orientation angle as described in section 5.2. However, the real orientation angle during a manoeuvre is equal to the kinematic orientation angle

plus the slip angle (appendix B), because a tyre needs a certain slip angle to generate a lateral force, which is needed to fore example drive a corner. The result is that there will be an error in the positions x, y and or the orientation angle θ while driving the manoeuvre, even if $z_{1i} = z_{1iref}$ for every "unicycle". The situation while driving a circle with an orientation angle of zero is illustrated in figure 5.9.

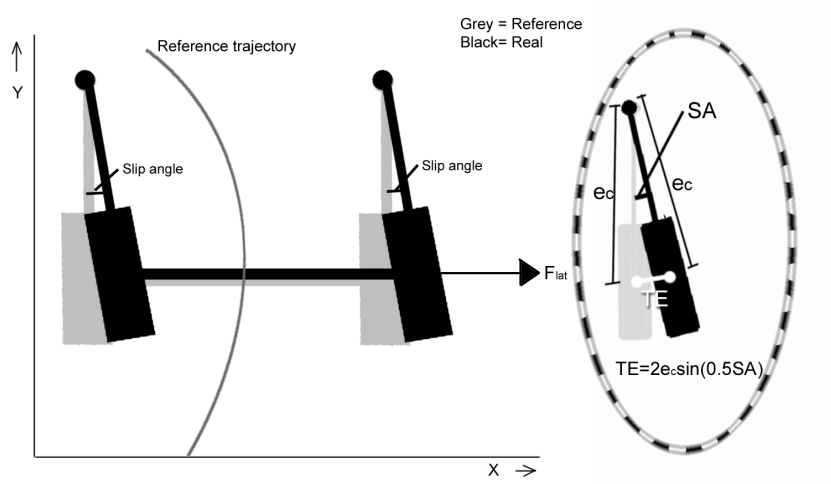

Figure 5.9: Error due to the chosen control method of input output linearization (SA is the slip angle of the tyre, grey is the reference and black is the real bicycle model if $z_{1i} = z_{1iref}$).

The position error at a corner (TE in figure 5.9 when $z_{1i} = z_{1iref}$) is:

$$TE = 2e_c \sin(0.5SA) \tag{5.34}$$

where SA is the slip angle of the tyre (also often described as α). The smaller the variable e_c, the smaller the error (TE) which results in a smaller error of the center of the bicycle. Using simulations with position errors, it is determined that a value for e_c of 0.25 (or lower) - 0.5 m is desired for medium and high velocity trajectories. The slip angles of non-linear tyres normally will be between 0^o-8^o (appendix B) if the tyres are used up to the maximum performance possible. The TE will have a value of 0-7 cm for these slip angles and an e_c of 0.5.
The result of this analysis is that slip compensation is expected to have a positive influence on the tracking behaviour if $z_{1i} \neq z_{1iref}$, but the slip compensation in combination with the chosen output linearization cannot assure that the error of the center of the bicycle is equal to zero when for example a circle is driven while $z_{1i} = z_{1iref}$.
The main reason for this is that the reference orientation angle is calculated using a kinematic approach. It would be better if the reference orientation angle would consists of the reference kinematic orientation angle plus the estimated slip angle. It is however difficult to estimate the exact slip angle(s) in reality because of the non-linearities of tyres in general.

For this moment, the choice is made to accept the error of the center of the bicycle. The error is accepted, because the error is related to the error TE, which has a relatively low maximum (7 cm) compared to the maximum allowable error (0.5 m) for the position of the center. Another reason why the error is accepted is that a good estimator of the real slip angle is not available for the real 4ws4wd car for which the controller is developed.
A recommendation for further research is that it would be useful to develop a good estimator of the slip angle so that the currently uncompensatable error (TE) is removed, while still maintaining the advantage of the steering angle behaviour of the chosen control method (see section 5.3.1).

5.7 Simulations of the effect of the tyre slip compensation

Simulations will be performed to see if the tyre slip compensation in the controller has a positive influence on the performance compared to the performance with the controller without tyre slip compensation. It is known that perfect tracking cannot be obtained (section 5.6), but it is still expected that the slip compensation improves the tracking.
It is important to find a proper (simulation) model of a bicycle with tyre slip before the simulations with the double unicycle controller with and without slip compensations can be started. A bicycle model with slip in singular perturbation form, which expendability is limited, is not available. Therefore, a physical model is designed, the so called one track model in combination with a linear tyre model (see appendix B). The one track model describes the vehicle body dynamics in the horizontal plane using three degrees of freedom, i.e. the displacements in x- and y-direction and the rotation around the vertical z-axis (yaw). Although there are only three degrees of freedom, it is possible to account for the distribution of the gravitation force between the front and rear axle as a function of the longitudinal acceleration. The one track model is a non-linear six order model: two orders for every degree of freedom. Non-linearities are caused by the geometrical relations.
First of all, simulations with the configuration dynamic model (of the bicycle without slip) and the one track model are done to see if the results of the simulations with the one track model convert to the results with the configuration dynamic model if the tyre stiffness is increased (and thus the slip is decreased). The tyres used for the simulations with the one track model are (based on) simple linear tyres (see appendix B):

$$\begin{aligned} F_{lati} &= D\alpha \\ F_{longi} &= G\kappa \end{aligned} \tag{5.35}$$

where D is the cornering stiffness and G is the slip stiffness. The parameters of the car are described in table 5.1. For the tyres, the standard parameters are: $G = 46F_{zi}$ and $D = 70F_{zi}$, where F_{zi} is the vertical load on tyre i.
All the parameters are chosen, so that the results also can be used for the controller of the 4ws4wd car.
The e_c variable that is used is 0.35 m, which is a value between 0.25 and 0.5 m, which is a valid choice looking at the conclusion of section 5.3.1. The value

Table 5.1: Specifications

m:	310 kg
I_z:	194 kgm^2
I_{φ_i}:	0.36 kgm^2
$I_{\theta_{li}}$:	2 kgm^2
L:	0.7 m
e_c:	0.35 m
r_i:	0.23 m

is relatively high, because it also has to work well at low velocities, because the variable e_c is not velocity dependent yet. The result(s) of the simulations can be found in appendix F. The conclusion of the simulations is that the results of the simulations with the one track model convert to the results with the configuration dynamic model if the tyre stiffness is increased, so the one track model is a valid simulation model.

The following step is to perform simulations to study if the tyre slip compensation improves the tracking of a trajectory. The choice is made to not perform simulations with starting errors, because these type of simulations are considered to be less relevant for the goal of the simulations. Therefore, two different trajectories with high accelerations (longitudinal and lateral) will be simulated. The first trajectory is an eight shaped trajectory with a fixed orientation angle ($\theta = 0$) of the car and a maximum lateral and longitudinal acceleration of 10 m/s^2. This trajectory has two corners with a fixed radius. This means that there will be a constant (sideways) slip, which is why this trajectory is useful. The second trajectory is a lane change with the orientation angle of the bicycle tangential to the trajectory and a maximum lateral and longitudinal acceleration of 10 m/s^2. This trajectory has two places where the steering angles have to increase and decrease fast while the car is driving with a fixed forward velocity, which means that the slip will rise and decrease fast. It also has two straight lines in which the bicycle will accelerate and de-accelerate from zero to its maximum velocity and visa versa. So this is also a very useful trajectory to see if the tyre slip compensation has a positive influence on the performance.

The double unicycle controller used for the simulations has K_p and K_v gains of respectively 3 and 4.5, which result in a natural damped system (in longitudinal direction). The resulting errors (measured-reference) for the center of the car for the two trajectories are plotted in figure 5.10 and figure 5.11.
The conclusion from the simulations is that the tyre slip compensation has a positive influence on the tracking performance of the system, but the error of the center is (as expected) not reduced to zero (see section 5.6). For the eight shaped trajectory the difference between the controller with and without tyre slip compensations is most obvious during the fixed radius corners of the trajectory. This is as expected, because this is the phase of the trajectory with the largest (lateral) tyre slip. For the lane change manoeuvre the difference between the controller with and without tyre slip compensations is most obvious during the start and end of the evasive manoeuvre. The overshoot at the start and

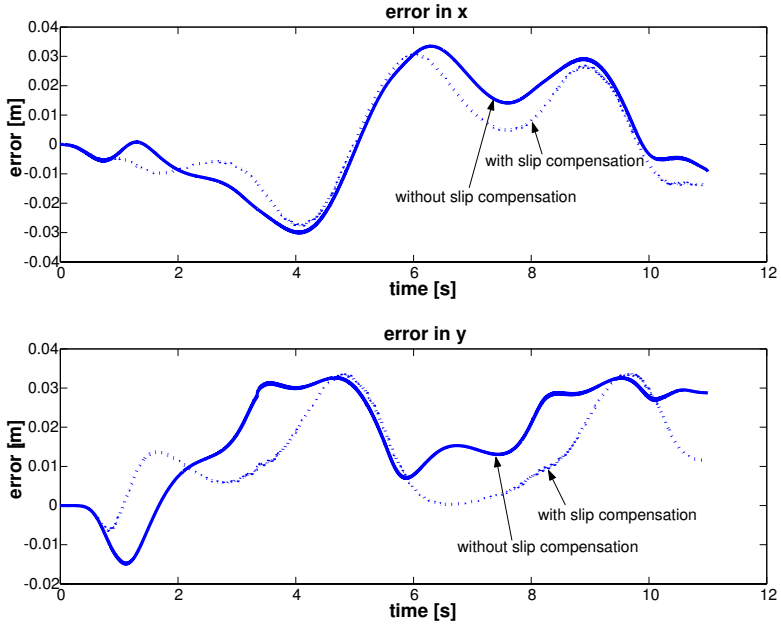

Figure 5.10: Errors of the eight shaped trajectory using the double unicycle controller with and without slip compensation.

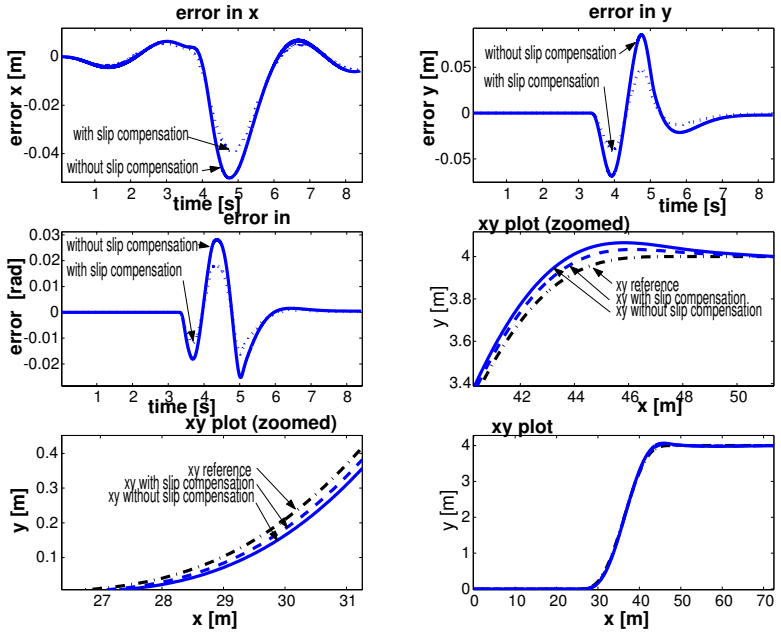

Figure 5.11: Errors of the lane change using the double unicycle controller with and without slip compensation.

end of the evasive manoeuvre is decreased when the controller with tyre slip compensation is used.
Overall the error is 30-40 procent less when the controller with tyre slip compensation is used, which is considered a satisfying result.

5.8 Summary

A controller for the bicycle model is presented. It appears that the standard controllers, described in the theory on wheeled mobile robots, have singular steering angles (e.g. 90 degrees). The trajectories normally driven by the 4wswd car often are constructed in such a way that these problem steering angles will be reached, so another type of controller is designed. This is the double unicycle controller, which is a controller consisting of two unicycle controllers, which each are a controller for a wheel that can be driven and steered. This control method can be easily adapted to a 4ws4wd car. So if a car is equipped with wheels that can be steered and driven independently, then the controller can be used. Therefore, the more general name of the controller will be multicycle controller (**multi**ple uni**cycle** controller).
Some simulations with the double unicycle controller are performed to tune the parameters of the controller. The conclusion is that especially the parameter e_c can influence the steering and tracking response of the car on position errors at low and high velocities.
Also a double unicycle controller with tyre slip compensation is developed for the bicycle model. For the double unicycle controller with slip compensation, simulations, using a physical model of the car, prove that the tyre slip compensation has a positive influence on the tracking error of the system. It is an extra performance gain without increasing the K_p and K_v values of the controller. It is also determined that the tracking error of the center will not be equal to zero while driving trajectories if there is slip. This is because the reference orientation angles of the tyres are equal to the kinematic steering angles in stead of the kinematic steering angles plus the (estimated) slip angles. It is however difficult to estimate the slip angle and therefore it is accepted that the tracking error cannot be reduced to zero.
Although the tracking error will not reduce to zero, it is still useful to extend the double unicycle controller to a "double unicycle controller with tyre slip compensation". The following step will be to introduce the multicycle controller with slip compensation for the 4ws4wd car.

Chapter 6

Multicycle control design

A controller is designed for a simplified model of the 4ws4wd car, called the bicycle model. The controller assures that the car will follow a prescribed trajectory in the horizontal plane in combination with a prescribed orientation angle of the car. The controller that has proven to be the best choice is the double unicycle controller with tyre slip compensation. The double unicycle controller consists of two "separate" unicycle controllers, one for each wheel of the car, which each has his own reference trajectory. The following step will be to expand this controller so that it can be used for a 4ws4wd car model. The controller will also be tested to obtain the best gains settings and to check the performance and robustness. In section 6.1, the controller for the 4ws4wd car model will be developed. In section 6.2, simulations with a complete dynamic model [15] of the 4ws4wd car used in VEHIL will be performed. If the controller works on this model, it is expected to work on the real 4ws4wd car as well.

6.1 Multicycle controller

The multicycle control method is inspired on the idea presented in a paper of Borenstein [10]. The basic idea is to decentralize the tracking problem. The tracking problem is to let the center of the car (x, y, θ) follow the reference trajectory $(x_{ref}, y_{ref}, \theta_{ref})$. The concept is to convert the (reference) position of the center to a (reference) position x_{ij} and y_{ij} $(i = f(ront), r(ear), j = l(eft), r(ight))$ at the four corners where the wheels are attached (figure 6.1)). The same procedure is followed for the first and second derivative of the (reference) positions of the corners.
The (reference) orientation angles of the wheels (θ_{ij}) are calculated using the kinematic approach, which means that the orientation angles are calculated using the reference velocity signals of the corners. This approach guarantees that the wheels are oriented so that an instantaneous center of rotation (ICR figure 6.1) is present during the total manoeuvre. The ICR represents the point around which the WMR is moving, so it is the point where the perpendiculars to the plane of each wheel (drawn from the center of the wheel) are all concurrent.
In the previous chapter it is suggested that the reference orientation angle ideally should consist of the kinematic orientation angle and the estimated slip angle of the tyre. It is however hard to estimate the slip angle of the tyre, so the

kinematic reference orientation angle is used as the reference orientation angle instead.
The (reference) positions, velocities and accelerations for the corners are:

$$\begin{aligned}
x_{fl} &= x + L_b \cos(\theta + \arctan(\tfrac{W}{L})) \\
y_{fl} &= y + L_b \sin(\theta + \arctan(\tfrac{W}{L})) \\
\dot{x}_{fl} &= \dot{x} - L_b\dot{\theta} \sin(\theta + \arctan(\tfrac{W}{L})) \\
\dot{y}_{fl} &= \dot{y} + L_b\dot{\theta} \cos(\theta + \arctan(\tfrac{W}{L})) \\
\ddot{x}_{fl} &= \ddot{x} - L_b\ddot{\theta} \sin(\theta + \arctan(\tfrac{W}{L})) - L_b\dot{\theta}^2 \cos(\theta + \arctan(\tfrac{W}{L})) \\
\ddot{y}_{fl} &= \ddot{y} + L_b\ddot{\theta} \cos(\theta + \arctan(\tfrac{W}{L})) - L_b\dot{\theta}^2 \sin(\theta + \arctan(\tfrac{W}{L})) \\
&\ldots
\end{aligned} \tag{6.1}$$

where $L_b = \sqrt{L^2 + W^2}$, where the variables L and W are illustrated in figure 6.1.
The kinematic orientation angles of the wheels are:

$$\theta_{ij} = \arctan(\frac{\dot{y}_{ij}}{\dot{x}_{ij}}) \tag{6.2}$$

and $\dot{\theta}_{ij}$ and $\ddot{\theta}_{ij}$ are the first and second time derivative of (6.2). The system with some of the new coordinates is illustrated in figure 6.1.

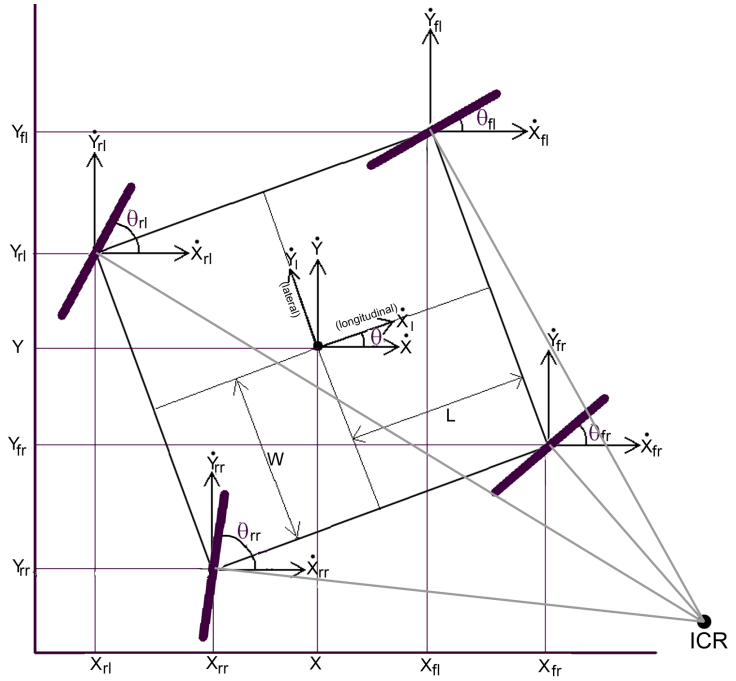

Figure 6.1: 4ws4wd model - Rewritten for multicycle controller.

Looking at the corners of the car the conclusion is that the car consists effectively of four systems, which are all wheels that can be oriented and driven. All these systems have their own reference signal $(x_{ijref}, y_{ijref}, \theta_{ijref})$, so effectively four

tracking problems remain. A single wheel that can be driven and that can be steered can be modelled as a unicycle system, so every "corner" of the car is a unicycle system. Especially for a real car with tyres, it is important to implement a certain weight transfer effect. This is important, because the more vertical force on a normal tyre, the more lateral and longitudinal force a tyre can deliver. For example the driving torque rear has to be larger than front to obtain the maximum performance if a car is accelerating in longitudinal direction.
This effect can be implemented in the multicycle controller by implementing a (varying) mass according to [11]:

$$\begin{aligned} m_{fl} &= \tfrac{1}{4}m - \tfrac{h_{car}m}{4Lg}a_{long} - \tfrac{h_{car}m}{4Wg}a_{lat} \\ m_{fr} &= \tfrac{1}{4}m - \tfrac{h_{car}m}{4Lg}a_{long} + \tfrac{h_{car}m}{4Wg}a_{lat} \\ m_{rl} &= \tfrac{1}{4}m + \tfrac{h_{car}m}{4Lg}a_{long} - \tfrac{h_{car}m}{4Wg}a_{lat} \\ m_{rr} &= \tfrac{1}{4}m + \tfrac{h_{car}m}{4Lg}a_{long} + \tfrac{h_{car}m}{4Wg}a_{lat} \end{aligned} \tag{6.3}$$

where a_{long} and a_{lat} are the longitudinal and lateral acceleration of the car during the manoeuvre. a_{long} points in the positive x_l direction and a_{lat} points in the positive y_l direction. m is the total mass of the 4ws4wd car and h_{car} is the height of the center of gravity of the 4ws4wd car.
The unicycle model has two inputs, which are the driving and the steering motor. The driving motor is implemented so that a positive torque will result in an increase of the longitudinal acceleration of the unicycle. The steering motor is implemented so that a positive torque will result in an increase of the orientation acceleration of the unicycle. The procedure to derive a model and a controller for a unicycle is described in chapter 5. The control method used is the slow manifold approach. The idea behind this approach is to define an invariant and attractive slow manifold on which the system is output linearizable. The result is that a linearized subsystem and a nonlinear subsystem remain. A PD controller with acceleration feedforward is designed for the linearized subsystem.
The output of the unicycle controller is a driving and an orientation torque. However, the motor that orients the wheels on the 4ws4wd car only has to steer the wheels relative to the body of the car. This angle is the so called "steering angle" (β_{ij}). The steering angle is equal to the orientation angle of the wheel minus the orientation angle of the car ($\beta_{ij} = \theta_{ij} - \theta$). The total steering torque (5.16) from the unicycle controller is equal to $I_{\theta_{ij}}\ddot{\theta}_{ij}$. The steering torque that has to be sent to the car is equal to $I_{\theta_{ij}}\ddot{\beta}_{ij}$. So a compensation term of $-I_{\theta_{ij}}\ddot{\theta}$ has to be added to the calculated steering torque (5.16) to get the real steering torque for the motors on the car.
The resulting torque input is:

$$\begin{aligned} \tau_{\varepsilon ij} = &\begin{pmatrix} \frac{m_{ij}r_{ij}^2 + I_{\varphi_{ij}}}{r_{ij}} \\ \frac{I_{\theta_{ij}}}{e_c} \end{pmatrix} \left(\begin{pmatrix} c(\theta_{ij}) & s(\theta_{ij}) \\ -s(\theta_{ij}) & c(\theta_{ij}) \end{pmatrix} \begin{pmatrix} w_{1ij} \\ w_{2ij} \end{pmatrix} + \begin{pmatrix} e_c\eta_{2ij}^2 \\ -\eta_{1ij}\eta_{2ij} \end{pmatrix} \right) \\ &+\varepsilon TCRT_{tij} - \begin{pmatrix} 0 \\ I_{\theta_{ij}}\ddot{\theta} \end{pmatrix} \end{aligned} \tag{6.4}$$

where θ_{ij} etc are illustrated in figure 6.1, $TCRT_{tij}$ (5.30) is the tyre slip compensation factor for tyre ij, m_{ij} is the (varying) mass of the unicycle, $I_{\theta_{ij}}$ is the inertia of the wheel around the vertical axis, $I_{\varphi_{ij}}$ is the rotation inertia of the

wheel, η_{1ij} is the forward velocity of the unicycle, η_{2ij} is the orientation velocity of the unicycle and w_{1ij} and w_{2ij} are:

$$\begin{aligned} w_{1ij} &= \ddot{z}_{1xijref} - K_v(\dot{z}_{1xij} - \dot{z}_{1xijref}) - K_p(z_{1xij} - z_{1xijref}) \\ w_{2ij} &= \ddot{z}_{1yijref} - K_v(\dot{z}_{1yij} - \dot{z}_{1yijref}) - K_p(z_{1yij} - z_{1yijref}) \end{aligned} \tag{6.5}$$

where K_v and K_p are the "PD" controller gains and $z_{1ijref} = [z_{1xijref}\ z_{1yijref}] = [x_{ijref} + e_c\cos\theta_{ijref}\ y_{ijref} + e_c\sin\theta_{ijref}]$ (z_{1ij} is the output linearization variable). A schematic overview of the control method can be found in appendix G.

6.2 Simulations

The multicycle (double unicycle) controller has proven to be the best controller for the bicycle model of the 4ws4wd car (chapter 5). The goal of the simulations here is to check if the multicycle controller can be used to control the real 4ws4wd car in the VEHIL test facility. A complete dynamic model of the 4ws4wd car [15], e.g. with steering motor dynamics, will be used to get an idea of the usefulness of the controller. First of all the transfer functions in longitudinal and lateral directions will be determined. These tests are used to determine the controller parameters and test the robustness of the controller. The following step will be to test trajectories with low velocities and low acceleration levels. During these tests the tyres are not used up to their limits and will still operate in their linear region. Also the steering and driving motor dynamics are not that important at low velocities and low acceleration levels. So the system is "close" to an ideal system, where the multicycle controller is derived for. The last part of the simulations will be to simulate trajectories with high velocities and high accelerations. These tests are chosen, so that the 4ws4wd car is used up to the maximum performance possible. It is interesting to determine the performance of the controller for these severe trajectories.

6.2.1 Frequency response

The frequency response in longitudinal direction (reference to measured signal) is determined using a swept sine, superposed on a forward velocity, for the full dynamic model [15]. The swept sine used for the responses has a frequency range of 0-10 Hz. The modelled dynamics of the full dynamic model are all present in this region and also the used trajectories have their frequency range (0-1 Hz, see appendix A) in this region. First, the frequency response using an "ideal controller", which is the multicycle controller with tyre slip compensation without parameter errors, is determined. For example the mass in the multicycle controller is equal to the mass of the model. Secondly the frequency response using the multicycle controller with parameter errors is determined to check the robustness. It is important to study this, because in reality the parameters of the 4ws4wd system are not (always) known in detail. Therefore, this frequency response will give a more realistic result for the real frequency response of the controlled 4wd4ws car. The mass used in the controller with parameter errors is 0.8 times the mass used in the model. The rotation and orientation inertia of the wheel used in the controller with parameter errors is 0.5 times the inertia used in the model.

The parameters of the vehicle model are the parameters of the 4ws4wd car summarized in table (2.1). The e_c variable that is used is 0.35 m, which is a compromise between the error due to the slip angle, the steering angle behaviour and the response on a (lateral) position error (section 5.3.1). The simulations are performed with three different settings for the PD values of the controllers, which all result in natural damped systems (see appendix A). Matlab/Simulink with an ode5 solver with a fixed step time of 0.002s is used for the simulations. In figure 6.2 the resulting magnitude and phase characteristic of the frequency response in longitudinal directon for the controllers with and without parameter errors are shown. It follows from the frequency response in longitudinal direction

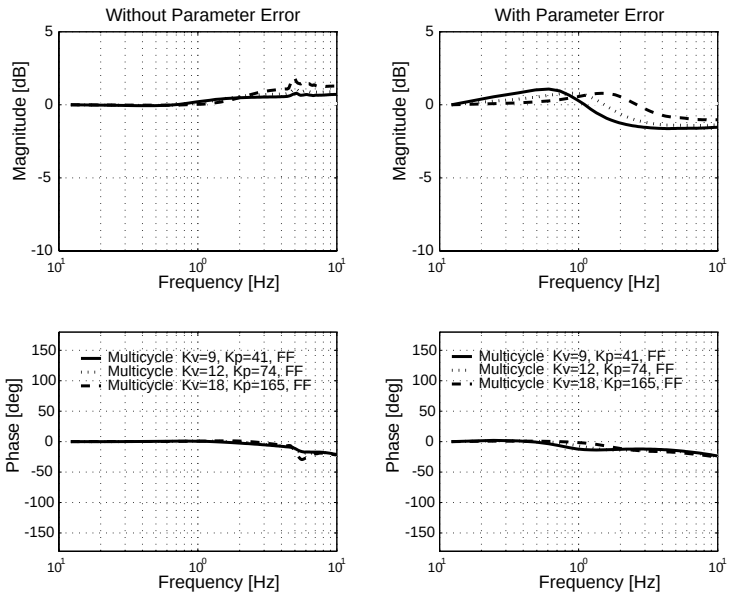

Figure 6.2: Frequency response in longitudinal direction for a controller with and without parameter errors.

that the magnitude, using the controller without parameter errors, is about 0 dB up to 1-2 Hz. The magnitude of about 0 dB is expected because of the output linearization in combination with the feedforward of the reference trajectory. It also follows that there is a resonance frequency around 5 Hz, which is equal to the damped pitch eigenfrequency of the 4ws4wd model. The frequency response using the controller with parameter errors shows a different behaviour. The linearization is not perfect anymore, because the torque input partly consists of the PD controller with feedforward that is multiplied by a factor, which is inaccurate because it consists of e.g. the mass of the unicycle. Therefore, the feedforward is not perfect anymore, so the response is more like a response of a system with a PD controller. The "weakest" controller has a closed loop bandwidth of 1.5 Hz and the "strongest" controller has a closed loop bandwidth of 4 Hz. The controller shows that it can handle parameter variations, so the controller is robust with respect to parameter variations. For performance reasons, the strongest controller is preferred, because the phase

delay with this controller is up to 1 Hz almost zero. This is desired, because the most common trajectories that are driven by the 4ws4wd car have a frequency range where frequencies below 1 Hz are most dominant (appendix A).
The frequency response function in lateral direction is also determined using a swept sine while driving with a forward velocity and an orientation angle of zero. The swept sine used for the response has again a frequency range of 0-10 Hz. In figure 6.3 the resulting magnitude and phase characteristic of the frequency response in lateral direction for the controllers with and without parameter errors are drawn. The conclusion from the frequency response in

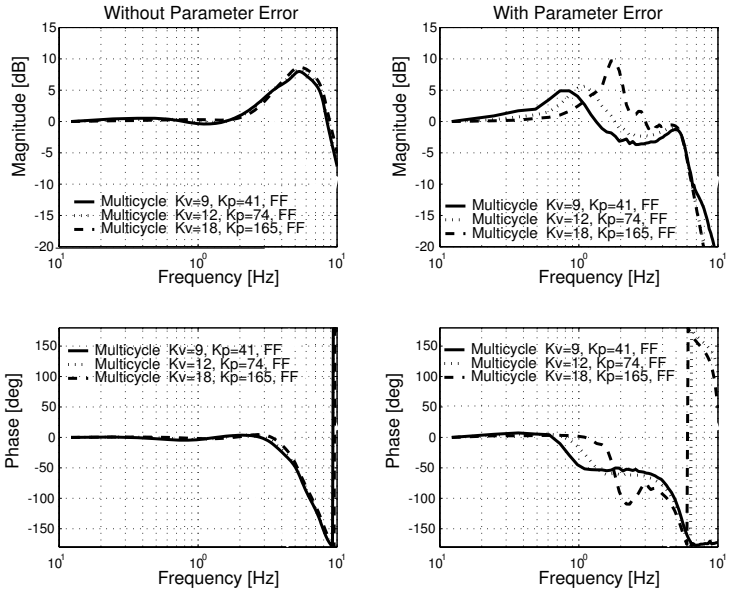

Figure 6.3: Frequency response in lateral direction for a controller with and without parameter errors.

lateral direction is that the magnitude using the controller without parameter errors is about 0 dB up to 1-2 Hz. The magnitude of about 0 dB is, as described before, expected. A resonance frequency around 5 Hz, which is equal to the damped roll eigenfrequency of the 4ws4wd model, is again visible. The frequency response using the controller with parameter errors shows again the behaviour of the "PD" part of the controller.
The conclusions from both the frequency responses is that the controller with feedforward, a K_p value of 165 and a K_v value of 18 is desired, so this controller will be used for the simulations and the experiments later on.

6.2.2 Trajectories

Two different types of trajectories will be used to test the performance of the multicycle controller in combination with the full dynamic model of the 4ws4wd car [15]. The trajectories are an eight shaped trajectory with a fixed orientation angle and a lane change with an orientation angle tangential to the trajectory. They are all obtained using a tool developed by TNO [15] that constructs the

trajectories from 5th order polynomials.
All the trajectories have a non-rolling start, from which the velocity tangential to the track is increased to a prescribed velocity level with a prescribed acceleration. At the end of the trajectory the velocity is decreased to zero with a prescribed deceleration. The velocity is kept constant between these two phases.
The maximum acceleration levels tangential to the trajectory are prescribed during the calculation. The acceleration levels perpendicular to the trajectory (centripetal acceleration) are a combination of the velocity tangential of the track and the radius of the corner(s) of the trajectory.
Different simulations with trajectories that have both low ($<3\ m/s^2$) and high ($>8\ m/s^2$) acceleration levels are performed. The errors of the position and the orientation angle of the center are, as expected, smaller if the acceleration levels are lower. This is expected, because the tyre slip is smaller if the accelerations are lower. Also the steering motor dynamics etc. are not that important if the trajectory has a low acceleration level profile.
The error of the position and the orientation angle of the center increase if the acceleration levels are increased. This is expected, because the tyre slip and the influence of the motor dynamics increase. To give a more absolute measurement for the position and orientation angle error, the root mean square error (6.6) values of two high acceleration trajectories (appendix H) are given in table 6.1.

$$RMSE = \sqrt{\frac{\sum_{i=1:n} e_i^2}{n}} \tag{6.6}$$

where e_i is the error and n is the total number of data-points.
The root mean square error is overall rather small (<2 cm for the position). The conclusion is that the RMSE for the eight shaped trajectory is larger than the RMSE for the lane change. This is because the region in time with tyre slip is larger for the eight shaped trajectory due to the two large corners. The peaks in the position errors of these trajectories, and also other trajectories that are simulated, also remain within the limits (e.g. maximum position error 0.05-0.1 m where a maximum of 0.5 is allowed). Also the orientation angle error that is measured is acceptable. Therefore, the conclusion is that the multicycle performs well over the whole working range with this WMR on simulation level. A more detailed discussion of some of these simulations in combination with experiments with the real 4ws4wd car of these trajectories can be found in the following chapter.

Table 6.1: Root mean square error for two different trajectories

high acceleration lane change	**high acceleration 8 trajectory**
x: 0.0045949	x: 0.016821
y: 0.0072361	y: 0.019394
θ: 0.00066521	θ: 0.0016563

6.3 Summary

A so called "multicycle controller" for the 4ws4wd car is derived and studied using a complete dynamic model of the 4ws4wd car used in the VEHIL test

facility. First, the longitudinal and lateral frequency responses are determined. Secondly, both high and low acceleration level manoeuvres are performed. The conclusion is that the controller performs well on the whole working range (0-10 m/s^2, 0-50 km/h). The following step is to test the controller in reality.

Chapter 7

Experimental results

The final step in the control design process is the testing of the controller in the reality. Here this means that the controller is used by the 4ws4wd car that is used in VEHIL. The trajectories that will be driven are trajectories that are already simulated in chapter 6, so the controller can handle the trajectories on simulation level. The trajectories that will be shown in this chapter have high acceleration levels, because these are the most challenging trajectories.
The maximum velocity during the experiments is 20 km/h, which is so low because of safety reasons. Two different trajectories will be used to test the multicycle controller in combination with the real 4ws4wd car. The trajectories are an eight shaped trajectory with a fixed orientation angle and a lane change with an orientation angle tangential to the trajectory. As already discussed in chapter 6, the eight shaped trajectory is chosen, because of the long fixed radius corner that causes a constant sideways slip. The lane change is chosen, because of the high frequency spectrum (appendix A). The trajectories are all obtained using a tool developed by TNO [15] that constructs a trajectory of 5th order polynomials.
All the trajectories have a non-rolling start, from which the velocity tangential to the track is increased to a prescribed velocity level with a prescribed acceleration. During the last part of the trajectory, the velocity is decreased to zero with a prescribed deceleration. The velocity is kept constant between these two phases. At the end, the car will stand still for a few seconds before the data logging will be stopped.
The controller is implemented in a real time Simulink model, which is capable of communicating with the 4ws4wd car. The actual position and velocity of the 4ws4wd car is estimated using a discrete Kalman filter in combination with a magnetic grid in the road surface [15]. Additional sensors, like encoders, are used in the design of the state estimator. This estimator is also implemented in the full dynamic model of the 4ws4wd car used for the simulations. The estimated position and velocity are used to evaluate the tracking of the 4ws4wd car.
The goal of the experiments is to check the performance of the multicycle controller in reality. It is chosen to compare the results with the simulations to see if the complete dynamic model is a correct representation of the real car. Known differences between the simulation model and the reality are:

1. The tyre parameters used in the model are not known in detail (in combination with the floor).
2. The floor in the simulation model is flat, but the floor in the hall is not totally flat.
3. The friction torque between the tyre and the road is not modelled in the simulation model.

Another goal of the experiments is to see if the slip compensation is a real advantage. The errors of the center of the car will be shown in different figures and also the root mean square error values will be calculated to check the performance. Sometimes also other figures (e.g. the steering torque) will be shown to explain non-expected results. The controller settings used are: K_p=165, K_v=18 and e_c=0.35, which have shown to be the best compromise for simulations (chapter 6).
In section 7.1.1 the results of the experiment of the high acceleration eight shaped trajectory will be presented. In section 7.1.2 the results of the experiment of the high acceleration lane change will be presented. Also a comparison will be made between the multicycle controller and the original controller that is used at this moment. Finally, a summary with some conclusions regarding the usefulness of the multicycle controller and the usefulness of the slip compensation will be given.

7.1 Experiments with multicycle controller

7.1.1 High acceleration eight shaped trajectory

First of all a high acceleration eight shaped trajectory with a fixed orientation angle is driven (see figure 7.1 and appendix H). From a non-rolling start (lon-

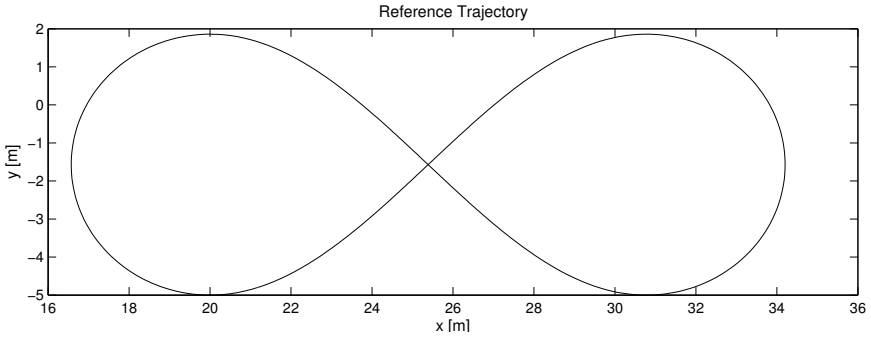

Figure 7.1: The reference xy of the high acceleration eight shaped trajectory

gitudinal direction is the x direction), the 4ws4wd car accelerates to 20 km/h with a maximum acceleration of 5 m/s^2. The tangential velocity of the track is kept constant at 20 km/h. The maximum acceleration in perpendicular direction of the trajectory is 9 m/s^2, which is a result of the tangential velocity and the radius of the corners of the eight shaped trajectory. At the end of the

trajectory, the velocity is reduced to zero again with a maximum deceleration of 5 m/s^2. The final part of the trajectory is a stand-still of three seconds.
The resulting errors for the high acceleration eight shaped trajectory with fixed orientation angle are drawn in figure 7.2. The errors of the experiment and the simulation with the multicycle controller without slip compensation (NSC) and the multicycle with slip compensation (WSC) are drawn. The two most

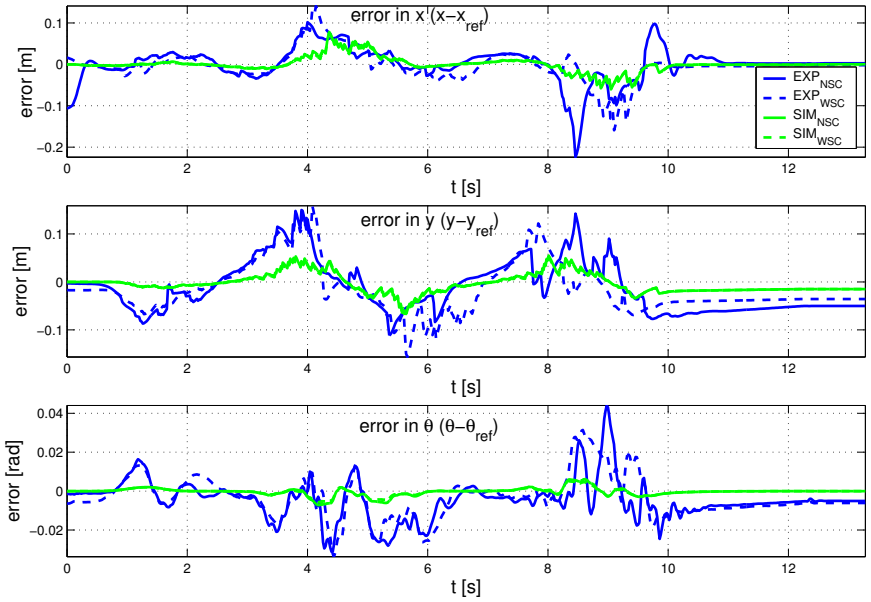

Figure 7.2: The resulting error in x, y, θ for the high acceleration eight shaped trajectory (error=measured-reference)

pronounced conclusions from the plots are that a difference is visible between the simulations and the experiments and that the advantage of the slip compensation is small compared to the total error for the experiments and (almost) not visible for for the simulations. First, the difference between the simulations and the experiments will be discussed.
The error in the x direction shows a starting error for one of the experiments. This is because the robot is put in its initial position using the original controller for the 4ws4wd car [15], which is not accurate in longitudinal directions at low velocities.
The error in the y direction shows a static error for the last 3 seconds of the trajectory. This is the phase that the car stands still at a fixed position. The car is standing still with the longitudinal direction in positive x direction. This error is the result of the chosen control method, which is output linearization. The zero-dynamics, which are the dynamics that remain if the car stands still, are that $\dot{\theta}_{ij} = 0$, so the orientation angle can have any fixed (θ_{ijt}) value as long as $z_{1ij} = z_{1ijref}$, so $z_{1xij} = x_{ijt} + e_c \cos(\theta_{ijt}) = z_{1xijref}$ and $z_{1yij} = y_{ijt} + e_c \sin(\theta_{ijt}) = z_{1yijref}$ are (ideal) solutions for the situation that the tyre stands still at the reference position of the virtual control point z_{1ij}. The car ends the trajectory with an error in the y direction, so $z_{1ij} \neq z_{1ijref}$.

Therefore, the car will steer the wheels so that that the measured output coordinates are equal to reference output coordinates, so that $z_{1ij} = z_{1ijref}$.
Overall the largest difference (spikes) in x and y direction for the simulations and the experiments can be found around 9 seconds. This is the moment that the car is reducing its velocity to zero again by braking. It was visible during the experiments that the car "moved" up and down during this phase, which is caused by bumps in the floor. This causes that e.g. the mass distribution is very different from what is expected, which finally results in the spikes in the position errors. During the rest of the trajectory a smaller difference is visible. The main reason for this difference can be found using figure 7.3 and 7.4. The real steering torque at the tyre is equal to the steering torque of the motors, which is illustrated in the figure(s), multiplied with a factor 59, which is the gearbox ratio. The real drive torque at the tyre is equal to the drive torque of the motors, which is illustrated in the figure(s), multiplied with a factor 5, which is the gearbox ratio.

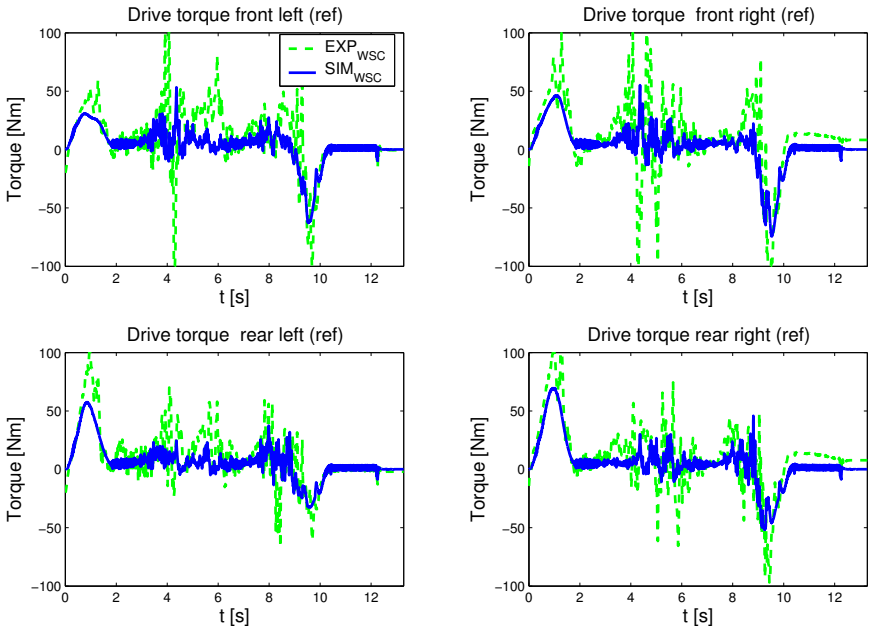

Figure 7.3: Drive torque eight shaped trajectory; actual torque with slip compensation (light), simulated torque with slip compensation (dark).

Figure 7.3 shows that the driving torque for the experiments is larger than the driving torque of the simulations. During the braking and acceleration phase of the trajectory this difference can be partly explained by a larger mass of the car than expected, because the mass of the car at this moment is not known in detail. The mass can be larger than expected due to the newest modifications of the 4ws4wd car. Also some non-modelled friction and losses in the drive motors and gearboxes is a factor [16]. In the "middle" phase of the trajectory, the difference can also be explained by the extra corrections that the controller has to make to compensate for the larger position errors.

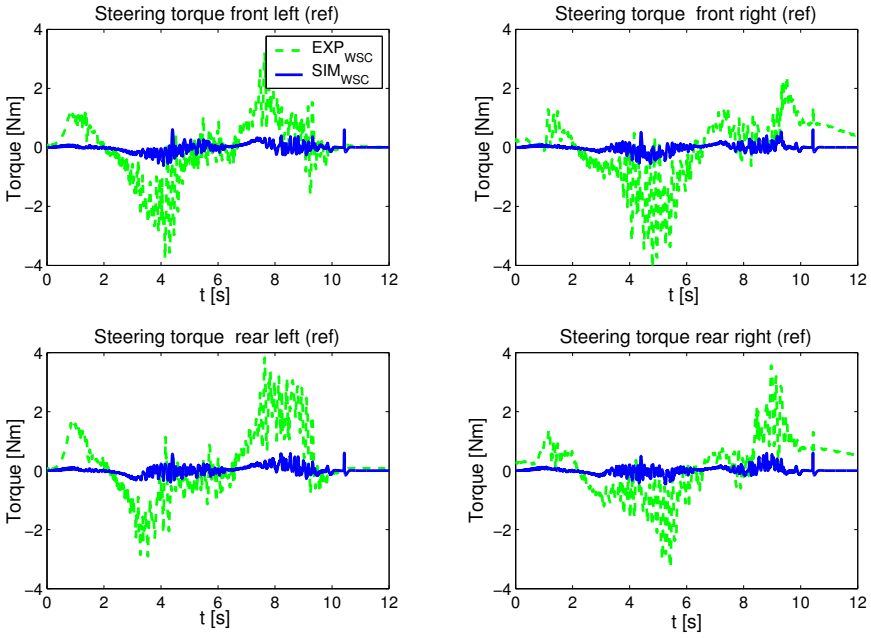

Figure 7.4: Steering torque eight shaped trajectory; actual torque with slip compensation (light), simulated torque with slip compensation (dark).

Figure 7.4 shows that the steering torque for the experiments is completely different than the steering torque of the simulations. The main reason for this is that the friction torque between the road and the tyre is not modelled in the full dynamic model of the 4ws4wd car that is used for the experiments. The most important non-modelled torque is the so-called "parking torque", which is the friction moment due to the width of the tyre. Due to the parking torque of the tyre a certain "deadzone" will result in the steering torque. Also some non-modelled friction torque in the bearings of the steering motors is present. This non-modelled friction torques are the main reason for the difference in position error between the results of the simulations and the experiments.

Overall the difference between the simulated and calculated orientation angle is large. This is due to a combination of the non-modelled friction torque and the further uncertainties in the parameters of the car (e.g. exact height of the center of gravity). However the error for the experiments is smaller than 2.5^o, so the error is still rather small compared to the error with the controller that is used at this moment. A brief discussion about the comparison between the multicycle and the controller that is used at this moment controller will follow later on in this chapter and a detailed discussion can be found in appendix I. The following step is to see if the slip compensation has a real advantage on the position error. It is hard to see the effect of the slip compensation in figure 7.2. Because of this, the root mean square error is calculated (see table 7.1). The result is that the controller with slip compensation, most of the time, performs better in the experiments and the simulations. The difference between the error

Table 7.1: Root mean square error for the high acceleration eight shaped trajectory

Exp NSC	Exp WSC	Sim NSC	Sim WSC
x: 0.041494	x: 0.036556	x: 0.017759	x: 0.016821
y: 0.054095	y: 0.053752	y: 0.020183	y: 0.019394
θ: 0.011029	θ: 0.011031	θ: 0.0020043	θ: 0.0016563

with slip compensation and without slip compensation is however rather small. The main reasons are the error due to the use of the kinematic orientation angle and the error due to the position and velocity estimator, which cause that the slip is just a small part of the total error. Another reason is that the measured signals are subjected to noise (especially the acceleration signals). The slip compensation uses these signals and also the derivatives of these signals. This causes that the calculated slip compensation term will not be as effective as possible.

7.1.2 High acceleration lane change

A high acceleration lane change with an orientation angle tangential to the trajectory is driven (see figure 7.5 and appendix H). From a non-rolling start,

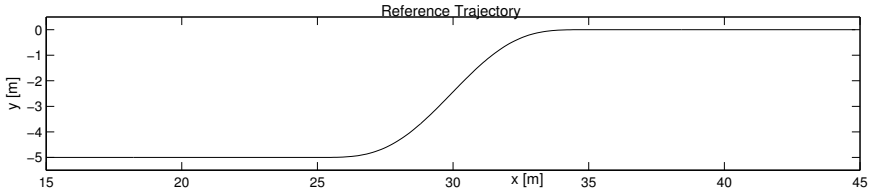

Figure 7.5: The reference xy of the high acceleration lane change

the 4ws4wd car accelerates in a straight line in x direction to 20 km/h with a maximum acceleration of 5 m/s^2. The tangential velocity of the track is kept constant at 20 km/h. The maximum acceleration in perpendicular direction of the trajectory is 9 m/s^2, which is a result of the tangential velocity and the radius of the corners of the lane change. At the end of the trajectory, the velocity is reduced to zero again in a straight line with a maximum deceleration of 5 m/s^2. The final part of the trajectory is a stand-still of two seconds.
The resulting errors for the high acceleration lane change with varying orientation angle are shown in figure 7.6. The errors of the experiments and the simulations with the multicycle controller without slip compensation (NSC) and the multicycle with slip compensation (WSC) are drawn. The two most pronounced conclusions from the plots are that the difference between the simulations and the experiments is larger compared to the difference for the high acceleration eight shaped trajectory and that the advantage of the slip compensation is again small compared to the total error for the experiments and (almost) not visible for for the simulations.
The trajectory starts with an error in the x and y direction, which is again

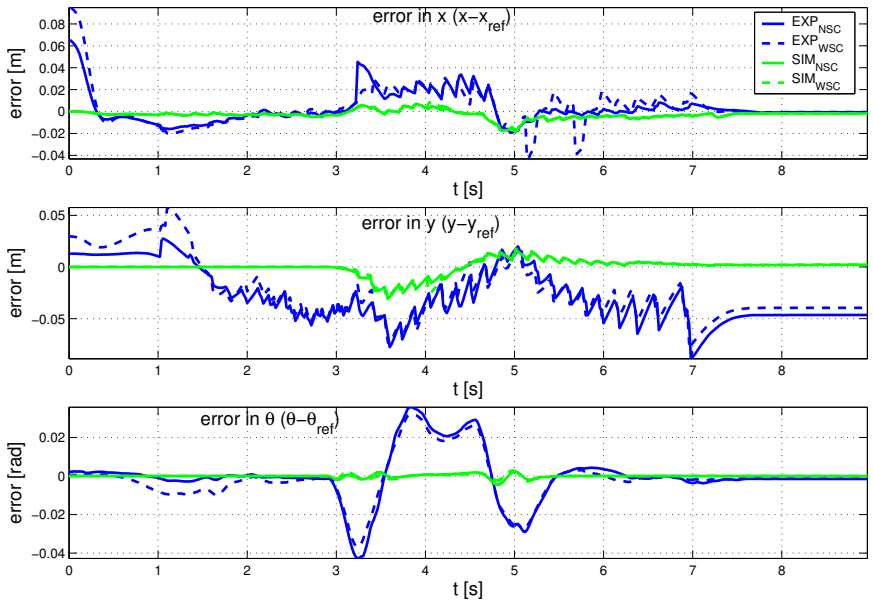

Figure 7.6: The resulting error in x, y, θ for the high acceleration lane change (error=measured-reference)

caused by the positioning of the 4ws4wd car at the start using the original controller [15]. The multicycle controller is capable of controlling the error in x direction, but has some problems controlling the error in the y direction. The main reason for this are the non-modelled friction torques that cause a certain deadzone in the steering torque. The controllers are trying to steer the wheels as can be seen in figure 7.7, but this does not result in a decrease of the error in the y directions directly. At 1.5 seconds the controller "suddenly" decreases the error in y direction, but an overshoot is visible. The controller again tries to steer the wheels, but now in different direction (different sign of the torque). Figure 7.8 shows what happens with the steering angles. The left wheels of the car are steered, but the right wheels are (almost) not steered during the first 3 seconds which is the acceleration phase in a straight line. The center of gravity is in the center of the car, so the explanation cannot be that the mass is distributed different as expected. The main reason is expected to be that the friction torque that causes the deadzone is larger at the right side of the 4ws4wd car compared to the left side of the car.
At the end of the trajectory, which is again a standstill of three seconds, the static error in the y direction is visible. This error is the result of the zero-dynamics in combination with the fact that the error in y at the end of the braking phase of the trajectory is not equal to zero. It is visible that the right steering angles are smaller than the left steering angles during the last three seconds. It is also visible that the right steering motors still have a static steering torque and that the left steering motors do not have a static steering torque. These two effects can be combined and be explained using the friction torque that causes a deadzone. Near the end of the braking phase of the trajectory

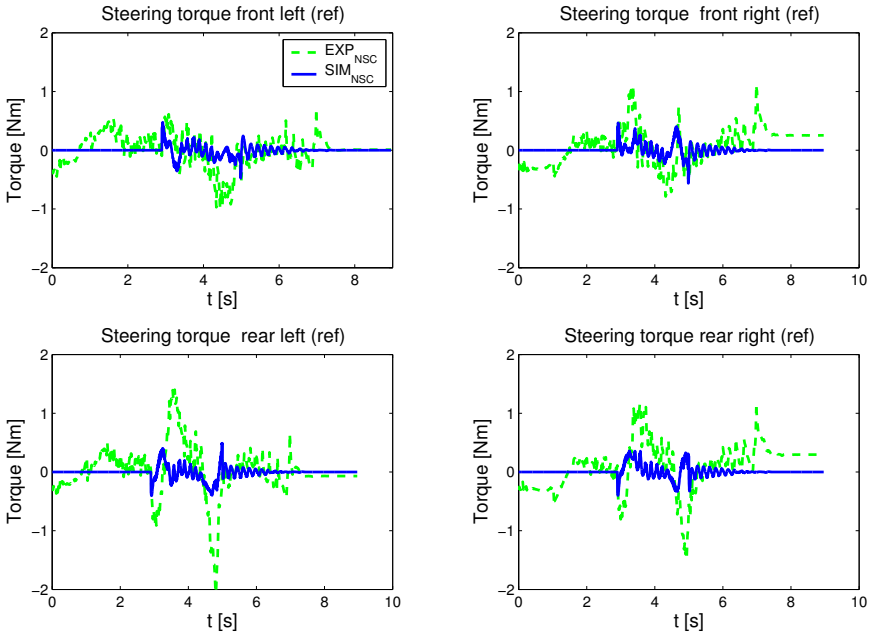

Figure 7.7: Steering torques lane change; actual torque without slip compensation (light), simulated torque without slip compensation (dark).

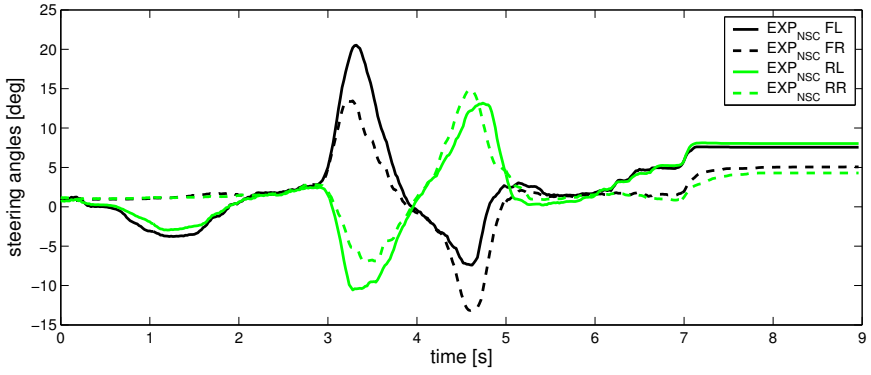

Figure 7.8: Steering angles for the lane change

a certain error in z_{1yij} remains for every tyre due to the error in y direction. This error is equal for all the tyres, because the orientation angle of the car is close to zero. The controller tries to reduce this error to zero (mostly) using a steering action. However, on the right side the friction torque is so large that a static error in z_{1yij} will remain for the right tyres causing a smaller steering angle and a residue steering torque.
During the evasive manoeuvre and the braking part of the trajectory it can be seen that the error is sawtooth shaped. As figure 7.9 shows, the measured position is sawtooth shaped. This shape is a result of the estimator that suddenly fails to deliver a smooth signal. A jump in the measured position is visible every time the estimator sees a magnet, which is every half meter. The controller is capable of handling this sawtooth shaped signal, so the controller proves to be robust. However the sawtooth shaped signal has a negative influence on the performance of the controller, so it is one of the reasons why the difference between the simulations and the experiments is so clear.
Overall the difference between the simulated and calculated orientation angle is large. This is due to a combination of the non-modelled friction torque, the further uncertainties in the parameters of the car (e.g. exact height of center of gravity) and the sawtooth shaped measured position. However the error for the experiments is smaller than 2.5^o, so the error is still rather small compared to the error with the controller that is used at this moment (see appendix I).

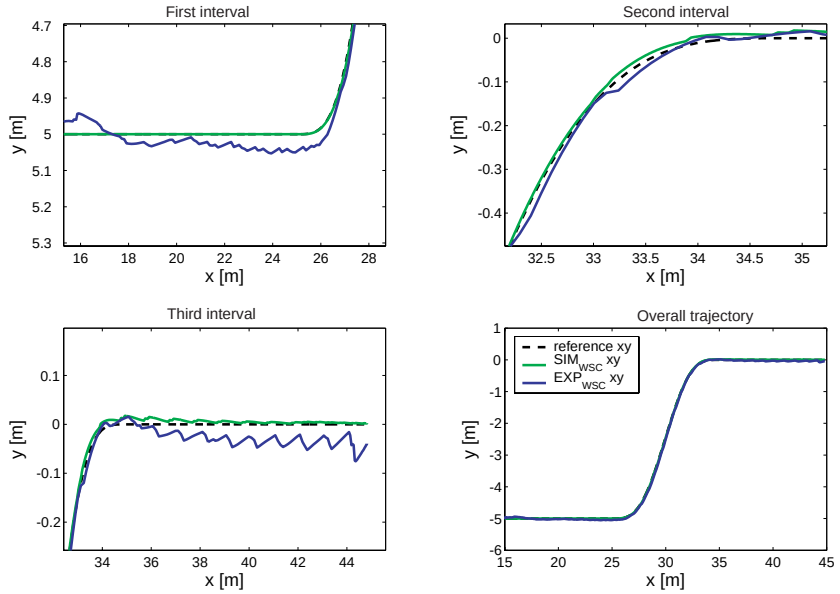

Figure 7.9: The lane change estimated xy plots

The following step is to see if the slip compensation has a real advantage on the position error. It is hard to see the effect of the slip compensation in figure 7.6. It is however visible that the slip compensation has a positive influence on the orientation angle error during the evasive manoeuvre. To get a more detailed

overview of the advantage, the root mean square error is calculated (see table 7.2).

Table 7.2: Root mean square error for the high acceleration lane change

Exp NSC	Exp WSC	Sim NSC	Sim WSC
x: 0.014156	x: 0.018113	x: 0.0046146	x: 0.0045949
y: 0.038248	y: 0.036089	y: 0.0072083	y: 0.0072361
θ: 0.013002	θ: 0.01179	θ: 0.00074871	θ: 0.00066521

The result is that the controller with slip compensation performs, in most cases, better in the experiments and the simulations. Only for the root mean square error in x direction for the experiments, it seems like the experiment with the slip compensation is far worse than the experiment without slip compensation. The reasons for this are, first that the starting error for the experiment with slip compensation is larger than for the experiment without slip compensation (figure 7.6) and secondly that two strange peaks in the x error, which are the result of the estimator, are visible around 5.5 seconds in figure 7.6.
Overall the difference between the error with slip compensation and without slip compensation is small, which has the same reasons as reported in section 7.1.1.

7.2 Comparison between multicycle and original controller

Here, a brief comparison will be made between the original controller, which is used at this moment for the path control of the 4ws4wd car used in VEHIL, and the multicycle controllers. The comparison will be done using the high acceleration lane change. The controllers are also compared using the low and high acceleration eight shaped trajectories. These results and also the total comparison can be found in appendix I.
The controller that is used at this moment for the path control has proven to be the best choice for the control for the 4ws4wd car over the last few years. This controller is a master slave controller. The master controller controls the position of the center of the vehicle and its orientation. To this end, the master controller outputs are a desired longitudinal and lateral force and a moment around the vertical axis, as if the vehicle is equipped with a virtual force actuator located in the center. The slave controller in fact 'distributes' these reference forces to the steering and driving torque of each wheel assembly, also taking essential tyre behaviour into account. The slave controller thus implements the virtual force actuator.
The resulting errors of the original controller, the multicycle controller without slip compensation and the multicycle with slip compensation for the high acceleration lane change with varying orientation angle are drawn in figure 7.10.
The conclusion is that there is a large difference between the original controller and the multicycle controllers. This difference is visible during the manoeuvre, but also at the end of the manoeuvre. This is the first sign that both controllers are totally different.

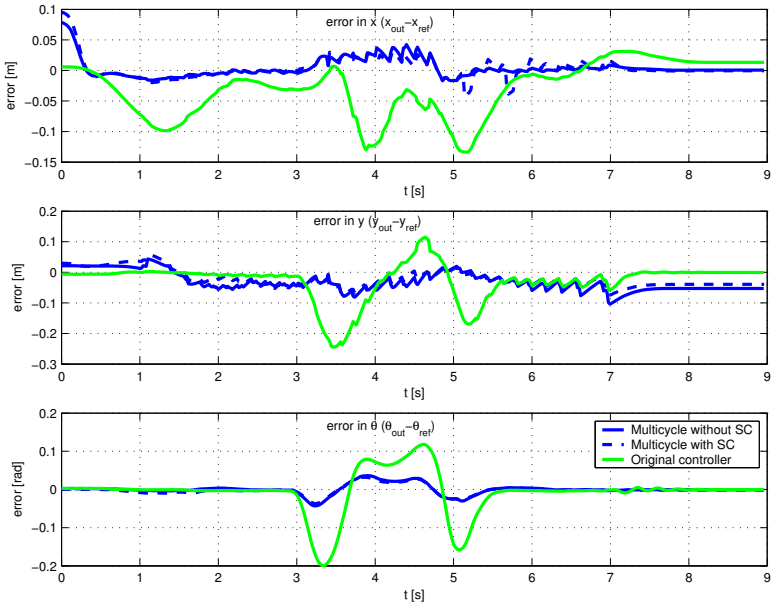

Figure 7.10: The resulting error in x, y, θ for the high acceleration lane change (error=measured-reference)

The steering and driving torque of the front left wheel are drawn in figure 7.11. The conclusions is that the original controller compensates the error more by steering its wheels and that the multicycle controller compensates the error more by driving the wheels. This can be concluded, because the steering torque signal for the original controller is larger and spikier than the steering torque signals of the multicycle controllers and the driving torque signal for the original controller is very different than the driving torque signals of the multicycle controllers.
Finally, the lateral and longitudinal accelerations are plotted in figure 7.12. Here it is visible that the response in lateral direction is far better for the multicycle controller than for the original controller. It looks like the original controller has a certain phase delay (lateral).
A comparison is made between the original and the multicycle controller. The conclusion is that the multicycle controller performs better than the original controller if high acceleration trajectories are driven. The difference is very clear for the lane change track. This can partly be explained looking a the frequency spectrum of a lane change and the frequency response in lateral direction of the car in combination with the controllers (appendix I). The frequency spectrum of a lane change has frequencies up to 1 Hz. The lateral frequency response of the car in combination with the multicycle controller is far better than the lateral frequency response of the car in combination with the original controller around 1 Hz (appendix I).
Another conclusion is that both control methods (original controller and multicycle controller) have a different way of compensating the error. The original controller compensates more by steering the wheels rather than driving

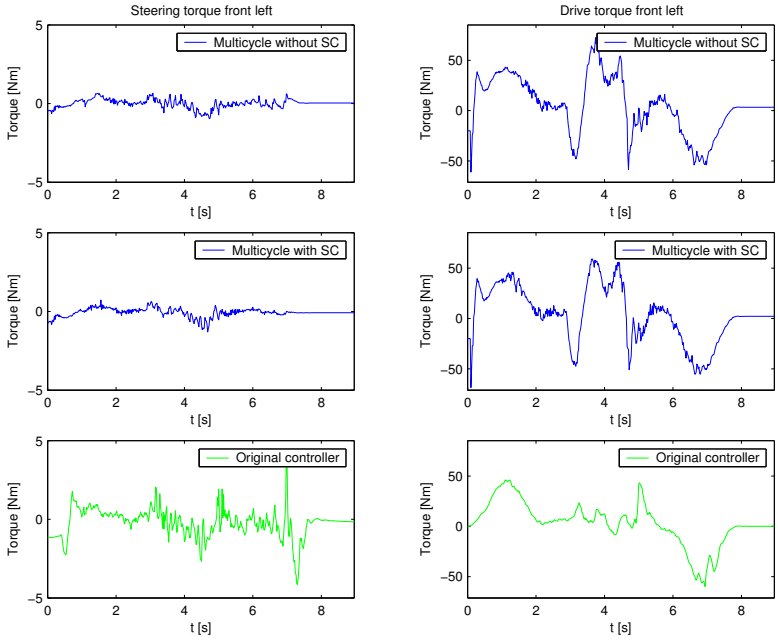

Figure 7.11: The steering and driving torques for the front left wheel for the high acceleration lane change.

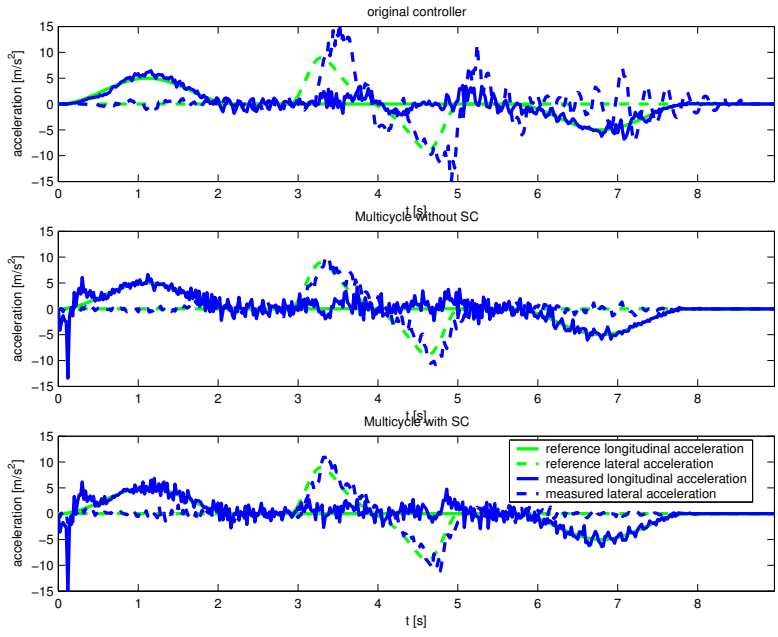

Figure 7.12: The lateral and longitudinal acceleration for the high acceleration lane change.

the wheels. The multicycle controller compensates more by driving the wheels rather than steering the wheels.
Whether the multicycle controller keeps performing well if the velocities are increased has to be determined. It is however expected that the multicycle controller remains to have a better tracking performance for high acceleration (lateral) manoeuvres where the accelerations increase and decrease fast.

7.3 Summary

The multicycle controller is reviewed using experiments and it is studied whether the tyre slip compensation has a positive influence on the resulting error in real situation.
Both the results of the simulations and the experiments are compared. The result is that the maximum position error for high acceleration reference signals is about 0.1 m, where a maximum position error of 0.5 m is allowed. The results of the simulations and the experiments are quite different. Overall the position error of the experiments is larger than expected from the simulations. The main reasons for this difference are:

1. Some non-modelled friction forces/torques (gearbox, parking moment tyres etc)

2. Parameter uncertainties (e.g. the mass of the car is not known in detail at this moment)

The result of the investigation of the tyre slip compensation is that the tyre slip compensation has a positive influence, but this influence is small. The main reasons for this are expected to be that:

1. The total error consists of an error due to the slip, but also consists of other errors, such as position estimation errors.

2. The slip compensation term consists of signals with a large signal to noise ratio (e.g. acceleration), so the slip compensation, as suggested by Motte and Campion [5], is not as effective as possible.

From the simulations and the experiments, the conclusion is that the multicycle controller itself is a good controller for the 4ws4wd car. It is however desired to perform more experiments to investigate how well the controller can handle more complicated trajectories (e.g. spinning around its vertical axis at a fixed point). Finally a comparison is made between the original controller that is used at this moment and the multicycle controller. The conclusion is that the multicycle controller has a better tracking performance than the original controller for the tested trajectories.

Chapter 8

Conclusions and recommendations

The control design for a four wheel steered and four wheel driven (4ws4wd) overactuated vehicle is considered in this report. Most attention is paid to the minimization of the position error during the driving of the trajectories. This is for example achieved by the implementation of a tyre slip compensation in the controller. Next to this, attention is paid to the steering behavior, especially for the reaction on lateral errors. The following conclusions and recommendations are the result of the research.

8.1 Conclusions

The first objective of this report is the development of a controller that can independently track the time dependent x and y positions of the center and the orientation angle θ of the 4wd4ws car over the whole working range (0-10 m/s^2, 0-50 km/h). The control objective over the velocity range differs. At high and medium velocities it is most important that the position error is as small as possible. At low velocities ($<$2 km/h) the steering angle behavior, as a reaction on position errors, is also or even more important.
The 4ws4wd car has eight actuators, which are the four steering and the four driving motors, and three degrees of freedom. Therefore, the system is an overactuated system.
In this report it is considered if the controllers that are developed in the wheeled mobile robot world can be used for the 4ws4wd car. During the literature survey it appeared that a lot of literature is available of the so called "unicycle" model, which is a model of a wheel that can be driven and steered. A control method, called the multicycle controller, that uses one of the available controllers for a unicycle model is developed.
The idea of the multicycle controller is to decentralize the control problem so that four subsystems remain (four corners). For every corner, a unicycle controller is developed. The controller itself consists of a state feedback controller, which in combination with the right output linearizing coordinates ("virtual control point"), linearizes the (sub)system. A PD feedback controller with acceleration feedforward is designed for this linearized system. In total,

the system consists of four unicycle controllers that together assure that the 4ws4wd robot car follows its desired trajectory.
The control method that is used in this report assures that the position error at high and medium velocities is low. The control method also assures that the steering behavior (as a reaction on position errors) is relaxed at low velocities.
The second objective of this report is the implementation of the tyre behavior in the controller. The most important tyre behavior that has to be modelled is the tyre slip. The tyre slip is implemented by investigating a unicycle with linear tyres. A controller from the field of robotics is developed for this system. The controller is based on the slow manifold approach. The idea behind the slow manifold approach is to define an invariant and attractive "slow manifold" on which the system is output linearizable. The same output coordinates and the same PD controller with feedforward is used to be able to compare the two controllers. The result is that both controllers are comparable, only the controller for the system with tyre slip has an extra term, the so called slip compensation term.

The controller is tuned and tested by means of simulations and experiments using the model and the real 4ws4wd robot car used in VEHIL.
The simulations show that the controller is capable of controlling the position of the center and the orientation angle of the car while driving different trajectories. On simulation level, the controller with slip compensation shows a better tracking behaviour than the controller without slip compensation. The controller with slip compensation is however not able to fully compensate for the position error due to the tyre slip. This is because the reference orientation angles of the wheels are calculated using a kinematic approach (i.e. neglecting tyre slip). This error reduces if the distance of the virtual control point from the center of the tyre is decreased. To fully reduce the error, the reference orientation angle has to be the kinematic orientation angle plus the estimated slip angle. It is however not possible yet to estimate the slip angle with great accuracy. That is the reason why the kinematic orientation angles are used as the reference signals instead.
The result of the experiments is that the controller is capable of controlling the position of the center and the orientation angle of the car while driving different trajectories. The trajectories that are driven have a relatively low velocity (max 20 km/h) because of safety reasons. The difference between the controller with and without slip compensation is less visible. This is mainly because the total error not only consists of an error related to the slip of the tyre, but also consists of other errors (e.g. position estimator). Another important reason is that the tyre slip compensation uses measured signals that have a large signal to noise ratio (e.g. acceleration), so the tyre slip compensation is not as effective as possible.

The final conclusion is that the multicycle controller is a controller that links two worlds, because it combines the control methods of the field of robotics (e.g. unicycle controllers) with the real world of complicated (e.g. a lot of weight transfer) cars with multiple steerable wheels. The control method for the unicycle that is used in this report is suited for the specific requirements of the 4ws4wd car used by TNO in VEHIL.
The slip compensation that is used in this report is one of the few slip compen-

sations found in the robotics literature. The conclusion is that the suggested slip compensation has an advantage for the tracking, but the advantage is rather small. Another method to compensate for the slip (angle) is suggested in this report (slip angle estimation), but the method is not yet implemented. The multicycle controller that is developed is a controller that meets the given objectives, but improvements are possible. Improvements and other remarks will be summed up in the recommendations.

8.2 Recommendations

Velocity dependency
The controller that is designed is a controller that controls a virtual point in front of the real tyre. This is done, so that a point tracking problem remains. The virtual point is at this moment attached at a fixed distance from the center of the wheel. However, it would be desired to reduce this distance at medium and high velocities to reduce the error due to the tyre slip. It also would be desired to increase this distance at low velocities to maintain the advantage of the steering behavior of the controller. Therefore it is recommended to implement a distance of the virtual control point (e_c) that is velocity dependent.

Estimator
A part of the position error from the experiments is the result of the estimator. The actual position and velocity of the 4ws4wd car is estimated using a discrete Kalman filter in combination with a magnetic grid in the road surface. The result is that the position estimation is not ideal, which has as a result that the controller doesn't work perfectly. The result is a larger position error than expected from simulations with a perfect feedback of the position and the velocity of the center. If an estimator that constantly measures the right position would be used, it is expected that the tracking error is decreased. A possible solution could be a local measuring system that is equal to a miniaturized GPS system.

Different unicycle controllers
The control method described in this report is suited for the specific requirements of the used WMR. However a lot of other control methods are known for the unicycle system, so it would be interesting to investigate if other control methods for the unicycle are suited for the control of a multiple wheeled mobile robot that has steerable wheels.

Slip angle feedforward
It would be an advantage if the reference orientation angle of the unicycles would consist of the kinematic orientation angle plus the estimated slip angle of the unicycle/tyre in stead of only the kinematic orientation angle. Therefore an estimator that can predict the slip angles of the tyres is desired.

Friction torque
It would be useful to expand the full dynamic model with the friction torque between the tyre and the road. The results of the simulations and the experiments are expected to be closer related to each other if the full dynamic model

is expanded with this friction torque. If the friction torque is known, then it is also possible to implement a feedforward of this signal in the controller so that the controller performance is improved.

Parameters
The multicycle controller is a state feedback controller. The exact values of the parameters of the system (mass, height of the center of gravity etc) are therefore important to achieve the maximum performance possible with the controller. At this moment not all the parameters of the car are known in detail so it is useful to determine them in detail. Also it would be useful to determine the tyre parameters, such as cornering stiffness and slip stiffness, in detail.

Tyre saturation
Real tyres can deliver a certain maximum force (lateral and longitudinal), which is dependent on the vertical force on the tyre. Above a certain slip angle, the lateral force will not increase anymore. Therefore, it is not desired that the controller steers the tyres even further if this certain slip angle is present because this will have no effect for the lateral force that is delivered. It can even decrease the lateral force for certain tyres and so the system can be destabilized. Therefore, a smart controller that can handle the tyre saturation has to be developed to stabilize the car around the maximum performance region.

Control method
In this report, a control method that decentralizes the tracking problem is suggested. It has proven to be a useful concept for the control of the 4ws4wd car and more general for WMR's with conventional steerable wheels. It is interesting to investigate if this control method can be used for other control problems such as positioning platforms that are equipped with multiple positioning motors.

Bibliography

[1] C. Canudas de Wit and P. Tsiotras, Dynamic tire friction models for vehicle traction control, 38th IEEE Conference on Decision and Control , Phoenix, AZ, Dec. 7-11, pp. 3746–3751, 1999.

[2] J.D. Bendtsen, P. Anderson and T.S. Pedersen, Robust feedback linearization-based control design for a wheeled mobile robot, 6th International Symposium on Advanced Vehicle Control, Hiroshima, Japan 9-13 September 2002

[3] G. Campion, G. Bastin and B. D'Andrea-Novel, Structural properties and classification of kinematic and dynamic models of wheeled mobile robots, IEEE transactions on robotics and automation, vol 12, no 1, February 1996

[4] B. D'Andrea-Novel and G. Campion and G. Bastin, Control of wheeled mobile robots not satisfying ideal velocity constraints: a singular perturbation approach, International Journal of Robust and Nonlinear Control, vol 5, 243-267(1995)

[5] I. Motte, G. Campion, Control of sliding mobile robots: a slow manifold approach, Mathematical Theory of Networks and Systems (MTNS 2000)

[6] M.L. Corradin and G. Orlando, Robust tracking control of mobile robots in the presence of uncertainties in the dynamical model, Journal of robotic Systems, vol 18(6), 317-323 (2001)

[7] M.L. Corradin, T. Leo and G. Orlando, Experimental testing of a discrete-time sliding mode controller for trajectory tracking of a wheeled mobile robot in the presence of skidding effects, Journal of robotic Systems, vol 19(4), 177-188 (2002)

[8] C. Canudas de Wit, B. Siciliano and G. Bastin, Theory of Robot Control, Springer 1996 ISBN 3-540-76054-7

[9] J.E. Slotine and W. Li, Applied Nonlinear Control, Prentice-Hall 1991, ISBN 0-13-040890-5

[10] J. Borenstein, Control and kinematic design of multi-degree-of-freedom mobile robots with compliant linkage, IEEE Transactions on Robotics and Automation,February 1995, Vol. 11, No. 1, pp. 21-35

[11] Mitschke, M., Dynamik der Kraftfahrzeuge, Band C: Fahrverhalten, Springer-Verlag Berlin, Heidelberg, Germany, 1990.

[12] G.F. Franklin, J.D. Powell and A. Emami-Naeini, Feedback control of dynamic systems, third edition, Addison-Wesley Publishing Company, Inc, 1994, ISBN 0-201-53487-8

[13] H. B. Pacejka, Tire and Vehicle Dynamics, October 2002, ISBN 0-7680-1126-4

[14] S. Sastry, Nonlinear systems; analysis, stability and control, Springer-Verslag New York, Inc, 1999, ISBN 0-387-98513-1

[15] TNO workdocument, werkpakket 02: Regeling en Simulatie

[16] S.H. van der Meulen, Validation, Improvement and Analysis of Moving Base Simulation Model, May 2004, DCT 2004.56

Appendix A

Tuning of the feedback controller

The tuning of the PD controller will be described in this appendix .
The concept of the control method described in this report is that, after the state feedback in combination with output linearization coordinates, a linear system of the form $\ddot{z}_1 = w$ remains. The variable w is an input that can consists of a feedforward acceleration signal and a position and velocity feedback loop (PD controller). The values of the PD controller have to be determined. The system is plotted in figure A.1.

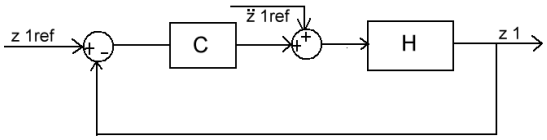

Figure A.1: z_1 system

To estimate the values of the PD controller the choice is made to neglect the feedforward for this moment, so the following system remains:

$$\ddot{z}_1 = K_p(z_{1ref} - z_{1mes}) + K_v(\dot{z}_{1ref} - \dot{z}_{1mes}) \tag{A.1}$$

where K_p is the P value of the controller and K_v is the D value of the controller. The remaining system is effectively a mass of 1 kg to where a damper and a spring are added by the PD controller.
The closed loop system can be written as $\frac{HC}{1+HC}$, where C is the PD controller and H is the representation of the mass of 1 kg, which is $\frac{1}{s^2}$.

$$Closedloop = \frac{something}{s^2 + K_v s + K_p} \tag{A.2}$$

where the dominator in general can be written as $s^2 + 2\beta\omega_n s + \omega_n^2$, where β is the damping ratio and ω_n is the undamped natural frequency. A common choice for the damping ratio is 0.7 [12], which results in a natural damped system.

The controller will be designed using the "bandwidth" design method. The idea is to design the controller so that the closed loop system will respond to signals that have a frequency smaller than the bandwidth and that the closed loop system will not respond to signals that have a frequency larger than the bandwidth. the normal time domain and the frequency spectra of some (severe) trajectories will be illustrated in figure A.2 - A.7 to evaluate how large the bandwidth of the system has to be.

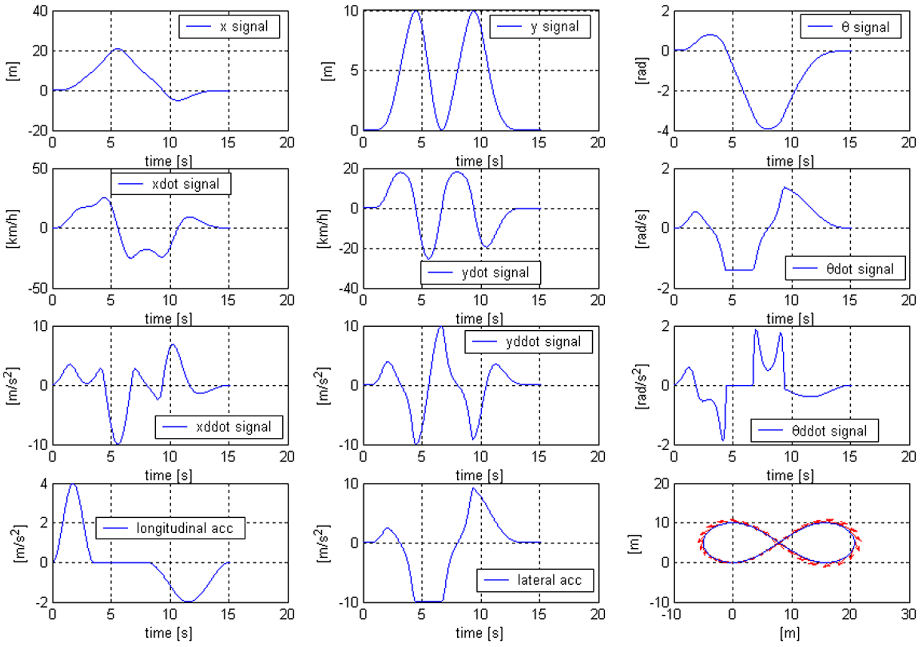

Figure A.2: Eight shaped trajectory - Time Domain

The result from the frequency spectra is that the lane change with varying orientation angle is the most demanding/severe reference signal. The most dominant frequencies can be found in the frequency range of 0-1 Hz. For this moment the choice is made to design three different controllers; one controller with a bandwidth of about 1.5 Hz, one controller with a bandwidth of about 2.5 Hz and one controller with a bandwidth of about 4 Hz. The first one should be good enough for the "normal" reference signals and the second and the third one can be used for the more "severe" reference signals. In the tuning process it is always possible to change the values of the PD controller, but these three controllers will give a good "estimation" of the minimum values of K_p and K_v. The closed loop systems are plotted in figure A.8 - A.10

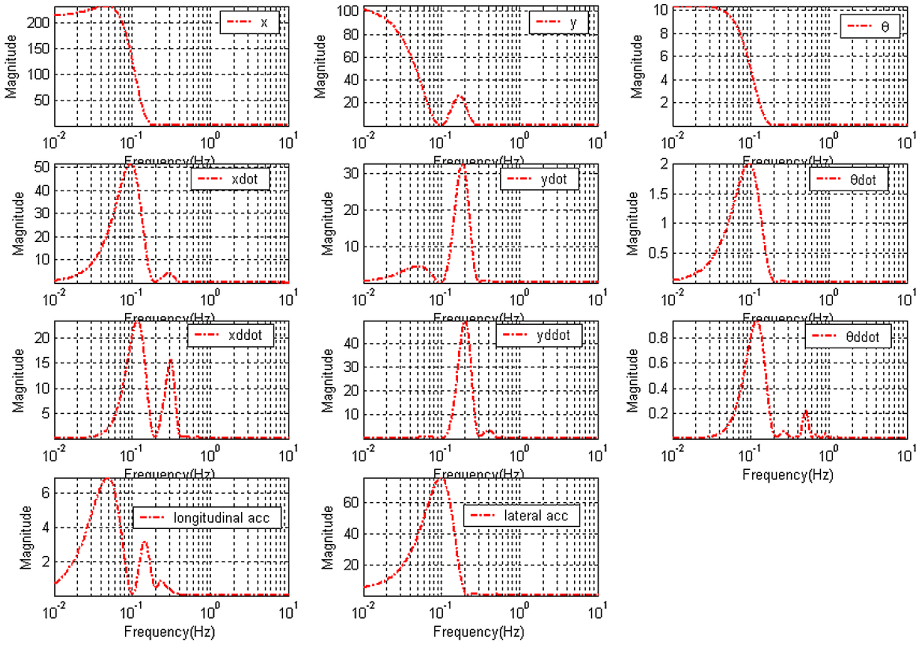

Figure A.3: Eight shaped trajectory- Frequency Spectrum

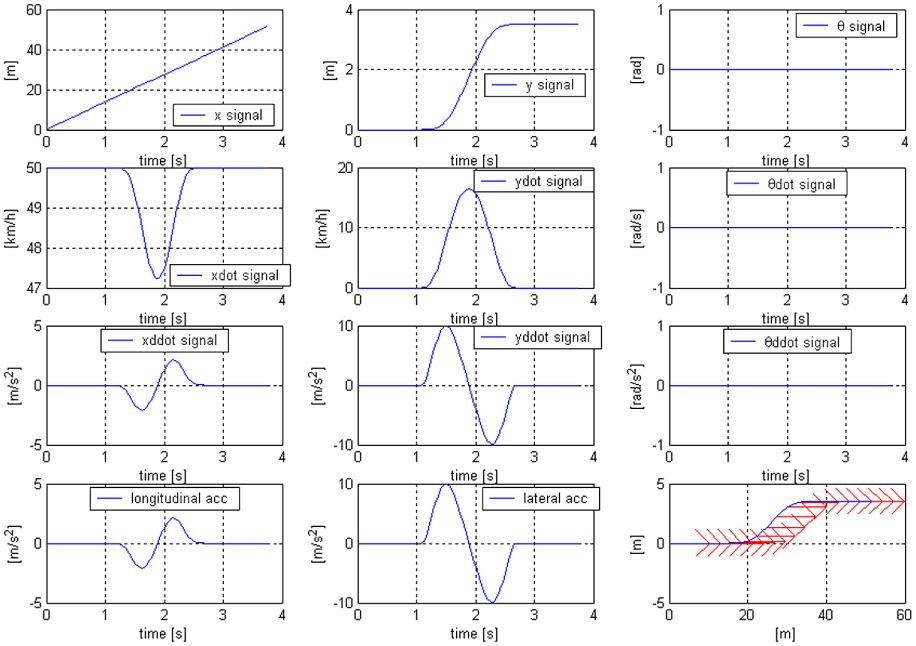

Figure A.4: Lane change (fixed orientation angle) - Time Domain

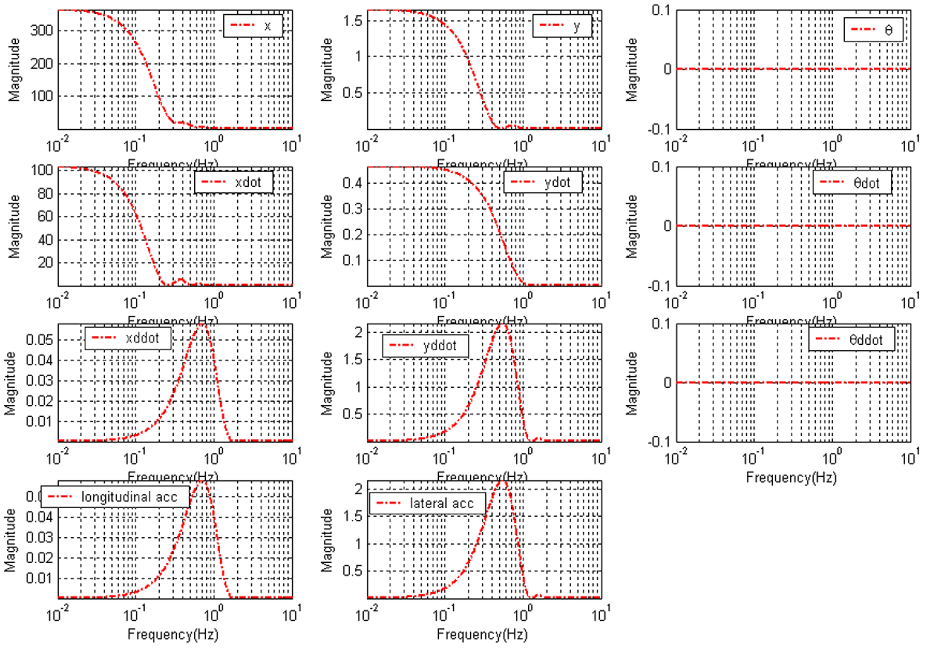

Figure A.5: Lane change (fixed orientation angle) - Frequency Spectrum

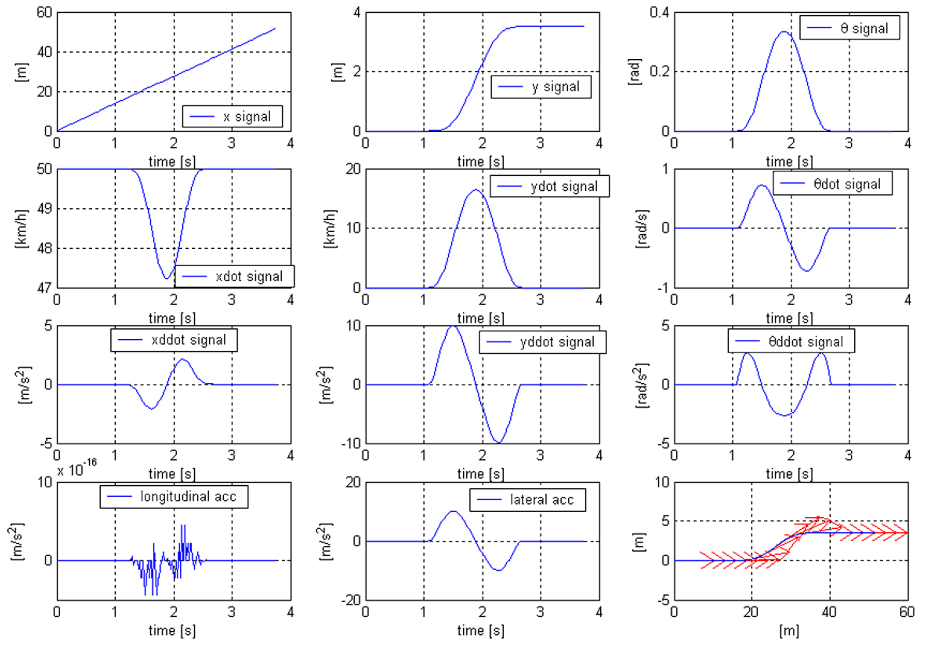

Figure A.6: Lane change (varying orientation angle) - Time Domain

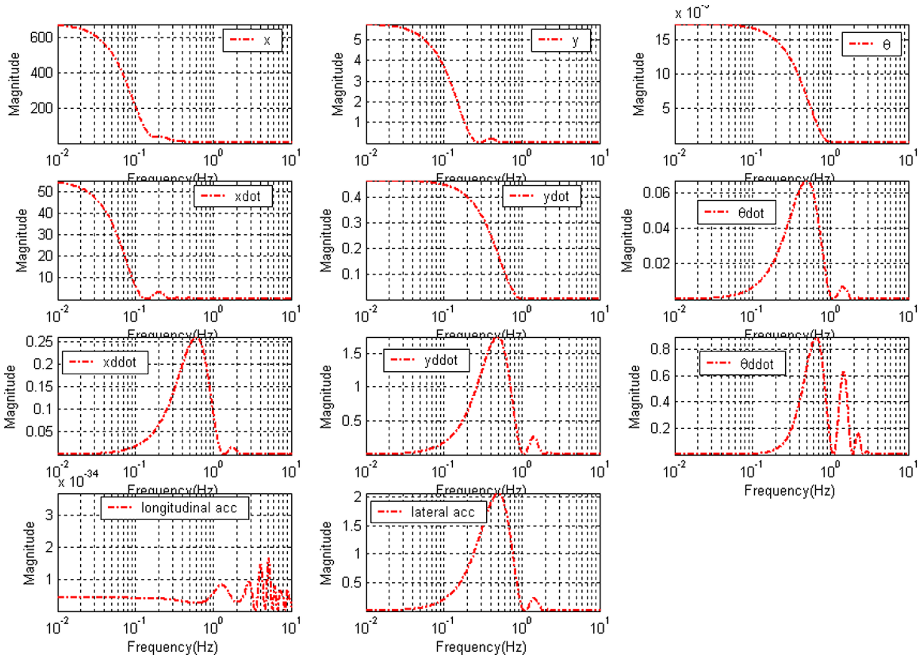

Figure A.7: Lane change (varying orientation angle) - Frequency Spectrum

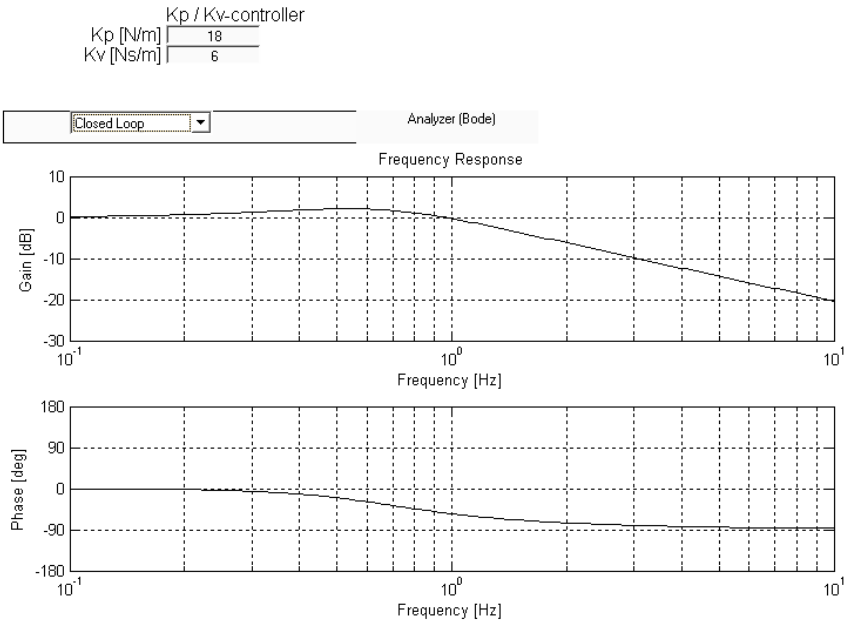

Figure A.8: Closed loop - 1.5 Hz

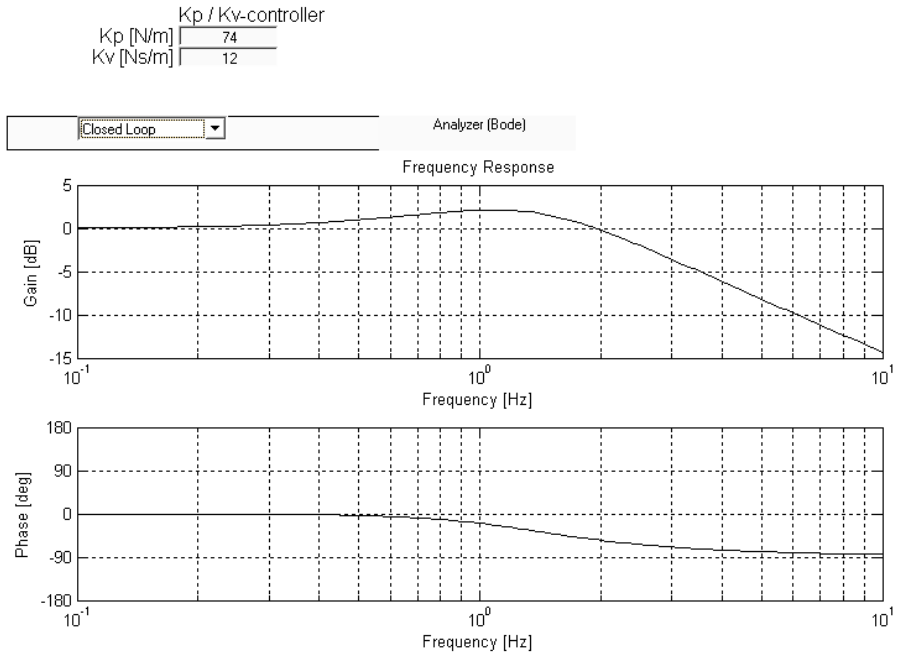

Figure A.9: Closed loop - 2.5 Hz

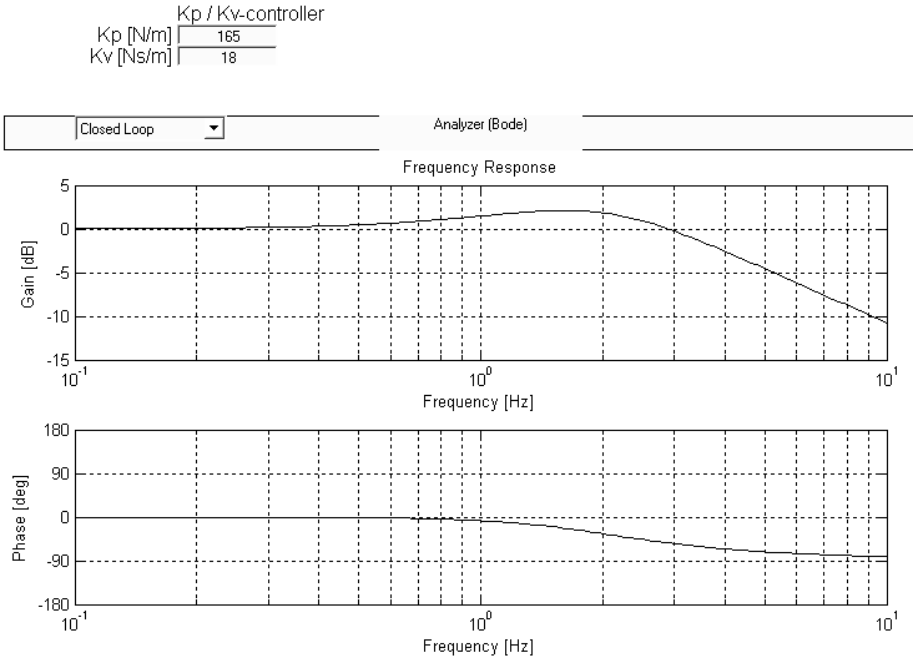

Figure A.10: Closed loop - 4 Hz

Appendix B

Fundamental tyre behavior

In this appendix, some fundamentals of the tyre-road contact behavior will be explained. In the first section the term "slip" is introduced. Then the pure slip characteristics on the basis of the so called Magic Formula [13] are discussed. These characteristics describe the relation between slip value and tyre force in the contact patch of tyre and road. Although these characteristics are highly non-linear (caused by the influence of vertical load and friction level), it is managed to describe them with a limited set of input parameters. It is not claimed that this model is a full proof representation of the behaviour of a real tyre. Nevertheless, this model allows a vehicle model to manoeuvre at limit performance without harming the reality notoriously.

B.1 Slip values

In figure B.1 a side and top view of a tyre is drawn. The left part (side view) shows the construction parts of the tyre and its rotational velocity ω. The wheel rim and thus the tyre center are towed over the road in longitudinal direction with a velocity v_{long}. The center of the rim is located at a distance above the road surface, which is defined by the loaded tyre radius R_l. This radius is smaller than the unloaded tyre radius due to the fact that the vertical load deflects and flattens the tyre near the contact patch. The slip point S is introduced. This imaginary point is attached to the wheel rim. In a free rolling condition, the point S is the momentary pole of the rotation of the wheel body. The distance of point S to the wheel center is defined as the effective rolling radius R_e. In general the effective rolling radius is larger than the loaded tyre radius but smaller than the unloaded tyre radius. By definition, the velocity of rolling v_r equals:

$$v_r = R_e\omega \tag{B.1}$$

In case of acceleration the longitudinal traction force F_{long} causes the slip point S to slide backwards over the road surface. This so called longitudinal slip velocity $v_{s,long}$ is defined as the difference between the rolling velocity of the wheel v_r and the forward velocity of the wheel center v_{long} :

$$v_{s,long} = R_e\omega - v_{long} \tag{B.2}$$

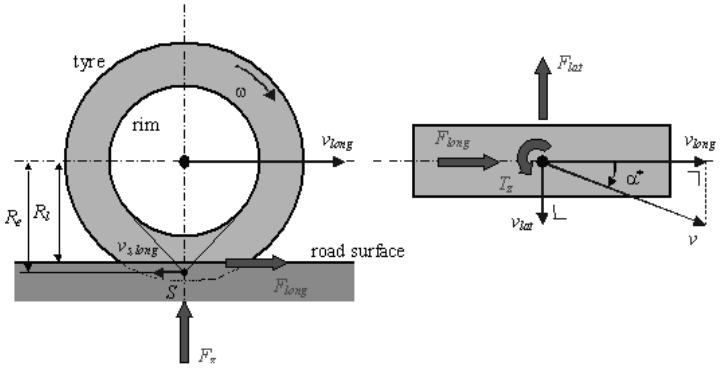

Figure B.1: The forces acting in the contact patch of slipping tyre during accelerating and cornering.

In vehicle dynamics the longitudinal slip κ is used as an input variable for computing the longitudinal tyre force and is defined by:

$$\kappa = \frac{v_{s,long}}{|v_{long}|} = \frac{R_e\omega - v_{long}}{|v_{long}|} \tag{B.3}$$

The absolute value of the longitudinal velocity v_{long} is used in the slip definition to make sure that the direction of the longitudinal slip velocity $v_{s,long}$ coincides with the direction of the generated slip force. For calculating the lateral tyre slip force F_{lat} the lateral slip velocity $v_{s,lat} = v_{lat}$ is used for determining the input slip value. In a lot of vehicle dynamics literature the orientation of the slip velocity v to the wheel plane, called the slip angle α^*, is used as an input for the lateral tyre force. In the Magic Formula [13] however, lateral slip is defined by the tangent of this slip angle, probably for consistency reasons with the longitudinal slip κ, reading:

$$\alpha = \tan(\alpha^*) = \frac{v_{lat}}{|v_{long}|} \tag{B.4}$$

The same argumentation for the absolute value of v_{long} in this formula can be used as in B.3. At low levels of longitudinal and lateral slip the relationship between slip force and slip value can be approximated by linear functions containing the coefficient G_b and D_b:

$$F_{long} = G_b\kappa \tag{B.5}$$

$$F_{lat} = D_b\alpha \tag{B.6}$$

At large levels of slip, these relationships no longer hold as the increase of traction and cornering forces are no longer proportional to the increasing slip values. The friction between tyre and road limits the maximum level of forces and moments. In the Steady-State Tyre Characteristics section a formula is introduced which is capable of describing the non-linear relationship between force and slip: the Magic Formula model.

B.2 Steady-State Tyre Characteristics (pure slip condition)

The steady-state force generation of the tyre is highly non-linear with respect to slip. In figure B.2 a typical diagram of a tyre force under pure longitudinal or lateral slip conditions are shown.

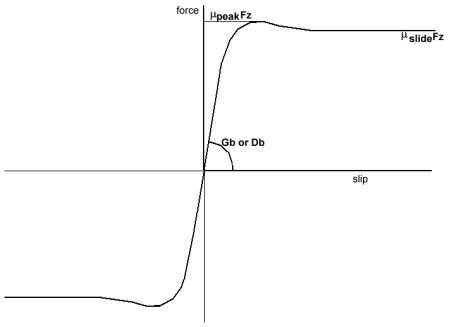

Figure B.2: Typical tyre force-slip diagram

The conclusion can be that at low values of the slip (B.5) and (B.6) are valid. At higher values of the slip, a saturation point is reached. The tyre forces reach a maximum value, that is equal to:

$$F_{long} = \mu_{long} F_z \tag{B.7}$$

$$F_{lat} = \mu_{lat} F_z \tag{B.8}$$

where μ_{long} and μ_{lat} are the longitudinal and lateral friction coefficient.
The longitudinal force generation is influenced by lateral slip and vice versa. This is because a tyre can deliver a certain total force. So if there is a certain lateral force, then the maximum longitudinal force that can be generated will be lower. So if there is both a lateral slip and a longitudinal slip, then both forces will be influenced by each other. This effect is the reason why a normal front wheel driven passenger car will loose grip in a corner if the driver has to brake hard in the corner. This effect is called combined slip, which can be plotted as a circle, the so called friction circle. An example of a a friction circle is shown in figure B.3.
In practice the friction circle will be more elliptically shaped.
Another important aspect in the behavior of the tyre is the influence of the vertical wheel load F_z. The basis coulomb friction law states that the maximum friction force is proportional to the friction coefficient multiplied by the load between the two surfaces. However, in practice, the tyre behavior also has non-linearities in this respect. Both μ_{long} and μ_{lat} are a function of the wheel load.
For modelling the non-linear tyre characteristics an empirical tyre model, the Magic Formula, is chosen. This model is based on a set of mathematical expressions, with coefficients that are strongly related to the physical tyre properties (friction level, slip stiffness, etc), representing experimental tyre data. The advantage of such an empirical model over modelling the tyre structure itself is

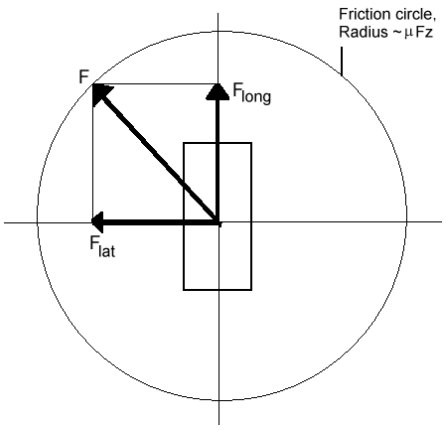

Figure B.3: Schematic description of the friction circle.

that its computational load in a computer simulation is much lower. The Magic Formula was first presented in 1987, and since then many revisions have been made. A short summary and an explanation of the adaptation to reduce the number of input parameters to a minimum will be given here.
The general shape of the Magic Formula for describing the pure slip characteristics is a sine function with an arctangent as an argument:

$$F = D\sin(C\arctan(Bx)) \tag{B.9}$$

where F stands for the steady-state tyre characteristic and x denotes the slip value κ or α . The coefficients B, C and D characterize the shape of the slip characteristics. Each coefficient represents a specific aspect of the slip characteristic: the shape factor C influences the overall shape of the characteristic and the peak factor D influences the maximum value of the characteristic. The coefficient B is called stiffness factor because, when multiplied by C and D, it defines the slip stiffness (G_b or D_b) ($= BCD$) and thus influences the slope of the characteristic at low values of slip. The real Magic Formula uses an enormous amount of parameters to describe the load, camber, ply-steer and friction dependencies of its coefficients. All these parameters have to be defined and validated for every new tyre mounted to the car.
As stated, the magnitude of the tyre forces is strongly dependent on the vertical wheel load F_z. Therefore the normalized slip characteristic is introduced, which is merely a division of the tyre force F (B.9) by the vertical wheel load F_z. The normalized characteristic is merely an approximation but well accepted in literature by Pacejka et al [13]. The normalized tyre model coefficients are denoted with the norm subscript. The result is that as an approximation the tyre behavior can be modelled with only one curve in longitudinal and lateral direction.
Finalizing, the non-linear steady-state combined longitudinal tyre force F_{long} and the lateral tyre force F_{lat} are given by:

$$F_{long}(\kappa, \alpha, F_z) = G(\kappa, \alpha)_{long} F_{long,norm}(\kappa) F_z \tag{B.10}$$

$$F_{lat}(\kappa, \alpha, F_z) = G(\kappa, \alpha)_{lat} F_{lat,norm}(\alpha) F_z \tag{B.11}$$

where $G(\kappa, \alpha)_{long}$ and $G(\kappa, \alpha)_{lat}$ are the weight functions for the interaction of the longitudinal and lateral slip.
In reality the steady state situation is not reached instantaneously. It takes a certain distance/time before the tyre can deliver the steady state forces. This effect is called the "transient behavior". The choice is made to not discuss this effect here. If one is interested in this effect, then the book called Tire and Vehicle Dynamics by Pacejka [13] is a good starting point to get more information.

Appendix C

Wheeled mobile robot bicycle controller

In this appendix, the model and controller for a bicycle will be discussed. The model and controller are directly derived from the theory on wheeled mobile robots without tyre slip. The appendix is written so that it can be read in combination with chapter 4, which is the chapter that describes the general procedure.

C.1 Bicycle model

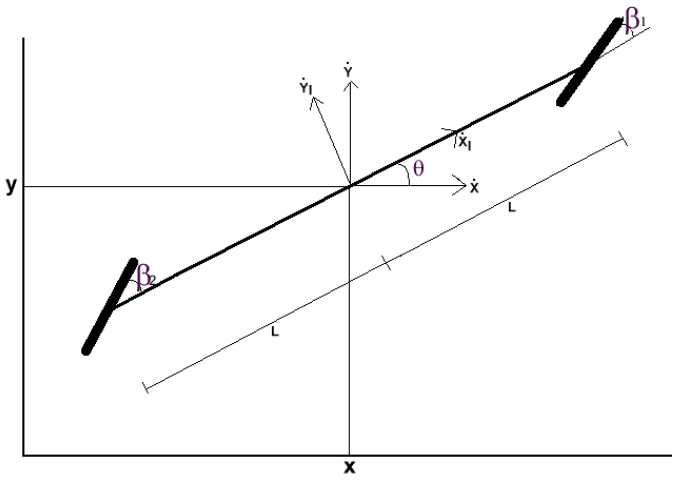

Figure C.1: Bicycle model

The bicycle model, that will be studied here, consists of two wheels that can be driven and steered separately (figure C.1). The seven global variables (n=7) are the position of the center x and y, the orientation angle θ, the steering angles

β_1 and β_2 and the rotation angles of the wheels φ_1 and φ_2.

$$q = \begin{pmatrix} x \\ y \\ \theta \\ \beta_1 \\ \beta_2 \\ \varphi_1 \\ \varphi_2 \end{pmatrix} \tag{C.1}$$

The bicycle itself has also local coordinates, which are x_l, y_l and θ. The transformation matrix $R(\theta)$ (4.1) can be used to switch between the local and global velocities and accelerations. In total there are four constraints (m=4); two roll constraints and two slip constraints.
It is important to define some variables (see figure 4.2) for both wheels before the constraints can be defined. These variables for wheel 1 are: $\alpha = 0$, $\beta = \beta_1$ and $L = L$. These variables for wheel 2 are: $\alpha = \pi$, $\beta = \beta_2$ and $L = L$. The slip constraints can now be written, using 4.3, as:

$$C_1 R(\theta)\dot{\xi} = \begin{pmatrix} \sin(\beta_1) & -\cos(\beta_1) & -L\cos(\beta_1) \\ -\sin(\beta_2) & \cos(\beta_2) & -L\cos(\beta_2) \end{pmatrix} R(\theta) \begin{pmatrix} \dot{x} \\ \dot{y} \\ \dot{\theta} \end{pmatrix} = 0 \tag{C.2}$$

The roll constraints can be written, using 4.4, as:

$$J_1 R(\theta)\dot{\xi} + J_2\dot{\varphi} = \begin{pmatrix} \cos(\beta_1) & \sin(\beta_1) & L\sin(\beta_1) \\ -\cos(\beta_2) & -\sin(\beta_2) & L\sin(\beta_2) \end{pmatrix} R(\theta) \begin{pmatrix} \dot{x} \\ \dot{y} \\ \dot{\theta} \end{pmatrix} + \begin{pmatrix} r & 0 \\ 0 & r \end{pmatrix} \begin{pmatrix} \dot{\varphi}_1 \\ \dot{\varphi}_2 \end{pmatrix} = 0 \tag{C.3}$$

These constraints can be written in the standard form $A^T\dot{q} = 0$:

$$A^T\dot{q} = \begin{pmatrix} \sin(\beta_1+\theta) & -\cos(\beta_1+\theta) & -L\cos(\beta_1) & 0 & 0 & 0 & 0 \\ -\sin(\beta_2+\theta) & \cos(\beta_2+\theta) & -L\cos(\beta_2) & 0 & 0 & 0 & 0 \\ \cos(\beta_1+\theta) & \sin(\beta_1+\theta) & L\sin(\beta_1) & 0 & 0 & r & 0 \\ -\cos(\beta_2+\theta) & -\sin(\beta_2+\theta) & L\sin(\beta_2) & 0 & 0 & 0 & r \end{pmatrix} \begin{pmatrix} \dot{x} \\ \dot{y} \\ \dot{\theta} \\ \dot{\beta}_1 \\ \dot{\beta}_2 \\ \dot{\varphi}_1 \\ \dot{\varphi}_2 \end{pmatrix} = 0 \tag{C.4}$$

It is now possible to determine the degree of mobility and the degree of steerability using (4.12) and (4.13). The degree of mobility is equal to 1 and the degree of steerability is 2. The degree of steerability is 2, which is obvious, because there are two independent conventional steering wheels attached to the body. The degree of mobility is 1. Physically this means that the bicycle can only move in one direction without re-orienting its conventional steering wheels (e.g driving on a circle. The only direction in which the bicycle can move without

re-orienting the steering wheels is on the circle). So the only possible movement is the rotation about the instantaneous center of rotation that is constructed from the two perpendiculars to the planes of the wheels. The result is that a bicycle is a type-(1,2) robot as described in [3].
The following step is to define the posture kinematic model. First of all it is important to calculate the matrix $\Sigma(\beta)$, which is a matrix where the columns form a basis of the null-space of C_1 ($C_1\Sigma(\beta) = 0$). It is known that $R(\theta)\dot{\xi} = \Sigma(\beta)\eta_a$ (see section 4.1.1), where η_a is an input-vector of dimension δ_m. Because of this, a possible expression for $\Sigma(\beta)$ is:

$$\Sigma(\beta) = \begin{pmatrix} L\cos(\beta_1 - \beta_2) + L\cos(\beta_1 + \beta_2) \\ L\sin(\beta_1 + \beta_2) \\ \sin(\beta_1 - \beta_2) \end{pmatrix} \tag{C.5}$$

Knowing that there are two conventional steering wheels the *posture kinematic model* can be written as:

$$\begin{pmatrix} \dot{\xi} \\ \dot{\beta} \end{pmatrix} = \begin{pmatrix} R^T(\theta)\Sigma(\beta) & 0 \\ 0 & I \end{pmatrix} \begin{pmatrix} \eta_a \\ \zeta \end{pmatrix} = \begin{pmatrix} \frac{1}{2}L\cos(\theta+\beta_1-\beta_2) + \frac{1}{2}L\cos(-\theta+\beta_1-\beta_2) + L\cos(\theta+\beta_1+\beta_2) & 0 & 0 \\ \frac{1}{2}L\sin(\theta+\beta_1-\beta_2) - \frac{1}{2}L\sin(-\theta+\beta_1-\beta_2) + L\sin(\theta+\beta_1+\beta_2) & 0 & 0 \\ \sin(\beta_1-\beta_2) & 0 & 0 \\ 0 & 1 & 0 \\ 0 & 0 & 1 \end{pmatrix} \begin{pmatrix} \eta_a \\ \zeta_1 \\ \zeta_2 \end{pmatrix} \tag{C.6}$$

,where η_a is the "velocity" of the bicycle and ζ_1 and ζ_2 are the steering velocities of the wheels.

The following step is to define the *configuration kinematic model*, which is:

$$\begin{pmatrix} \dot{\xi} \\ \dot{\beta} \\ \dot{\varphi} \end{pmatrix} = \begin{pmatrix} R^T(\theta)\Sigma(\beta) & 0 \\ 0 & I \\ -J_2^{-1}J_1\Sigma(\beta) & 0 \end{pmatrix} \begin{pmatrix} \eta_a \\ \zeta \end{pmatrix} = \begin{pmatrix} \frac{1}{2}L\cos(\theta+\beta_1-\beta_2) + \frac{1}{2}L\cos(-\theta+\beta_1-\beta_2) + L\cos(\theta+\beta_1+\beta_2) & 0 & 0 \\ \frac{1}{2}L\sin(\theta+\beta_1-\beta_2) - \frac{1}{2}L\sin(-\theta+\beta_1-\beta_2) + L\sin(\theta+\beta_1+\beta_2) & 0 & 0 \\ \sin(\beta_1-\beta_2) & 0 & 0 \\ 0 & 1 & 0 \\ 0 & 0 & 1 \\ \frac{-2L\cos(\beta_2)}{r} & 0 & 0 \\ \frac{2L\cos(\beta_1)}{r} & 0 & 0 \end{pmatrix} \begin{pmatrix} \eta_a \\ \zeta_1 \\ \zeta_2 \end{pmatrix}$$
$$\rightarrow \dot{q} = S(q)\eta \tag{C.7}$$

The following step is to determine the configuration dynamic model. First of all an extra dynamic equation has to be introduced.

$$M(q)\ddot{q} = C(q,\dot{q}) + F + B\tau \tag{C.8}$$

The force vector consists of lagrange forces, which are (internal) forces that assure that the constraints are not violated. It is assumed that no resistance

forces are present. The bicycle has four different torque inputs; the driving and steering motor torques. These torques are implemented so that a positive torque will result in an increase of the acceleration in longitudinal direction if the steering angles are zero.
For the unicycle model the matrices M, C, τ and B are:

$$M = \begin{pmatrix} m & 0 & 0 & 0 & 0 & 0 & 0 \\ 0 & m & 0 & 0 & 0 & 0 & 0 \\ 0 & 0 & I_\theta & 0 & 0 & 0 & 0 \\ 0 & 0 & 0 & I_s & 0 & 0 & 0 \\ 0 & 0 & 0 & 0 & I_s & 0 & 0 \\ 0 & 0 & 0 & 0 & 0 & I_\varphi & 0 \\ 0 & 0 & 0 & 0 & 0 & 0 & I_\varphi \end{pmatrix} \tag{C.9}$$

$$C = 0 \tag{C.10}$$

$$F = A\lambda \tag{C.11}$$

$$\tau = \begin{pmatrix} \tau_{s1} \\ \tau_{s2} \\ \tau_{d1} \\ \tau_{d2} \end{pmatrix} \tag{C.12}$$

$$B = \begin{pmatrix} 0 & 0 & 0 & 0 \\ 0 & 0 & 0 & 0 \\ 0 & 0 & 0 & 0 \\ 1 & 0 & 0 & 0 \\ 0 & 1 & 0 & 0 \\ 0 & 0 & -1 & 0 \\ 0 & 0 & 0 & 1 \end{pmatrix} \tag{C.13}$$

where m is the mass of the bicycle, I_θ is the inertia of the bicycle around the vertical axis, I_φ is the rotation inertia of the steering wheels, I_s is the orientation inertia of the steering wheels, τ_{di} is the driving torque of wheel i ($i = 1, 2/f(ront), r(ear)$) and τ_{si} is the steering torque .
To be able to write down the configuration dynamic model, as described by (4.25), the matrix $\dot{S}(q, \dot{q})$ has to be defined.

$$\dot{S} = \begin{pmatrix} \dot{S}_{11} & 0 & 0 \\ \dot{S}_{21} & 0 & 0 \\ (\zeta_1 - \zeta_2)\cos(\beta_1 - \beta_2) & 0 & 0 \\ 0 & 0 & 0 \\ 0 & 0 & 0 \\ \frac{2\zeta_2 \sin(\beta_2)}{r} & 0 & 0 \\ \frac{-2\zeta_1 \sin(\beta_1)}{r} & 0 & 0 \end{pmatrix} \tag{C.14}$$

where

$$\begin{aligned} \dot{S}_{11} = &-\tfrac{1}{2}L(\eta_a \sin(\beta_1 - \beta_2) + \zeta_1 - \zeta_2)\sin(\theta + \beta_1 - \beta_2) - \\ &\tfrac{1}{2}L(-\eta_a \sin(\beta_1 - \beta_2) + \zeta_1 - \zeta_2)\sin(-\theta + \beta_1 - \beta_2) - \\ &L(\eta_a \sin(\beta_1 - \beta_2) + \zeta_1 + \zeta_2)\sin(\theta + \beta_1 + \beta_2) \end{aligned} \tag{C.15}$$

$$\begin{aligned}\dot{S}_{21} = &\tfrac{1}{2}L(\eta_a \sin(\beta_1 - \beta_2) + \zeta_1 - \zeta_2)\cos(\theta + \beta_1 - \beta_2) - \\ &\tfrac{1}{2}L(-\eta_a \sin(\beta_1 - \beta_2) + \zeta_1 - \zeta_2)\cos(-\theta + \beta_1 - \beta_2) + \\ &L(\eta_a \sin(\beta_1 - \beta_2) + \zeta_1 + \zeta_2)\cos(\theta + \beta_1 + \beta_2)\end{aligned} \tag{C.16}$$

Now the *configuration dynamic model* of a bicycle can be defined as:

$$\begin{aligned}\dot{q} &= S\eta \\ \dot{\eta} &= (S^T M S)^{-1} S^T(-M\dot{S}\eta + B\tau)\end{aligned} \tag{C.17}$$

The final step is to define the feedback equivalent (by static state feedback) of the configuration dynamic model. The torque input τ can be defined as:

$$\tau = (S^T B)^+ S^T M(S\nu + \dot{S}\eta) \tag{C.18}$$

where $\nu = [\nu_1 \ \nu_2 \ \nu_3]$ is an arbitrary reference input. Using this, the feedback equivalent (by static state feedback) of the configuration dynamic model is:

$$\begin{pmatrix} \dot{q} \\ \dot{\eta_a} \\ \dot{\zeta_1} \\ \dot{\zeta_2} \end{pmatrix} = \begin{pmatrix} S(q)\eta \\ \nu_1 \\ \nu_2 \\ \nu_3 \end{pmatrix} \tag{C.19}$$

C.2 Bicycle controller

The goal is to develop a controller such that a reference trajectory (x_{ref}, y_{ref} and θ_{ref}) will be tracked by the center of the bicycle. Next to this also the reference steering angles (β_{1ref} and β_{2ref}) will be controlled. The control method as described in section 4.1.2 will be used. The goal of the control method is to get a controllable linear subsystem with a dimension of $2(\delta_m + \delta_s) = 6$ ($\dot{z}_1, \dot{z}_2$) and a nonlinear subsystem of dimension of $3 - \delta_m = 2$ ($\dot{z_3}$) as described by (4.38). The first step is to select the linearizing output vector z_1 of dimension $\delta_m + \delta_s$. A possible choice is [8]:

$$z_1 = \begin{pmatrix} z_{11} \\ z_{12} \\ z_{13} \end{pmatrix} = \begin{pmatrix} x + L\cos(\theta) + e_c \cos(\theta + \beta_1) \\ y + L\sin(\theta) + e_c \sin(\theta + \beta_1) \\ \beta_2 \end{pmatrix} \tag{C.20}$$

where e_c is the distance between the center of the front-wheel and a virtual "control" point (see e.g. figure 5.4). So the position of a point, at a distance of e_c in the longitudinal direction of the front-wheel, will be controlled. Also the steering angle at the rear will be controlled. The following step is to define z_2, which is equal to $\dot{z}_1$, which is:

$$\dot{z}_1 = z_2 = H\eta \tag{C.21}$$

$$H = \begin{pmatrix} H_{11} & -e_c \sin(\theta + \beta_1) & 0 \\ H_{21} & e_c \cos(\theta + \beta_1) & 0 \\ 0 & 0 & 1 \end{pmatrix} \tag{C.22}$$

where H_{11} and H_{21} are:

$$H_{11} = L\cos(\theta+\beta_1-\beta_2)+L\cos(\theta+\beta_1+\beta_2)-\frac{1}{2}e_c\cos(\theta+\beta_2)+\frac{1}{2}e_c\cos(\theta+2\beta_1-\beta_2)$$

(C.23)

$$H_{21} = L\sin(\theta+\beta_1-\beta_2)+L\sin(\theta+\beta_1+\beta_2)-\frac{1}{2}e_c\sin(\theta+\beta_2)+\frac{1}{2}e_c\sin(\theta+2\beta_1-\beta_2) \tag{C.24}$$

Now z_1 and z_2 are known, but z_3 is still unknown. A possible choice for z_3 is $[\theta\ \beta_1]$ [8]. The following step is to determine $\dot{z}_2$. Using that $\dot{\eta} = \nu$ it is possible to define $\dot{z}_2$ as:

$$\dot{z}_2 = \ddot{z}_1 = H\dot{\eta} + \dot{H}\eta = H\nu + b \tag{C.25}$$

where H is described in (C.21) and b is:

$$b = \dot{H}\eta = \begin{pmatrix} \dot{H}_{11} & -e_c(\eta_a\sin(\beta_1-\beta_2)+\zeta_1)\cos(\theta+\beta_1) & 0 \\ \dot{H}_{21} & -e_c(\eta_a\sin(\beta_1-\beta_2)+\zeta_1)\sin(\theta+\beta_1) & 0 \\ 0 & 0 & 0 \end{pmatrix}\eta \tag{C.26}$$

where $\dot{H}_{11}$ and $\dot{H}_{21}$ are:

$$\begin{aligned}\dot{H}_{11} = &-L(\eta_a\sin(\beta_1-\beta_2)+\zeta_1-\zeta_2)\sin(\theta+\beta_1-\beta_2)- \\ &L(\eta_a\sin(\beta_1-\beta_2)+\zeta_1+\zeta_2)\sin(\theta+\beta_1+\beta_2)- \\ &\tfrac{1}{2}e_c(\eta_a\sin(\beta_1-\beta_2)+2\zeta_1-\zeta_2)\sin(\theta+2\beta_1-\beta_2)+ \\ &\tfrac{1}{2}e_c(\eta_a\sin(\beta_1-\beta_2)+\zeta_2)\sin(\theta+\beta_2)\end{aligned} \tag{C.27}$$

$$\begin{aligned}\dot{H}_{21} = &L(\eta_a\sin(\beta_1-\beta_2)+\zeta_1-\zeta_2)\cos(\theta+\beta_1-\beta_2)+ \\ &L(\eta_a\sin(\beta_1-\beta_2)+\zeta_1+\zeta_2)\cos(\theta+\beta_1+\beta_2)+ \\ &\tfrac{1}{2}e_c(\eta_a\sin(\beta_1-\beta_2)+2\zeta_1-\zeta_2)\cos(\theta+2\beta_1-\beta_2)- \\ &\tfrac{1}{2}e_c(\eta_a\sin(\beta_1-\beta_2)+\zeta_2)\cos(\theta+\beta_2)\end{aligned} \tag{C.28}$$

Finally using that $\nu = H^{-1}(w-b)$ it is possible to state that $\ddot{z}_1 = w$.

$$\ddot{z}_1 = \begin{pmatrix} w_1 \\ w_2 \\ w_3 \end{pmatrix} \tag{C.29}$$

where $w_e = \ddot{z}_{1eref} - K_{ve}(\dot{z}_{1e} - \dot{z}_{1eref}) - K_{pe}(z_{1e} - z_{1eref})$, where K_{pe} and K_{ve} are gains and $e = 1, 2, 3$.
The total controller is now a combination of $\nu = H^{-1}(w-b)$ and (C.18). The inverse of the matrix H is used, which causes problems for certain steering angles, because the determinant of H is $2e_cLcos(\beta_2)$. The controller works well as long as the determinant of H is nonzero.
The total system that remains is:

$$\begin{aligned}\dot{z}_1 &= z_2 \\ \dot{z}_2 &= w \\ \dot{z}_3 &= Q(q_1)z_2\end{aligned} \tag{C.30}$$

The final step is to define the zero-dynamics, so the dynamics if the bicycle stands still. The internal dynamics are determined by the equation $\dot{z}_3 = Qz_2$.

The variable z_1 and z_2 are zero if the bicycle stands still at the desired output $z_1 = [0\ 0\ 0]$. The result is that $\dot{z}_3$ is also zero. The zero-dynamics are then also:

$$\begin{aligned} \theta(t) &= \theta_0 \\ \beta_1(t) &= \beta_{10} \end{aligned} \tag{C.31}$$

Stable solutions for the problem of the bicycle standing still at $z_1 = [0\ 0\ 0]$ are:

$$\begin{aligned} x_0 + L\cos(\theta_0) + e_c\cos(\theta_0 + \beta_{10}) &= 0 \\ y_0 + L\sin(\theta_0) + e_c\sin(\theta_0 + \beta_{10}) &= 0 \\ \beta_{20} &= 0 \end{aligned} \tag{C.32}$$

where the variables with subscript $_0$ can have any value as long as the equations are not violated.

Appendix D

Unicycle model and controller

In this appendix, the unicycle model and controller will be derived using the theory on wheeled mobile robots. The appendix is written so that it can be read in combination with chapter 4, which is the chapter that describes the general procedure.

D.1 Unicycle model

The model for a unicycle, as shown in figure D.1, using the wheeled mobile theory presented in section 4.1.1, will be described in this appendix.

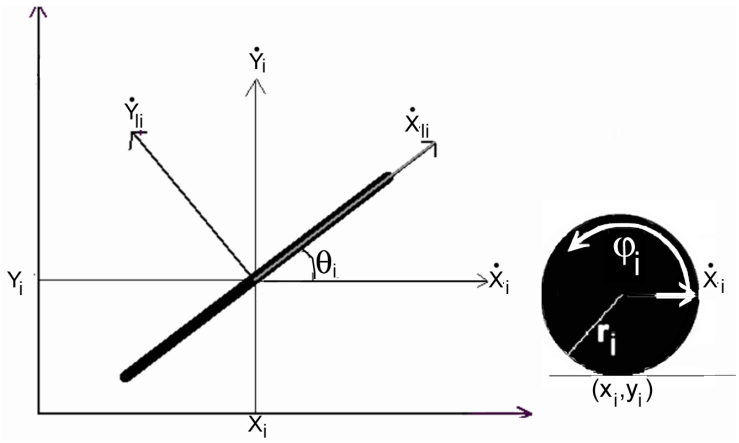

Figure D.1: Unicycle model

A unicycle as described here has four configurations variables (n=4), which are the position of the center (x_i and y_i), the orientation angle θ_i and the rotation of the wheel φ_i ($i = f(ront), r(ear)$).

$$q_i = \begin{pmatrix} x_i \\ y_i \\ \theta_i \\ \varphi_i \end{pmatrix} \tag{D.1}$$

The wheel itself has also local coordinates, which are x_{li}, y_{li} and θ_i. The transformation matrix $R(\theta_i)$ (4.1) can be used to switch between the local and global velocities and accelerations. In total there are two constraints (m=2), because there is one wheel. These constraints are the roll constraint and the slip constraint.
A few extra variables for the unicycle are needed to determine the constraints using (4.3) and (4.4). L_i is zero, α_i is zero and β_i is zero. Using (4.3), the slip constraint can now be written as:

$$\begin{pmatrix} 0 & -1 & 0 \end{pmatrix} R(\theta_i) \begin{pmatrix} \dot{x}_i \\ \dot{y}_i \\ \dot{\theta}_i \end{pmatrix} = C_1 R(\theta_i) \dot{\xi}_i = 0 \tag{D.2}$$

which simply states that there is a restriction on the velocity in y_l direction. Using (4.4), the roll constraint can now be written as:

$$\begin{pmatrix} 1 & 0 & 0 \end{pmatrix} R(\theta_i) \begin{pmatrix} \dot{x}_i \\ \dot{y}_i \\ \dot{\theta}_i \end{pmatrix} + r_i \dot{\varphi}_i = J_1 R(\theta_i) \dot{\xi}_i + J_2 \dot{\varphi}_i = 0 \tag{D.3}$$

which states that the longitudinal velocity of the unicycle $\dot{x}_{li}$ is equal to $-r_i\dot{\varphi}_i$. The constraints rewritten in the standard form $A_i^T \dot{q}_i = 0$ are:

$$A_i^T \dot{q}_i = \begin{pmatrix} \sin(\theta_i) & -\cos(\theta_i) & 0 & 0 \\ \cos(\theta_i) & \sin(\theta_i) & 0 & r_i \end{pmatrix} \begin{pmatrix} \dot{x}_i \\ \dot{y}_i \\ \dot{\theta}_i \\ \dot{\varphi}_i \end{pmatrix} = 0 \tag{D.4}$$

It is now possible to determine the degree of mobility and the degree of steerability using (4.12) and (4.13). The degree of mobility (δ_m) is equal to two and the degree of steerability (δ_s) is zero. The degree of mobility is two, because two movements are possible. The wheel can be driven forward/backward in x_{li} direction. The second possible movement is the orientation of the unicycle (θ_i). It is now already possible to see the connection with a normal wheel on the 4ws4wd/2ws2wd car, because one driving motor is available that drives the wheel in the x_{li} direction and one steering motor is available that can orient the wheel (θ_i). The conclusion can be that a unicycle is a type-(2,0) robot as described in [3].
The following step is to define the posture kinematic model. First of all it is important to calculate the matrix $\Sigma(\beta)$, which is a (3x2) matrix where the columns form a basis of the null-space of C_1 so that $C_1\Sigma(\beta) = 0$. It is known that $R(\theta_i)\dot{\xi}_i = \Sigma(\beta)\eta_{ai}$ (see section 4.1.1), where η_{ai} is an input-vector of dimension 2. The result from this is that a possible expression for $\Sigma(\beta)$ is:

$$\Sigma(\beta) = \begin{pmatrix} 1 & 0 \\ 0 & 0 \\ 0 & 1 \end{pmatrix} \tag{D.5}$$

Knowing that there are no conventional steering wheels the *posture kinematic model* can be written as:

$$\dot{\xi}_i = (R^T(\theta_i)\Sigma(\beta))\eta_{ai} = \begin{pmatrix} \cos(\theta_i) & 0 \\ \sin(\theta_i) & 0 \\ 0 & 1 \end{pmatrix} \begin{pmatrix} \eta_{1i} \\ \eta_{2i} \end{pmatrix} \tag{D.6}$$

where η_{1i} is the forward velocity of the unicycle ($\dot{x}_{li}$) and η_{2i} is the orientation velocity of the unicycle ($\dot{\theta}_i$).

The following step is to define the *configuration kinematic model*, which is:

$$\begin{pmatrix} \dot{\xi}_i \\ \dot{\varphi}_i \end{pmatrix} = \begin{pmatrix} R^T(\theta_i)\Sigma(\beta) \\ -J_2^{-1}J_1\Sigma(\beta) \end{pmatrix} \eta_{ai} = \begin{pmatrix} \cos(\theta_i) & 0 \\ \sin(\theta_i) & 0 \\ 0 & 1 \\ \frac{-1}{r_i} & 0 \end{pmatrix} \begin{pmatrix} \eta_{1i} \\ \eta_{2i} \end{pmatrix} \rightarrow \dot{q}_i = S_i(q)\eta_i \tag{D.7}$$

where the added equation simply is the roll-constraint, because $\eta_{1i} = \dot{x}_{li}$, so $r_i\dot{\varphi}_i = -\dot{x}_{li}$.
The following step is to determine the configuration dynamic model, because the real torque input cannot be determined using the kinematic model. First of all an extra dynamic equation has to be introduced (4.21) that e.g. describes how the motors are attached to the unicycle. It is again assumed that there are no disturbances etc, so the C_i matrix used in (4.21) is zero. The unicycle has two different torque inputs; the driving and steering motor torque. As a result of this the τ_i vector has two components. The steering motor is "implemented" so that a positive torque has as a consequence that $\ddot{\theta}_i$ increases. The driving motor is "implemented" so that a positive torque has as a consequence that $\ddot{x}_{li}$ increases. F_i is constructed from the constraint forces.

$$\begin{pmatrix} m_i & 0 & 0 & 0 \\ 0 & m_i & 0 & 0 \\ 0 & 0 & I_{\theta_i} & 0 \\ 0 & 0 & 0 & I_{\varphi_i} \end{pmatrix} \ddot{q}_i = A_i(q)\lambda_i + \begin{pmatrix} 0 & 0 \\ 0 & 0 \\ 0 & 1 \\ -1 & 0 \end{pmatrix} \begin{pmatrix} \tau_{di} \\ \tau_{si} \end{pmatrix} \tag{D.8}$$

where m_i is the mass of the unicycle, I_{θ_i} is the inertia of the unicycle around the vertical axis, I_{φ_i} is the rotation inertia of the wheel, λ_i is the Lagrange multiplier vector, τ_{di} is the driving torque and τ_{si} is the steering torque .
The matrix $\dot{S}_i(q_i, \dot{q}_i)$ has to be defined to be able to write down the configuration dynamic model, as described by (4.25).

$$\dot{S}_i(q_i, \dot{q}_i) = \begin{pmatrix} -\eta_{2i}\sin(\theta_i) & 0 \\ \eta_{2i}\cos(\theta_i) & 0 \\ 0 & 0 \\ 0 & 0 \end{pmatrix} \tag{D.9}$$

Now the *configuration dynamic model* of a unicycle can be defined as:

$$\begin{pmatrix} \dot{x}_i \\ \dot{y}_i \\ \dot{\theta}_i \\ \dot{\varphi}_i \\ \dot{\eta}_{1i} \\ \dot{\eta}_{2i} \end{pmatrix} = \begin{pmatrix} \cos(\theta_i)\eta_{1i} \\ \sin(\theta_i)\eta_{1i} \\ \eta_{2i} \\ \frac{-1}{r_i}\eta_{1i} \\ \frac{r_i\tau_{di}}{m_i r_i^2 + I_{\varphi_i}} \\ \frac{\tau_{si}}{I_{\theta_i}} \end{pmatrix} \tag{D.10}$$

Here the analogy with the configuration dynamic model of the 1DOF car is visible. The term for $\dot{\eta}_{1i}$ is equal to the term for $\dot{\eta}$ of the 1DOF car (4.45).
The final step is to define the feedback equivalent (by static state feedback) of the configuration dynamic model. The torque input τ_i can be defined as:

$$\begin{pmatrix} \tau_{di} \\ \tau_{si} \end{pmatrix} = \begin{pmatrix} \frac{\nu_{1i}(m_i r_i^2 + I_{\varphi_i})}{r_i} \\ \nu_{2i} I_{\theta_i} \end{pmatrix} \tag{D.11}$$

where $\nu_i = [\nu_{1i}\ \nu_{2i}]$ is an arbitrary reference input. The feedback equivalent (by static state feedback) of the configuration dynamic model is:

$$\begin{pmatrix} \dot{x}_i \\ \dot{y}_i \\ \dot{\theta}_i \\ \dot{\varphi}_i \\ \dot{\eta}_{1i} \\ \dot{\eta}_{2i} \end{pmatrix} = \begin{pmatrix} \cos(\theta_i)\eta_{1i} \\ \sin(\theta_i)\eta_{1i} \\ \eta_{2i} \\ \frac{-1}{r_i}\eta_{1i} \\ \nu_{1i} \\ \nu_{2i} \end{pmatrix} \tag{D.12}$$

The posture dynamic model is:

$$\begin{pmatrix} \dot{x}_i \\ \dot{y}_i \\ \dot{\theta}_i \\ \dot{\eta}_{1i} \\ \dot{\eta}_{2i} \end{pmatrix} = \begin{pmatrix} \cos(\theta_i)\eta_{1i} \\ \sin(\theta_i)\eta_{1i} \\ \eta_{2i} \\ \nu_{1i} \\ \nu_{2i} \end{pmatrix} \tag{D.13}$$

D.2 Unicycle controller

Looking at (D.12) the conclusion can be that it would be possible to directly have control of the forward velocity of the unicycle and the orientation angle of the unicycle. However to be able to control the position of the unicycle, a "master" controller should be introduced that transforms the position error in adapted velocity reference signals. Because of this and because of the requirement of the steering angle behaviour, the choice is made to design a controller that "directly" controls the reference trajectory (x_{iref}, y_{iref} and θ_{iref}) of the unicycle. It is important to control the orientation angle next to the position of the unicycle, because then the orientation angle will always be as close as possible to the ideal orientation angle (5.2). This is desired, because finally the controller will be used for a car with real tyres that have slip. Because of the tyre characteristic diagram of real tyres (See appendix B) it is desired to keep the orientation angle as close as possible to the ideal steering angle, because then the slip(angle) will be minimized.
The goal of the controller is to control the three variables (x_i, y_i and θ_i), but only two inputs are available (steering and driving motor). Because of this, the control method described in section 4.1.2, will be used. The goal of the control design method is to get a controllable linear subsystem with a dimension of $2(\delta_m + \delta_s) = 4$ ($\dot{z}_{1i}, \dot{z}_{2i}$) and a nonlinear subsystem of dimension of $3 - \delta_m = 1$ ($\dot{z}_{3i}$) as described by (4.38).
The first step is to select the linearizing output vector z_{1i} of, which is of dimension 2 because of the degree of mobility. The vector z_{1i} is constructed from

the posture variables ($q_i = [x_i, y_i, \theta_i]$) so that a controllable system will remain. The variable z_{1i} is of dimension 2, so effectively a point tracking problem will remain. If the point x_i, y_i would be chosen, then it would not be possible to assure that the orientation angle will be equal or convert to the reference orientation angle. However if a point in front of the wheels is chosen, then it is assured that the variables x_i, y_i, θ_i will convert to the reference variables if there is a forward velocity. An example that can illustrate this is a truck in combination with a trailer. It the trailer is oriented with a certain angle relative to the truck while the truck stands still, then this orientation angle will remain. However, if the truck starts driving in a straight line with a certain velocity, then the orientation angle of the trailer (relative to the truck) will convert to zero. This is not exactly what happens when a point in front of the unicycle is chosen, but it illustrates the concept.
The virtual control point z_{1i} in front of the wheel is illustrated in figure D.2 [8].

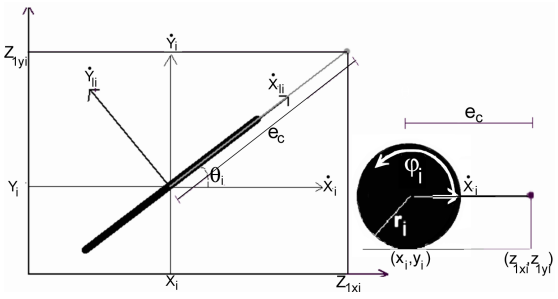

Figure D.2: Output linearizing coordinates z_{1i}.

$$z_{1i} = \begin{pmatrix} z_{1xi} \\ z_{1yi} \end{pmatrix} = \begin{pmatrix} x_i + e_c \cos(\theta_i) \\ y_i + e_c \sin(\theta_i) \end{pmatrix} \tag{D.14}$$

where e_c is the distance between the center of the unicycle and the virtual "control" point (z_{1i}). So instead of controlling the actual unicycle center position and the orientation angle, the z_{1xi} and the z_{1yi} position of the virtual "control" point will be controlled. So effectively a point tracking problem remains. The following step is to define z_{2i}, which is equal to $\dot{z}_{1i}$, which is:

$$\dot{z}_{1i} = z_{2i} = H_i \eta_i = \begin{pmatrix} \cos(\theta_i) & -e_c \sin(\theta_i) \\ \sin(\theta_i) & e_c \cos(\theta_i) \end{pmatrix} \begin{pmatrix} \eta_{1i} \\ \eta_{2i} \end{pmatrix} \tag{D.15}$$

The determinant of H_i is equal to e_c, so e_c has to be everything but zero, because the inverse of H_i will be used. Now z_{1i} and z_{2i} are known, but z_{3i} is still unknown. A possible choice for z_{3i} is θ_i [8]. The following step is to determine $\dot{z}_{2i}$ and $\dot{z}_{3i}$. Using that $\dot{\eta}_i = \nu_i$ it is possible to define $\dot{z}_{2i}$ as:

$$\dot{z}_{2i} = \ddot{z}_{1i} = H_i \dot{\eta}_i + \dot{H}_i \eta_i = H_i \nu_i + b_i \tag{D.16}$$

where H_i is equal to (D.15) and b_i is:

$$b_i = \begin{pmatrix} -\eta_{1i}\eta_{2i} \sin(\theta_i) - e_c \eta_{2i}^2 \cos(\theta_i) \\ \eta_{1i}\eta_{2i} \cos(\theta_i) - e_c \eta_{2i}^2 \sin(\theta_i) \end{pmatrix} \tag{D.17}$$

$\dot{z}_{3i}$ is equal to:

$$\dot{z}_{3i} = Q_i z_{2i} = Q_i \dot{z}_{1i} = \begin{pmatrix} \frac{-\sin(\theta_i)}{e_c} & \frac{\cos(\theta_i)}{e_c} \end{pmatrix} \begin{pmatrix} \dot{z}_{1xi} \\ \dot{z}_{1yi} \end{pmatrix} \tag{D.18}$$

Finally using that $\nu_i = H_i^{-1}(w_i - b_i)$ it is possible to state that $\ddot{z}_{1i} = w_i$.
So after feedback linearization the following expression for $\ddot{z}_{1i}$ remains:

$$\ddot{z}_{1i} = \begin{pmatrix} w_{1i} \\ w_{2i} \end{pmatrix} \tag{D.19}$$

$$\begin{aligned} w_{1i} &= \ddot{z}_{1xiref} - K_v(\dot{z}_{1xi} - \dot{z}_{1xiref}) - K_p(z_{1xi} - z_{1xiref}) \\ w_{2i} &= \ddot{z}_{1yiref} - K_v(\dot{z}_{1yi} - \dot{z}_{1yiref}) - K_p(z_{1yi} - z_{1yiref}) \end{aligned} \tag{D.20}$$

where K_p and K_p are arbitrary positive numbers and $z_{1iref} = [z_{1xiref}\ z_{1yiref}] = z_{1i}(x_{iref}, y_{iref}, \theta_{iref})$.
The total controller is now a combination of $\nu_i = H_i^{-1}(w_i - b_i)$ and (5.5).

$$\begin{pmatrix} \tau_{di} \\ \tau_{si} \end{pmatrix} = \begin{pmatrix} \frac{(m_i r_i^2 + I_{\varphi_i})}{r_i}(\cos(\theta_i)w_{1i} + \sin(\theta_i)w_{2i} + e_c\eta_{2i}^2 \\ I_{\theta_i}(\frac{-\sin(\theta_i)}{e_c}w_{1i} + \frac{\cos(\theta_i)}{e_c}w_{2i} - \frac{\eta_{1i}\eta_{2i}}{e_c}) \end{pmatrix} \tag{D.21}$$

Appendix E

Unicycle model and controller with slip compensation

In this appendix the complete procedure to derive the controller for a unicycle with tyre slip will be described. Some of the matrices already stated in appendix D, such as S_i, A_i etc will be used ($i = f(ront), r(ear)$). The appendix is written so that it can be read in combination with chapter 4, which is the chapter that describes the general procedure.

E.1 Unicycle model extended with tyre slip

A wheeled robot with tyre slip can be described with a model that can be written in the standard singular perturbation form (4.64). The procedure, described in section 4.3.1, will be used to get to this model for the unicycle.
The dynamical model can (again) be written in the standard form (4.21). It is assumed that there are no resistance torques etc, so $C_i = 0$. The generalized force vector consists of tyre contact forces. The resulting dynamical model is:

$$\begin{pmatrix} m_i & 0 & 0 & 0 \\ 0 & m_i & 0 & 0 \\ 0 & 0 & I_{\theta_i} & 0 \\ 0 & 0 & 0 & I_{\varphi_i} \end{pmatrix} \ddot{q}_i = -A_i K_i A_i^T A_i \mu_i + \begin{pmatrix} 0 & 0 \\ 0 & 0 \\ 0 & 1 \\ -1 & 0 \end{pmatrix} \begin{pmatrix} \tau_{di} \\ \tau_{si} \end{pmatrix} \quad \text{(E.1)}$$

,where K_i is a to be determined matrix.
The general procedure to derive K_i is described in section 4.3.1. A unicycle has two independent constraints (slip and roll) that both will be violated due to tyre slip, so the matrix K_i can be expressed as:

$$K_i = L_i^T(q_i) \frac{1}{V_i} \begin{pmatrix} D_0 & 0 \\ 0 & G_0 \end{pmatrix} L_i(q) \quad \text{(E.2)}$$

where $D_0 = \varepsilon D$ (D is the cornering stiffness), $G_0 = \varepsilon G$ (G is the slip stiffness) and V_i is the absolute velocity of the center of the tyre. The matrix L_i is still unknown, but it is known that:

$$\begin{pmatrix} V_{lat_i} \\ V_{long_i} - r_i \dot{\varphi}_i \end{pmatrix} = L_i(q) A_i^T(q) \dot{q}_i \quad \text{(E.3)}$$

A possible expression for L_i is determined using the matrix A_i for the unicycle and figure 5.3.

$$L_i = \begin{pmatrix} -1 & 0 \\ 0 & -1 \end{pmatrix} \tag{E.4}$$

so K_i can be expressed as:

$$K_i = \frac{1}{V_i} \begin{pmatrix} D_0 & 0 \\ 0 & G_0 \end{pmatrix} \tag{E.5}$$

The following procedure is to see what sign D_0 and G_0 have. The general forces (4.56) in this example will be calculated for an angle θ_i of zero degrees. In this case the first general force corresponds to F_{xi} and the second general force corresponds to F_{yi}.

$$F_i = -A_i L_i^T \begin{pmatrix} F_{lat_i} \\ F_{long_i} \end{pmatrix} = - \begin{pmatrix} 0 & 1 \\ -1 & 0 \\ 0 & 0 \\ 0 & r_i \end{pmatrix} \begin{pmatrix} -1 & 0 \\ 0 & -1 \end{pmatrix} \begin{pmatrix} F_{lat_i} \\ F_{long_i} \end{pmatrix} = \begin{pmatrix} F_{long_i} \\ -F_{lat_i} \\ 0 \\ r_i F_{long_i} \end{pmatrix} \tag{E.6}$$

The conclusion can be that F_{lat_i} is equal to $-F_{yi}$, so F_{lat_i} points in the negative y_i-axis direction, and that F_{long_i} is equal to F_{xi}, so F_{long_i} points in the positive x_i-axis direction. The following step is to see how the velocities are directed.

$$\begin{pmatrix} V_{lat_i} \\ V_{long_i} - r_i \dot{\varphi}_i \end{pmatrix} = L_i A_i^T \dot{q}_i =$$
$$\begin{pmatrix} -1 & 0 \\ 0 & -1 \end{pmatrix} \begin{pmatrix} 0 & -1 & 0 & 0 \\ 1 & 0 & 0 & r_i \end{pmatrix} \begin{pmatrix} \dot{x}_{li} \\ \dot{y}_{li} \\ \dot{\theta}_i \\ \dot{\varphi}_i \end{pmatrix} = \begin{pmatrix} 0 & 1 & 0 & 0 \\ -1 & 0 & 0 & -r_i \end{pmatrix} \begin{pmatrix} \dot{x}_{li} \\ \dot{y}_{li} \\ \dot{\theta}_i \\ \dot{\varphi}_i \end{pmatrix} \tag{E.7}$$

The conclusion is that V_{lat_i} is equal to $\dot{y}_i$ and that F_{lat_i} is pointing in the negative y_i-direction. The force and the slip-velocity are positioned in an opposite direction, because if the tyre is sliding in positive direction than the force will be pointed in negative direction. Using this, the conclusion can be that D_0 is a positive number. Using the same procedure it is possible to conclude that G_0 also has to be a positive number.

The standard configuration kinematic model ($\dot{q}_i = S_i(q_i)\eta_i$) is no longer valid. Instead of this $\dot{q}_i = S_i(q)\eta_i + A_i(q_i)\varepsilon\mu_i$ (4.59) has to be used.

$$\dot{q}_i = \begin{pmatrix} \cos(\theta_i) & 0 \\ \sin(\theta_i) & 0 \\ 0 & 1 \\ \frac{-1}{r_i} & 0 \end{pmatrix} \begin{pmatrix} \eta_{1i} \\ \eta_{2i} \end{pmatrix} + \begin{pmatrix} \sin(\theta_i) & \cos(\theta_i) \\ -\cos(\theta_i) & \sin(\theta_i) \\ 0 & 0 \\ 0 & r_i \end{pmatrix} \varepsilon \begin{pmatrix} \mu_{1i} \\ \mu_{2i} \end{pmatrix} \tag{E.8}$$

The derivative of this function with respect to the time is:

$$\ddot{q}_i = \begin{pmatrix} S_i & A_i \end{pmatrix} \begin{pmatrix} \dot{\eta}_i \\ \varepsilon\dot{\mu}_i \end{pmatrix} + \begin{pmatrix} \dot{S}_i & \dot{A}_i \end{pmatrix} \begin{pmatrix} \eta_i \\ \varepsilon\mu_i \end{pmatrix} \tag{E.9}$$

where

$$\dot{S}_i = \eta_{2i} \begin{pmatrix} -\sin(\theta_i) & 0 \\ \cos(\theta_i) & 0 \\ 0 & 0 \\ 0 & 0 \end{pmatrix} \quad \dot{A}_i = \eta_{2i} \begin{pmatrix} \cos(\theta_i) & -\sin(\theta_i) \\ \sin(\theta_i) & \cos(\theta_i) \\ 0 & 0 \\ 0 & 0 \end{pmatrix} \tag{E.10}$$

using that $\dot{\theta}_i = \eta_{2i}$.
The last steps are to implement $\ddot{q}_i$ (E.9) in (E.1) and front multiply (E.1) by $(S_i \ A_i)^T$. The resulting equation is:

$$\begin{aligned} J_i(q_i) \begin{pmatrix} \dot{\eta}_i \\ \varepsilon\dot{\mu}_i \end{pmatrix} = \begin{pmatrix} S_i^T(q_i) \\ A_i^T(q_i) \end{pmatrix} [B_i(q_i)\tau_i - M_i(q_i)(\dot{S}_i\eta_i + \dot{A}_i\varepsilon\mu_i)] + \\ \begin{pmatrix} 0 \\ -A_i^T(q)A_i(q_i)K_i(q_i,\dot{q}_i)A_i^T(q_i)A_i(q_i)\mu_i \end{pmatrix} \end{aligned} \tag{E.11}$$

where $J_i = \begin{pmatrix} S_i^T(q_i)M_i(q_i)S_i(q_i) & S_i^T(q_i)M_i(q_i)A_i(q_i) \\ A_i^T(q_i)M_i(q_i)S_i(q_i) & A_i^T(q_i)M_i(q_i)A_i(q_i) \end{pmatrix}$

The final step to come to a complete model in singular perturbation form is rewriting the equations to the standard form (4.64), which is:

$$\begin{aligned} \dot{q}_i &= S_i(q_i)\eta_i + A_i(q_i)\varepsilon\mu_i \\ \dot{\eta}_i &= f_{oi}(q_i,\eta_i) + \varepsilon f_{1i}(q_i,\eta_i,\mu_i) + \varepsilon^2 f_{2i}(q_i,\eta_i,\mu_i) + B_{1i}(q_i)\tau_i - R_{12i}A_i^T A_i K_i A_i^T A_i \mu_i \\ \varepsilon\dot{\mu}_i &= g_{oi}(q_i,\eta_i) + \varepsilon g_{1i}(q_i,\eta_i,\mu_i) + \varepsilon^2 g_{2i}(q_i,\eta_i,\mu_i) + B_{2i}(q_i)\tau_i - R_{22i}A_i^T A_i K_i A_i^T A_i \mu_i \end{aligned} \tag{E.12}$$

where in this case:

$$S_i = \begin{pmatrix} \cos(\theta_i) & 0 \\ \sin(\theta_i) & 0 \\ 0 & 1 \\ \frac{-1}{r_i} & 0 \end{pmatrix} \tag{E.13}$$

$$A_i = \begin{pmatrix} \sin(\theta_i) & \cos(\theta_i) \\ -\cos(\theta_i) & \sin(\theta_i) \\ 0 & 0 \\ 0 & r_i \end{pmatrix} \tag{E.14}$$

$$f_{0i} = \begin{pmatrix} 0 \\ 0 \end{pmatrix} \tag{E.15}$$

$$f_{1i} = \begin{pmatrix} \frac{-\mu_{1i}\eta_{2i}r_i^2}{r_i^2+1} \\ 0 \end{pmatrix} \tag{E.16}$$

$$f_{2i} = \begin{pmatrix} 0 \\ 0 \end{pmatrix} \tag{E.17}$$

$$B_{1i} = \begin{pmatrix} \frac{r_i}{(r_i^2+1)I_{\varphi i}} & 0 \\ 0 & \frac{1}{I_{\theta_i}} \end{pmatrix} \tag{E.18}$$

$$R_{12i}A_i^T A_i K_i A_i^T A_i = \begin{pmatrix} 0 & \frac{-(m_i - I_{\varphi_i})r_i^2 G_0}{V_i m_i I_{\varphi_i}} \\ 0 & 0 \end{pmatrix} \tag{E.19}$$

$$g_{0i} = \begin{pmatrix} \eta_{1i}\eta_{2i} \\ 0 \end{pmatrix} \tag{E.20}$$

$$g_{1i} = \begin{pmatrix} \eta_{2i}\mu_{2i} \\ \frac{-\mu_{1i}\eta_{2i}}{r_i^2+1} \end{pmatrix} \tag{E.21}$$

$$g_{2i} = \begin{pmatrix} 0 \\ 0 \end{pmatrix} \tag{E.22}$$

$$B_{2i} = \begin{pmatrix} 0 & 0 \\ \frac{-r_i}{(r_i^2+1)I_{\varphi i}} & 0 \end{pmatrix} \tag{E.23}$$

$$R_{22i}A_i^T A_i K_i A_i^T A_i = \begin{pmatrix} \frac{D_0}{V_i m_i} & 0 \\ 0 & \frac{(m_i r_i^2 + I_{\varphi_i})G_0}{V_i m_i I_{\varphi_i}} \end{pmatrix} \tag{E.24}$$

E.2 Unicycle controller with tyre slip compensation

Now the model is known, so the following step is to continue from the model in singular perturbation form to the slow manifold approach. The first step is to choose appropriate output linearization variables to perform the procedure described in section 4.3.2.
The largest linearizable subsystem of a WMR can be obtained by selecting $\delta_m + \delta_s = 2$ linearizing output functions (see section 4.1.2). So a smart combination of x_i, y_i, θ_i has to be chosen for the output linearizing coordinates. The same output linearizing coordinates as for the controller for the unicycle without slip will be chosen, so z_{1i} is:

$$z_{1i} = \begin{pmatrix} x_i + e_c \cos(\theta_i) \\ y_i + e_c \sin(\theta_i) \end{pmatrix} \tag{E.25}$$

The first derivative of this equation is:

$$\dot{z}_{1i} = S_{si}\eta_i + A_{si}\varepsilon\mu_i = \begin{pmatrix} \dot{x}_i - e_c\dot{\theta}_i \sin(\theta_i) \\ \dot{y}_i + e_c\dot{\theta}_i \cos(\theta_i) \end{pmatrix} \tag{E.26}$$

Using (E.12) S_{si} and A_{si} are:

$$S_{si} = \begin{pmatrix} \cos(\theta_i) & -e_c \sin(\theta_i) \\ \sin(\theta_i) & e_c \cos(\theta_i) \end{pmatrix} \tag{E.27}$$

$$A_{si} = \begin{pmatrix} \sin(\theta_i) & \cos(\theta_i) \\ -\cos(\theta_i) & \sin(\theta_i) \end{pmatrix} \tag{E.28}$$

The desired linearization condition is $\ddot{z}_{1i} = w_i$ (4.92), where w_i is a new input. The linearization condition for a unicycle is:

$$\ddot{z}_{1i} = S_{si}\dot{\eta}_i + A_{si}\varepsilon\dot{H}_{\varepsilon_i} + \dot{S}_{si}\eta_i + \dot{A}_{si}\varepsilon H_{\varepsilon_i} = w_i \tag{E.29}$$

where $\dot{S}_{si}$ and $\dot{A}_{si}$ are:

$$\dot{S}_{si} = \eta_{2i} \begin{pmatrix} -\sin(\theta_i) & -e_c \cos(\theta_i) \\ \cos(\theta_i) & -e_c \sin(\theta_i) \end{pmatrix} \tag{E.30}$$

$$\dot{A}_{si} = \eta_{2i} \begin{pmatrix} \cos(\theta_i) & -\sin(\theta_i) \\ \sin(\theta_i) & \cos(\theta_i) \end{pmatrix} \tag{E.31}$$

and a possible choice for w_i is:

$$w_i = \begin{pmatrix} w_{1i} \\ w_{2i} \end{pmatrix} = \ddot{z}_{1iref} - K_{pT}(z_{1i} - z_{1iref}) - K_{vT}(S_{si}\eta_i + A_{si}\varepsilon H_{\varepsilon_i} - \dot{z}_{1iref}) \tag{E.32}$$

where $S_{si}\eta_i + A_{si}\varepsilon H_{\varepsilon_i}$ is equal to $\dot{z}_{1i}$ on the slow manifold, $z_{1iref} = z_{1i}(x_{iref}, y_{iref}, \theta_{iref})$ and K_{pT} and K_{vT} are two positive definite matrices, e.g.:

$$K_{pT} = \begin{pmatrix} K_p & 0 \\ 0 & K_p \end{pmatrix} \tag{E.33}$$

$$K_{vT} = \begin{pmatrix} K_v & 0 \\ 0 & K_v \end{pmatrix} \tag{E.34}$$

It is now possible to describe the two equations (linearization and manifold condition) that are needed for the slow manifold approach (4.83). This can be done using the matrices (E.13) - (E.34).

The following step is to derive τ_{0i} and H_{0i} using the procedure described in 4.3.2. If $\varepsilon = 0$, then the linearizing condition and manifold condition are (4.84). This equation is an algebraic equation with the following solutions for τ_{0i} and H_{0i} for a unicycle:

$$\begin{aligned} \tau_{0i} &= \begin{pmatrix} \frac{(m_i r_i^2 + I_{\varphi_i})}{r_i}(\cos(\theta_i)w_{p101i} + \sin(\theta_i)w_{p102i} + e_c\eta_{2i}^2) \\ \frac{I_{\theta_i}}{e_c}(-\sin(\theta_i)w_{p101i} + \cos(\theta_i)w_{p102i} - \eta_{1i}\eta_{2i}) \end{pmatrix} \\ H_{0i} &= \begin{pmatrix} \eta_{1i}\eta_{2i}\frac{V_i m_i}{D_0} \\ \frac{-V_i m_i}{G_0(1+r_i^2)}(\cos(\theta_i)w_{p101i} + \sin(\theta_i)w_{p102i} + e_c\eta_{2i}^2) \end{pmatrix} \end{aligned} \tag{E.35}$$

where:

$$\begin{pmatrix} w_{p101i} \\ w_{p102i} \end{pmatrix} = \ddot{z}_{1iref} - K_{pT}(z_{1i} - z_{1iref}) - K_{vT}(S_{si}\eta_i - \dot{z}_{1iref}) \tag{E.36}$$

The following step is to determine τ_{1i} and H_{1i} using the method described in section 4.3.2. It is clear that there is an extra variable, which is $\dot{H}_{0i}$, that is not known yet. To derive $\dot{H}_{0i}$ the time derivative of H_{0i} has to be taken and as a second step ε has to be set to zero. It is used that m_i, G_0 and D_0 can be seen as fixed variable, because G_0 and D_0 are dependent of m_i. The result of this procedure on (E.35) is:

$$\dot{H}_{0i} = \begin{pmatrix} \eta_{1i}\eta_{2i}\frac{\dot{V}_i m_i}{D_0} + \dot{\eta}_{1i\varepsilon 0}\eta_{2i}\frac{V_i m_i}{D_0} + \eta_{1i}\dot{\eta}_{2i\varepsilon 0}\frac{V_i m_i}{D_0} \\ \frac{-\dot{V}_i m_i}{G_0(1+r_i^2)}(\cos(\theta_i)w_{p101i} + \sin(\theta_i)w_{p102i} + e_c\eta_{2i}^2) + \\ \frac{-V_i m_i}{G_0(1+r_i^2)}\eta_{2i}(-\sin(\theta_i)w_{p101i} + \cos(\theta_i)w_{p102i}) + \\ \frac{-V_i m_i}{G_0(1+r_i^2)}(\cos(\theta_i)\dot{w}_{p101i} + \sin(\theta_i)\dot{w}_{p102i} + 2e_c\dot{\eta}_{2i\varepsilon 0}\eta_{2i}) \end{pmatrix} \tag{E.37}$$

where:

$$\begin{pmatrix} \dot{\eta}_{1i\varepsilon 0} \\ \dot{\eta}_{2i\varepsilon 0} \end{pmatrix} = \begin{pmatrix} \frac{r_i}{(r_i^2+1)I_{\varphi_i}}\tau_{di0} + \frac{-(m_i - I_{\varphi_i})r_i^2 G_0}{V_i m_i I_{\varphi_i}}H_{02i} \\ \frac{1}{I_{\theta_i}}\tau_{si0} \end{pmatrix} \tag{E.38}$$

The solution for H_{1i} and τ_{1i} can now be determined. For the moment only the solution of τ_{1i} will be written down. The choice is made to only calculate τ_{0i} and τ_{1i}, because the contribution of τ_{2i} to the total τ_i is very small, because it is front multiplied by ε^2, which is a small parameter.

$$\tau_{1i} = \begin{pmatrix} \frac{m_i r_i^2 + I_{\varphi_i}}{r_i} \\ \frac{I_{\theta_i}}{e_c} \end{pmatrix} KSC_i \begin{pmatrix} H_{01i} \\ H_{02i} \end{pmatrix} + TCRT_i \tag{E.39}$$

where KSC_i and $TCRT_i$ (Tyre Characteristic Related Term) are:

$$KSC_i = -\begin{pmatrix} \cos(\theta_i) & \sin(\theta_i) \\ -\sin(\theta_i) & \cos(\theta_i) \end{pmatrix} K_{vT} A_{si} \tag{E.40}$$

$$TCRT_i = \begin{pmatrix} TCRT_{1i} \\ TCRT_{2i} \end{pmatrix} \tag{E.41}$$

where $TCRT_{1i}$ and $TCRT_{2i}$ are:

$$\begin{array}{l} TCRT_{1i} = \\ \frac{m_i I_{\varphi_i}}{r_i G_0}(V_i(\cos(\theta_i)\dot{w}_{p101i} + \sin(\theta_i)\dot{w}_{p102i} + \\ 2\eta_{2i}(-\sin(\theta_i)w_{p101i} + \cos(\theta_i)w_{p102i} - \eta_{1i}\eta_{2i})) + \\ \dot{V}_i(\cos(\theta_i)w_{p101i} + \sin(\theta_i)w_{p102i} + \\ e_c\eta_{2i}^2) + \eta_{2i}V_i(-\sin(\theta_i)w_{p101i} + V_i\cos(\theta_i)w_{p102i})) - \\ \frac{I_{\varphi_i}V_i m_i}{r_i D_o}\eta_{1i}\eta_{2i}^2 \end{array} \tag{E.42}$$

$$
\begin{array}{l}
TCRT_{2i} = \\
\frac{m_i I_{\theta_i}}{e_c^2 D_0}(e_c\eta_{2i}(V_i\cos(\theta_i)w_{p101i} + V_i\sin(\theta_i)w_{p102i} + V_i e_c\eta_{2i}^2 + \eta_{1i}\dot{V}_i)+ \\
\eta_{1i}V_i(-\sin(\theta_i)w_{p101i} + \cos(\theta_i)w_{p102i} - \eta_{1i}\eta_{2i}))+ \\
\frac{V_i m_i I_{\theta_i}}{e_c G_0(1+r_i^2)}\eta_{2i}(\cos(\theta_i)w_{p101i} + \sin(\theta_i)w_{p102i} + e_c\eta_{2i}^2)
\end{array}
\tag{E.43}
$$

The "total" controller $\tau_i = \tau_{0i} + \varepsilon\tau_{1i}$ is:

$$
\begin{array}{l}
\tau_i = \begin{pmatrix} \frac{m_i r_i^2 + I_{\varphi_i}}{r_i} \\ \frac{I_{\theta_i}}{e_c} \end{pmatrix} \left(\begin{pmatrix} c(\theta_i) & s(\theta_i) \\ -s(\theta_i) & c(\theta_i) \end{pmatrix} \left(\begin{pmatrix} w_{p101i} \\ w_{p102i} \end{pmatrix} - K_{vT}\varepsilon A_{si} H_{0i} \right) + \begin{pmatrix} e_c\eta_{2i}^2 \\ -\eta_{1i}\eta_{2i} \end{pmatrix} \right) \\
\quad +\varepsilon TCRT_i
\end{array}
\tag{E.44}
$$

If this controller is compared with the controller of the 1DOF example (4.104) then it can be concluded that they have a similar structure. Because of the similarities the controller for the unicycle that will be used for the simulation is:

$$
\begin{array}{l}
\tau_{i\varepsilon} = \begin{pmatrix} \frac{m_i r_i^2 + I_{\varphi_i}}{r_i} \\ \frac{I_{\theta_i}}{e_c} \end{pmatrix} \left(\begin{pmatrix} c(\theta_i) & s(\theta_i) \\ -s(\theta_i) & c(\theta_i) \end{pmatrix} \begin{pmatrix} w_{1i} \\ w_{2i} \end{pmatrix} + \begin{pmatrix} e_c\eta_2^2 \\ -\eta_{1i}\eta_{2i} \end{pmatrix} \right) + \\
\quad \varepsilon TCRT_{ti}
\end{array}
\tag{E.45}
$$

where $TCRT_{ti}$ is the $TCRT_i$ term with w_i and $\dot{w}_i$ instead of w_{p1i} and $\dot{w}_{p1i}$. In the 1DOF example, it was possible to see the similarity between the controller from the standard robot theory for a model without tyre slip and the controller with slip compensation with $\varepsilon = 0$. For the unicycle there is also such a similarity, because (E.45) with $\varepsilon = 0$ is equal to (5.16).
It is also possible to see the similarities between the controller with slip compensation for the 1 DOF model and the unicycle model. The driving part of the unicycle controller (first row of (E.45)) converts to (4.107) if $\theta_i = 0$ and $\dot{\theta}_i = \eta_{2i} = 0$ are implemented in (E.45).

Appendix F

Validation one-track model

In this appendix, a short validation of the physical one-track model will be given. This will be done by discussing a a lane change with a maximum lateral accelerations of 10 m/s^2 and a maximum longitudinal acceleration of 10 m/s^2. The simulations will be performed using the ode 5 solver with a fixed step size of 0.002 s. The first step in the process is to simulate the lane change using the configuration dynamic model of the bicycle. The double unicycle controller is "tuned" so that the error is (almost) zero. The 4 torque inputs of the model are saved. Now these torques are used as an input for the one track model. The expectation is that the error will convert to zero when the tyre stiffness is increased, because then the slip in lateral and longitudinal direction is reduced. This expectation is confirmed by the simulations, from which the results are plotted in figure F.1.
Now the conclusion can be that the one track model is validated.

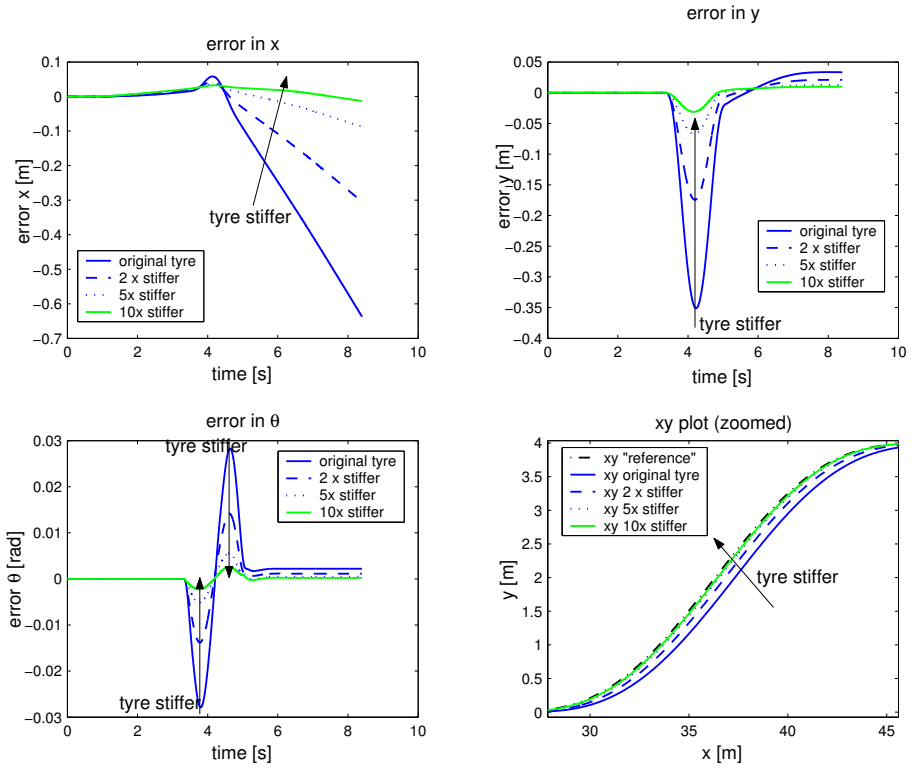

Figure F.1: Error (measured-reference) for the simulations with the one track model with increasing tyre stiffness. (Original tyre: $G = 46F_{zi}$ and $D = 70F_{zi}$, 10 x stiffer tyre: $G = 460F_{zi}$ and $D = 700F_{zi}$)

Appendix G

Schematic overview multicycle controller

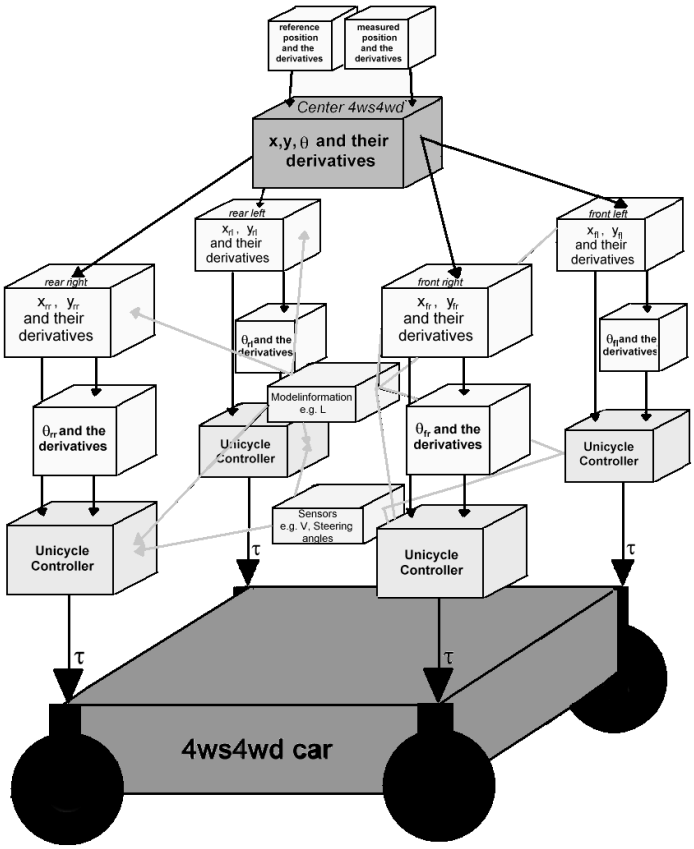

Figure G.1: Schematic overview of the multicycle controller for a 4ws4wd car.

Appendix H

Reference trajectories

In this appendix, the two high acceleration reference trajectories that are used for the simulations and the experiments with the 4ws4wd car are illustrated. The position, velocity and the accelerations signals are illustrated.

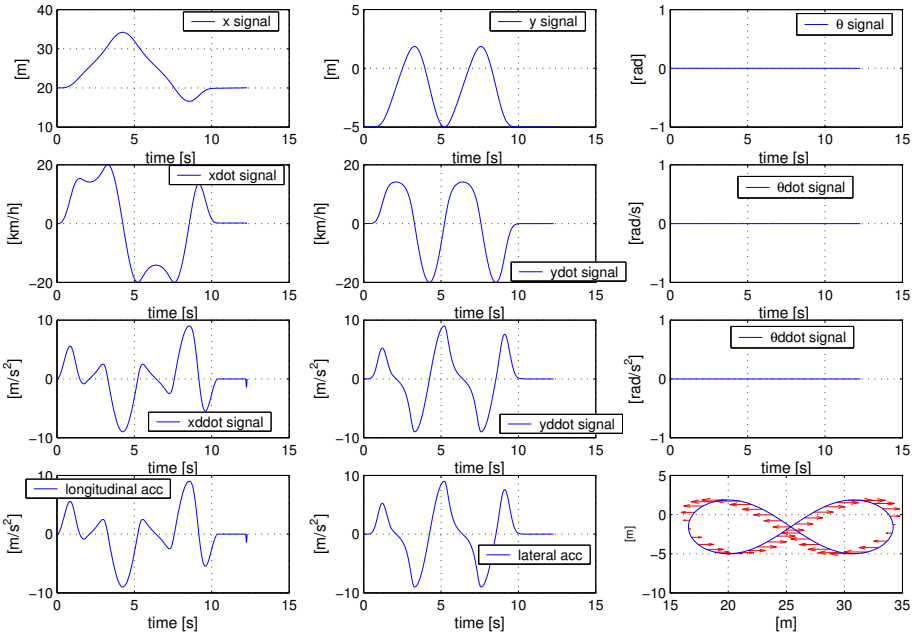

Figure H.1: The reference variables for the high acceleration eight shaped trajectory used for the simulations and the experiments with the 4ws4wd car.

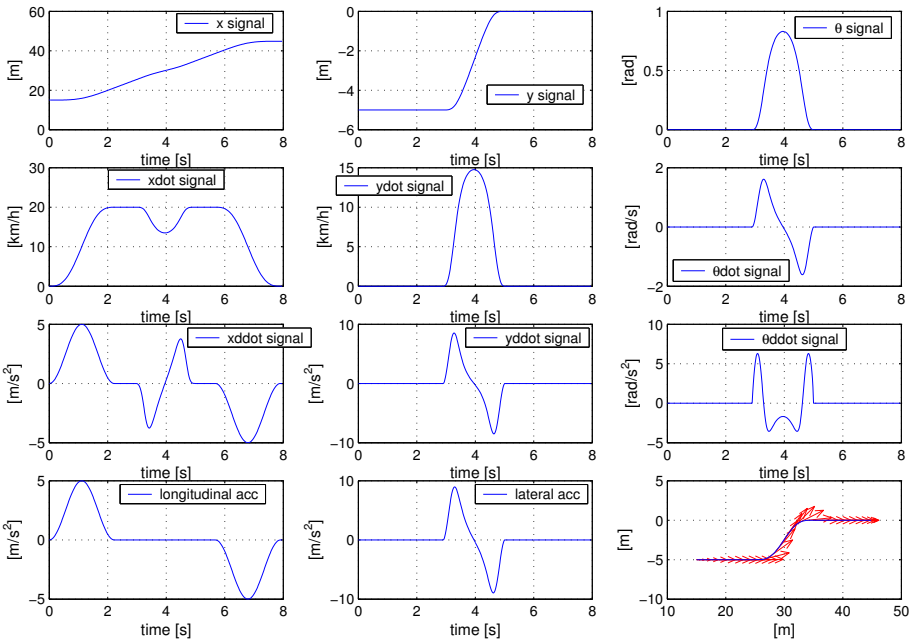

Figure H.2: The reference variables for the high acceleration lane change used for the simulations and the experiments with the 4ws4wd car.

Appendix I

Comparison between the multicycle controllers and the original controller

In this appendix, a comparison between the original controller, which is used at this moment for the path control of the 4ws4wd car used in VEHIL, and the multicycle controllers will be made. First a comparison will be made on simulation level. Finally a comparison will be made using experiments.

I.1 Simulations

The longitudinal and lateral frequency responses (x_{ref} to x and y_{ref} to y if the orientation angle is zero) while driving with a certain forward velocity are determined using the full dynamic simulation model of the 4ws4wd car (e.g. steering motor dynamics and roll dynamics of the car modelled) [15] . The multicycle controller with three different settings for the PD feedback controller is used. Also the original controller for the 4ws4wd car [15] is used. The simulations are split up in 2 sections: with and without parameter errors. The simulations with parameter errors are performed using the multicycle controller with parameter errors (e.g. the mass used in the controller is 0.8 times the mass of the model). The results of the simulations are drawn in figure I.1 and I.2.
The conclusion is that the lateral response of the original controller is not good compared to the lateral response of the multicycle controller without parameter errors. If parameter errors are introduced, then the multicycle controller with the strongest PD controller (highest bandwidth) is the only one that is better than the original controller. This is mainly, because the feedforward signal is not perfect anymore, so the response is more like the response of the PD controller.
The conclusion from the longitudinal response is that the original controller and the multicycle controller are comparable. Although it looks that the multicycle controller with the strongest PD settings is a little bit better.
A more detailed discussion about the frequency responses of the multicycle controller can be found in chapter 6.

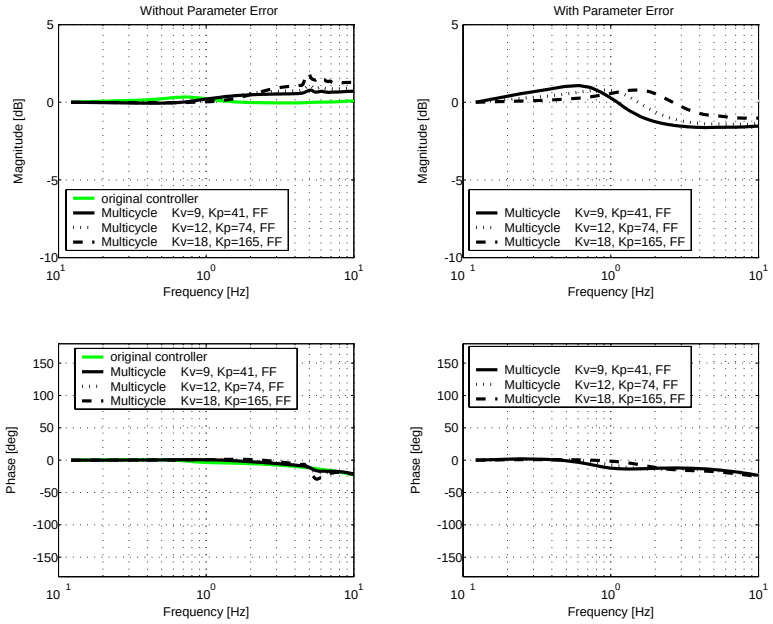

Figure I.1: Frequency response in longitudinal direction with and without parameter errors for the multicycle controller.

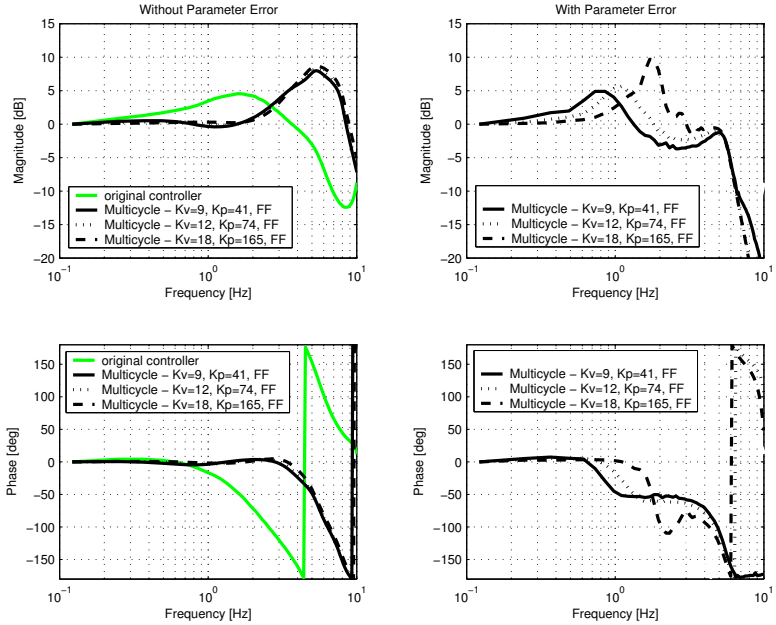

Figure I.2: Frequency response in lateral direction with and without parameter errors for the multicycle controller.

I.2 Experiments

The results of the experiments that are performed in the VEHIL test facility will be presented in this section. The trajectories used in the experiments are based on the trajectories used for the simulations performed in chapter 6. The experiments are performed using three different controllers: Original controller, Multicycle controller with tyre slip compensation ($K_p = 165, K_v = 18, e_c = 0.35$) and multicycle controller without tyre slip compensations ($K_p = 165, K_v = 18, e_c = 0.35$).
The results of three different experiments will be discussed. First a low acceleration eight shaped trajectory with a fixed orientation angle is driven. From a non-rolling start (longitudinal direction is the x direction), the 4ws4wd car accelerates to 15 km/h with a maximum acceleration of 3 m/s^2. The tangential velocity of the track is kept constant at 15 km/h. The maximum acceleration in perpendicular direction of the trajectory is 3 m/s^2, which is a result of the tangential velocity in combination with the radius of the corners of the eight shaped trajectory. At the end of the trajectory the velocity is reduced to zero again with a maximum de-acceleration of 3 m/s^2. The final part of the trajectory is a stand-still of a few seconds. Secondly a high acceleration eight shaped trajectory with a fixed orientation angle is driven (see appendix H). From a non-rolling start (longitudinal direction is the x direction), the 4ws4wd car accelerates to 20 km/h with a maximum acceleration of 5 m/s^2. The tangential velocity of the track is kept constant at 20 km/h. The maximum acceleration in perpendicular direction of the trajectory is 9 m/s^2, which is a result of the tangential velocity in combination with the radius of the corners of the eight shaped trajectory. At the end of the trajectory the velocity is reduced to zero again with a maximum de-acceleration of 5 m/s^2. The final part of the trajectory is a stand-still of a few seconds. Finally a high acceleration lane change with an orientation angle tangential to the trajectory is driven (see appendix H). From a non-rolling start, the 4ws4wd car accelerates in a straight line in x direction to 20 km/h with a maximum acceleration of 5 m/s^2. The tangential velocity of the track is kept constant at 20 km/h. The maximum acceleration in perpendicular direction of the trajectory is 9 m/s^2, which is a result of the tangential velocity in combination with the radius of the corners of the lane change. At the end of the trajectory the velocity is reduced to zero again in a straight line with a maximum de-acceleration of 5 m/s^2. The final part of the trajectory is a stand-still of two seconds.

I.2.1 Low acceleration eight shaped trajectory

The resulting errors for the low acceleration eight shaped trajectory with fixed orientation angle are drawn in figure I.3.
The errors using the original controller and the multicycle with slip compensation are drawn. The conclusion is that the difference between the controllers for this trajectory is rather small. The error is larger than expected from simulations of comparable trajectories (e.g. appendix A). One of the reasons that the error is larger is the fact that the position of the 4ws4wd car is determined using an estimator that estimates the position based on a discrete measuring tool (magnet grid) and a continuous measuring tool (wheel

velocities). The discrete measuring tool causes that the positions and velocity estimation is not ideal. The result is that the controller will not work perfect, which results in a larger error a the position error.
The error in the x direction at the end of the trajectory increases for the original controller. This is the phase when the car is close to the stop, so the velocity is low in the last few seconds of the trajectory. The original controller switches the feedback loop off at low velocities to overcome problems with the steering angle behavior. The error in the y direction at the end of the trajectory is not zero for the multicycle controller. This is the phase that the car (almost) stands still. The car is oriented with the longitudinal direction in positive x direction, so the error is due to the solutions of the zero-dynamics of the chosen control method, which is output linearization. The zero-dynamics are that $\dot{\theta}_{ij} = 0$, so the orientation angle can have any fixed (θ_{ijt}) value as long as $z_{1ij} = z_{1ijref}$, so $z_{1xij} = x_{ijt} + e_c \cos(\theta_{ijt}) = z_{1xijref}$ and $z_{1yij} = y_{ijt} + e_c \sin(\theta_{ijt}) = z_{1yijref}$ are (ideal) solutions for the situation that the tyre stands still at the reference position of the virtual control point z_{1ij}. The car ends the trajectory with an error in the y direction, so $z_{1ij} \neq z_{1ijref}$. Therefore, the car will steer the wheels so that that the measured output coordinates are equal to reference output coordinates, so that $z_{1ij} = z_{1ijref}$.

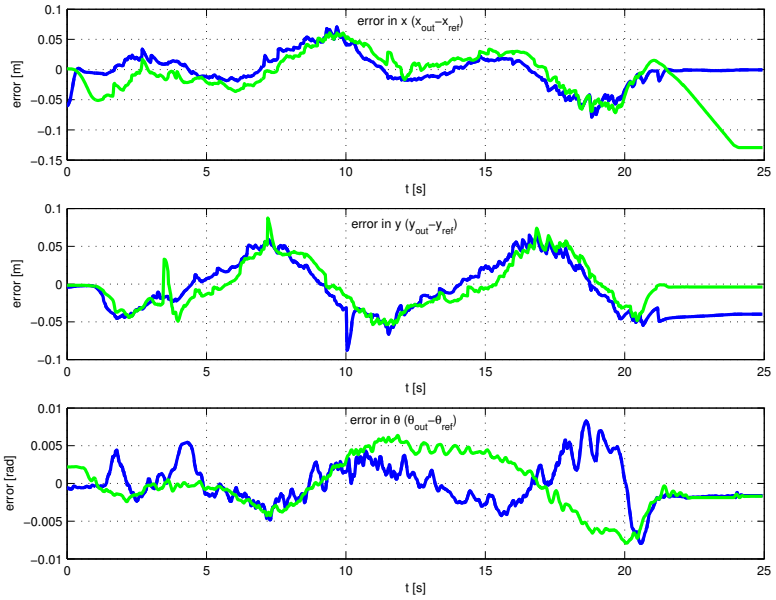

Figure I.3: The resulting error in x, y, θ for the low acceleration eight shaped trajectory (error=measured-reference). Dark signal: Multicycle controller with slip compensation. Light signal: Original controller

I.2.2 High acceleration eight shaped trajectory

The resulting errors for the high acceleration eight shaped trajectory with fixed orientation angle are drawn in figure I.4. The errors of the original controller, the multicycle controller without slip compensation and the multicycle with slip compensation are drawn. The conclusion is that the error using the multicycle controllers is smaller than the error using the original controller. This is visible in the error in the x direction and the error in the orientation angle θ. The difference between the multicycle with and without slip compensations is small. It is again visible that the original controller has an error in the x direction at the end of the trajectory and that the multicycle controllers have an error in the y direction at the end of the trajectory.

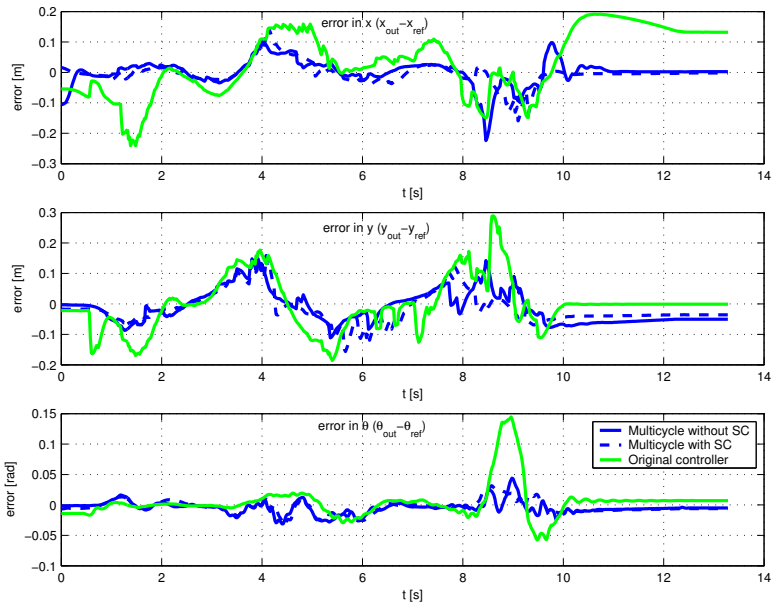

Figure I.4: The resulting error in x, y, θ for the high acceleration eight shaped trajectory (error=measured-reference)

The steering and driving torque of the front left wheel are drawn in figure I.5. The conclusions is that the original controller compensates the error more by steering its wheels and that the multicycle controller compensates the error more by driving the wheels. This can be concluded, because the steering torque signal for the original controller is larger and spikier than the steering torque signals of the multicycle controllers and the driving torque signal for the original controller is smaller and less spikier than the driving torque signals of the multicycle controllers.

I.2.3 High acceleration lane change

The resulting errors for the high acceleration lane change with varying orientation angle are drawn in figure I.6. The errors of the original controller, the

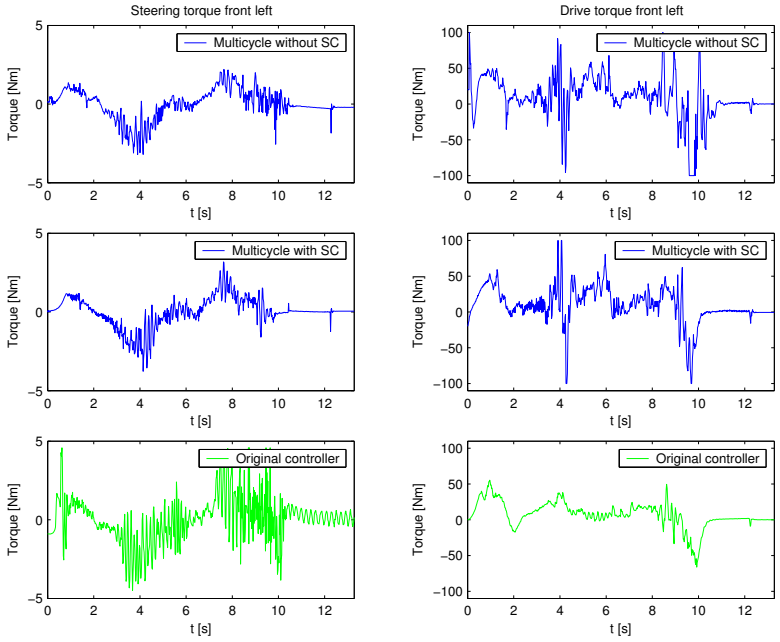

Figure I.5: The steering and driving torques for the front left wheel for the high acceleration eight shaped trajectory.

multicycle controller without slip compensation and the multicycle with slip compensation are drawn.
The conclusion is that there is a large difference between the original controller and the multicycle controllers. The errors using the multicycle controllers are smaller than the errors using the original controller. Also a small difference is visible between the multicycle controller with and without slip compensation.
The steering and driving torque of the front left wheel are drawn in figure I.7. The conclusions is again that the original controller compensates the error by steering its wheels and that the multicycle controller compensates the error by driving the wheels. This can be concluded, because the steering torque signal for the original controller is larger and spikier than the steering torque signals of the multicycle controllers and the driving torque signal for the original controller is very different than the driving torque signals of the multicycle controllers. The steering angles of the different controllers are drawn in figure I.8. Here it is visible that the steering angles are larger if the the original controller is used.
Finally, the lateral and longitudinal accelerations are plotted in figure I.9. Here it is visible that the response in lateral direction is far better for the multicycle controller than for the original controller. This corresponds with the results of the frequency response shown in the first section of this appendix.

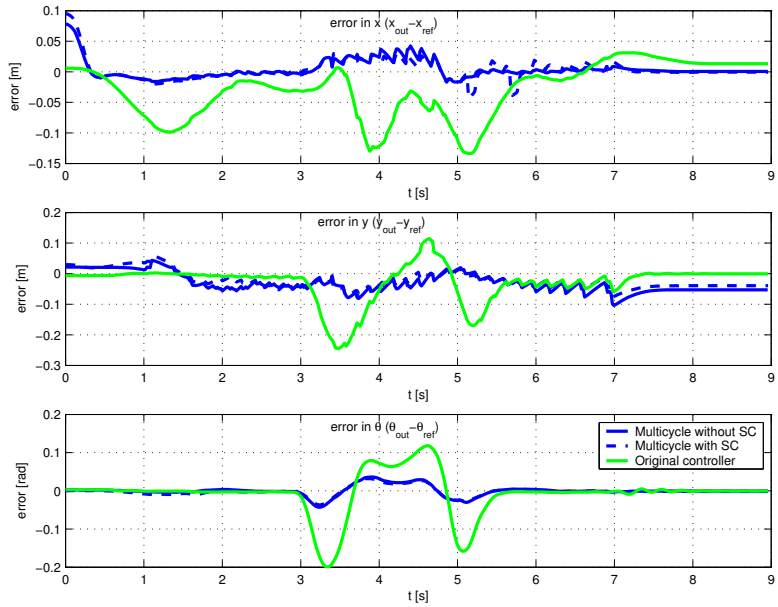

Figure I.6: The resulting error in x, y, θ for the high acceleration lane change (error=measured-reference)

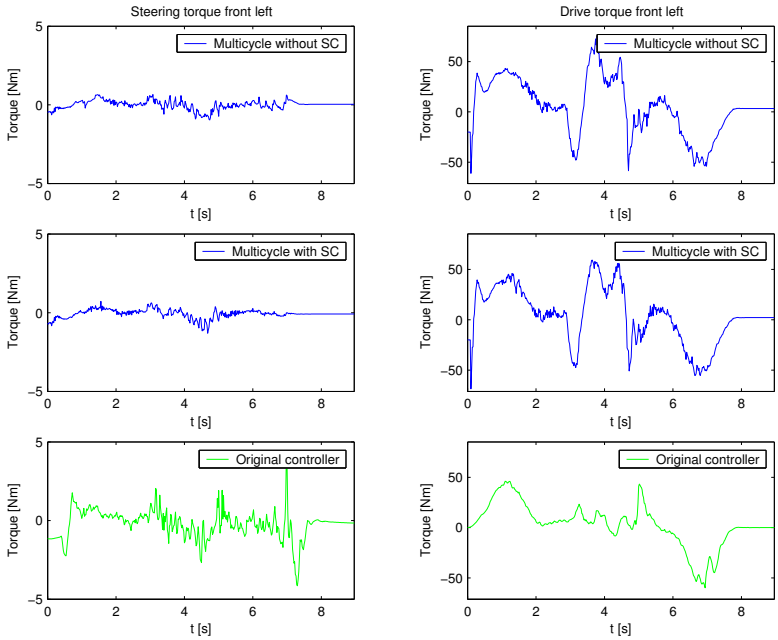

Figure I.7: The steering and driving torques for the front left wheel for the high acceleration lane change.

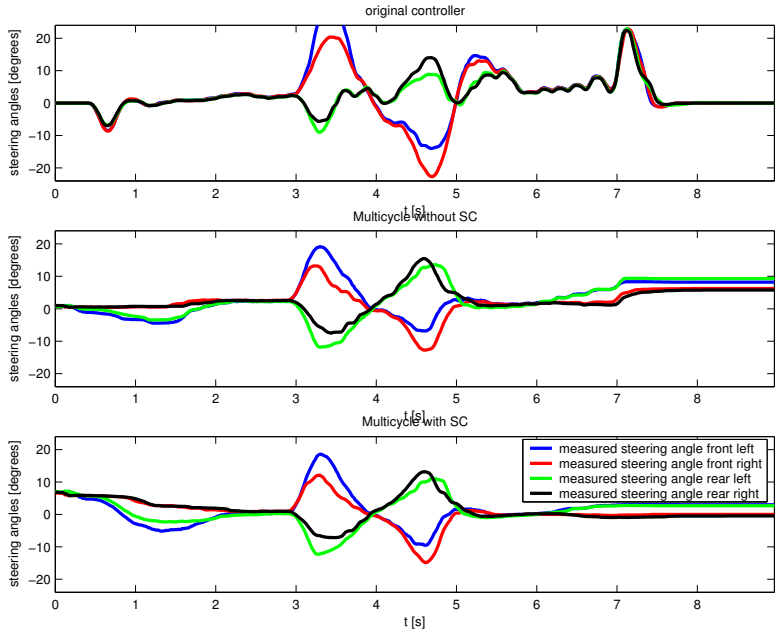

Figure I.8: The steering angles for the high acceleration lane change.

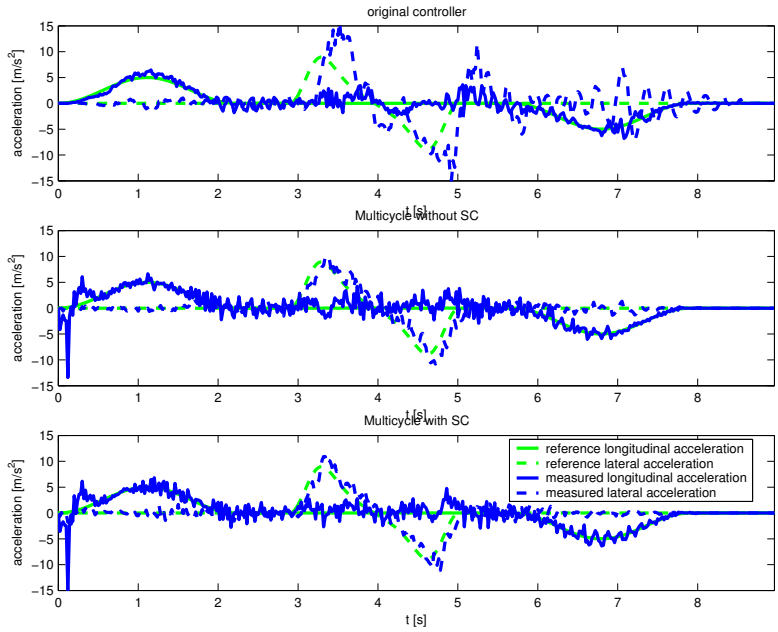

Figure I.9: The lateral and longitudinal acceleration for the high acceleration lane change.

I.3 Summary

A comparison is made between the original, the multicycle with and without slip compensation controller in this appendix. The conclusion is that the multicycle controller performs better than the original controller if high acceleration trajectories are driven. The difference is very clear for the lane change track. This can be explained looking a the frequency spectrum of a lane change and the frequency response in lateral direction. The frequency spectrum of a lane change has frequencies up to 1 Hz. The lateral frequency response of the multicycle controller is far better than the lateral frequency response of the original controller around 1 Hz. The difference for the eight shaped trajectories is not that large, because the frequency spectrum of the eighttrack is "lower" than the frequency spectrum of the lane change. The difference between the lateral frequency respons between the original controller and the multicycle controllers is smaller at those lower frequencies (0.2 Hz).
The second conclusion is that the multicycle with slip compensations is indeed better in reality than the multicycle without slip compensation. However the improvement is rather small. The simulations performed in chapter 5.4 show a more significant improvement than the experiments. One of the reasons is that slip is not the only reason for the error during the experiments because of other errors such as the position estimations errors. Another important factor is the large signal to noise ratio of the measured signals used for the slip compensation that cause that the slip compensation is not as effective as possible.
Another conclusion is that both control methods (original controller and multicycle controller) have a different way of compensating the error. The original controller compensates more by steering the wheels rather than driving the wheels. The multicycle controller compensates more by driving the wheels rather than steering the wheels.
Whether the multicycle controller keeps performing well if the velocities are increased has to be determined. It is however expected that the multicycle controller remains to have a better tracking performance for high acceleration (lateral) manoeuvres where the accelerations increase and decrease fast.